

CASSINI ATMOSPHERIC CHEMISTRY MAPPER

Volume I: Investigation and Technical Plan

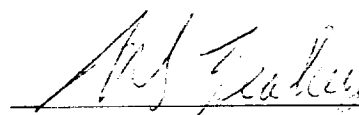
February 5, 1990

Principal Investigator:



Prof. Wm. Hayden Smith
Washington University
St. Louis, MO. 63130
(314) 889-5638

Authorizing Institutional Official



H.S. Leahey, Director
Washington University, Research Office
St. Louis, MO. 63130
(314) 889-5889

Co-Investigators:

Dr. Kevin H. Baines
Jet Propulsion Laboratory
California Institute of Technology
4800 Oak Grove Drive
Pasadena, Ca 91109
(818) 354-0481

Dr. M. Bruce Fegley
Max Planck-Institut für Chemie
Abteilung Kosmochemie
Mainz, F.R. Germany
49-6131-305-346

Dr. Harold J. Reitsema
Ball Aerospace Systems Group
P.O. Box 1062
Boulder, Co 80306-1062
(303) 939-5026

Dr. Gordon L. Bjoraker
Goddard Space Flight Center
Greenbelt, MD 20771
(301) 286-3139

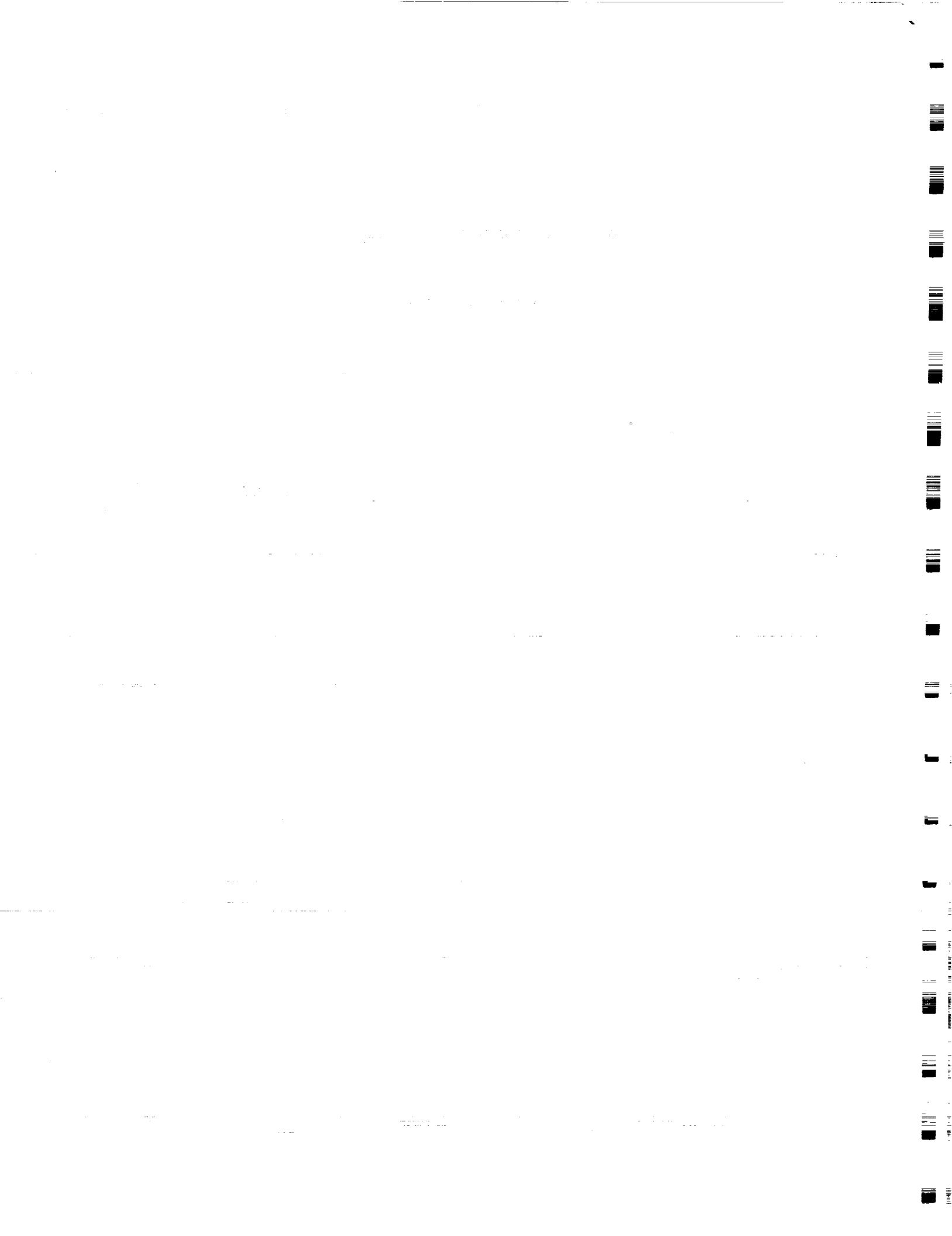
Dr. Keith S. Noll
Lunar and Planetary Lab
University of Arizona
Tucson, Az 85721
(602) 621-6362

Dr. Pierre Drossart
Observatoire de Meudon
92195 Meudon Principal
CEDEX, France
1-45077672

Dr. Glenn S. Orton
Jet Propulsion Laboratory
California Institute of Techn
4800 Oak Grove Drive
Pasadena, Ca 91109
(818) 354-2460

Industrial Collaborators:

Ball Aerospace, Prime Contractor
Rockwell International Science Center, Infrared Detector Arrays



ABSTRACT

The Cassini Atmospheric Chemistry Mapper (ACM) enables a broad range of atmospheric science investigations for Saturn and Titan by providing high spectral and spatial resolution mapping and occultation capabilities at 3 and 5 μm . ACM, consequently, can directly address the major atmospheric science objectives for Saturn and for Titan, as defined by the Announcement of Opportunity, with pivotal diagnostic measurements not accessible to any other proposed Cassini instrument.

ACM determines mixing ratios for atmospheric molecules from spectral line profiles for an important and extensive volume of the atmosphere of Saturn (and Jupiter). In particular, vertical profiles for H_2O and CO mixing ratios for the troposphere and stratosphere are determined as a function of latitude and longitude in order to delineate the dynamical and kinematic processes of the Saturnian atmosphere.

Spatial and vertical profiles of disequilibrium species abundances define Saturn's deep atmosphere, its chemistry, and its vertical transport phenomena. ACM spectral maps provide a unique means to interpret atmospheric conditions in the deep (~ 1000 bar) atmosphere of Saturn. Deep chemistry and vertical transport is inferred from the vertical and horizontal distribution of a series of disequilibrium species; in particular, CO , PH_3 , GeH_4 , AsH_3 , and HCN . ACM will detect the depth to which convective "storms" reach by sensing the abundance variations of specific disequilibrium species drawn upward to observable levels.

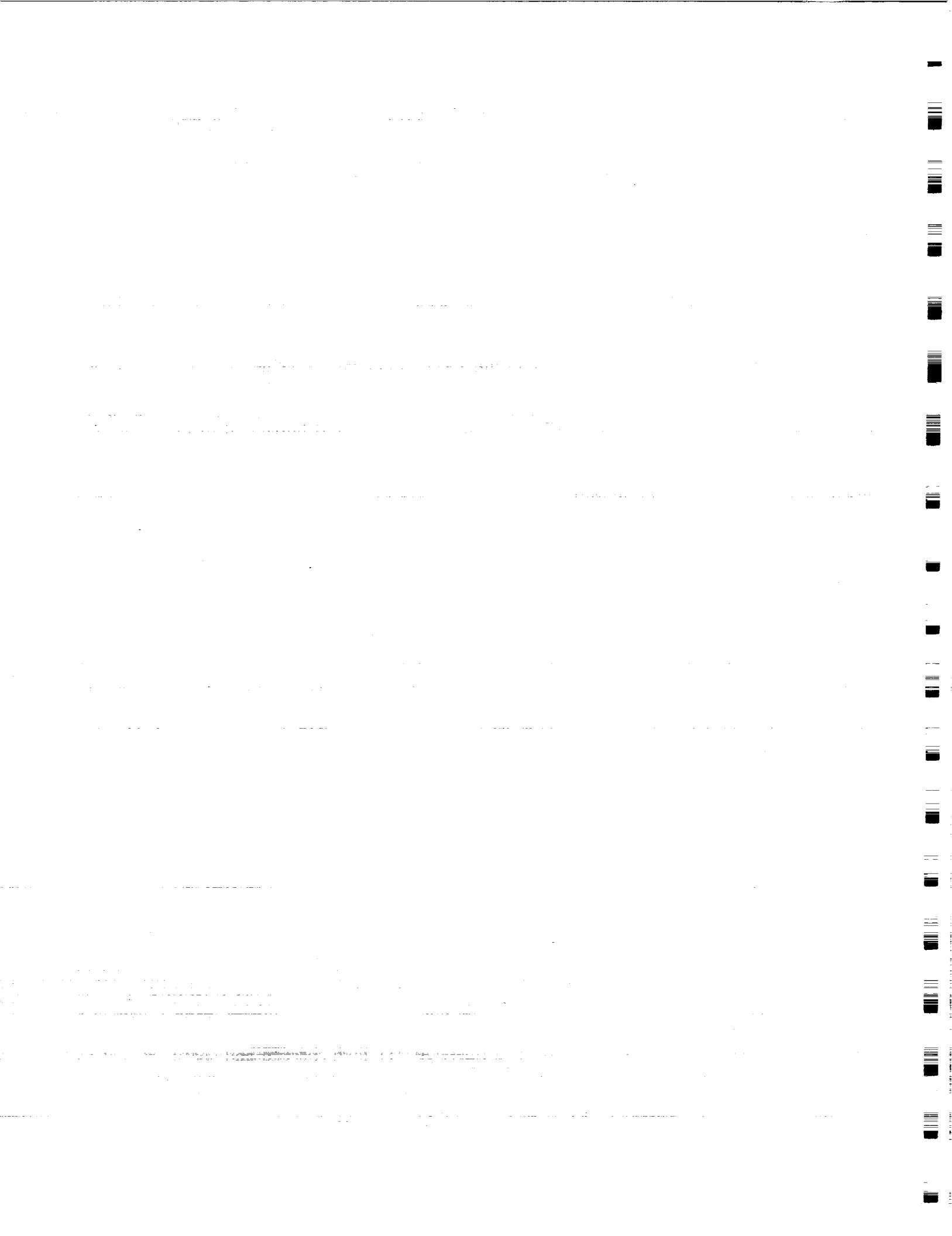
Solar occultations provide a method to bridge the altitude range in Saturn's (and Titan's) atmosphere that is not accessible to radio science, thermal infrared, and uv spectroscopy with temperature measurements to $\pm 2\text{K}$ from the analysis of molecular line ratios and to attain an high sensitivity for low-abundance chemical species in the very large column densities that may be achieved during occultations for Saturn.

For Titan, ACM solar occultations yield very well resolved ($1/6$ scale height) vertical mixing ratios column abundances for atmospheric molecular constituents, eg. CO , HCN , C_2H_2 , and C_2H_6 , that are important in defining atmospheric evolution of Titan and the rate for processes leading to methane depletion. Occultations also provide for detecting abundant species very high in the upper atmosphere, while at greater depths, detecting the isotopes of C and O, constraining the production mechanisms and/or sources for the above species. Reflectance spectrophotometry at 3 and 5 μm measures horizontal distributions for the above species.

ACM measures the vertical and horizontal distribution of aerosols via their opacity at 3 μm and, particularly, at 5 μm . ACM recovers spatially-resolved atmospheric temperatures in Titan's troposphere via 3- and 5- μm spectral transitions. Together, the mixing ratio profiles and the aerosol distributions are utilized to investigate the photochemistry of the stratosphere and consequent formation processes for aerosols.

Finally, ring opacities at 3.0 μm and 5.3 μm , observed during solar occultations and in reflected sunlight, provide a measurement of the particle size and distribution of ring material.

ACM will be the first high spectral resolution mapping spectrometer on an outer planet mission for atmospheric studies while retaining a high resolution spatial mapping capability. ACM, thus, opens an entirely new range of orbital scientific studies of the origin, physio-chemical evolution and structure of the Saturn and Titan atmospheres. ACM provides high angular resolution spectral maps, viewing nadir and near-limb thermal radiation and reflected sunlight; sounds planetary limbs, spatially resolving vertical profiles to several atmospheric scale heights; and measures solar occultations, mapping both atmospheres and rings. ACM's high spectral and spatial resolution mapping capability is achieved with a simplified Fourier Transform spectrometer with a no-moving parts, physically compact design. ACM's simplicity guarantees an inherent stability essential for reliable performance throughout the lengthy Cassini Orbiter mission.



Contents

1	Instrument Summary	
2	SCIENTIFIC OBJECTIVES	1
2.1	Introduction/ Scientific Rationale	1
2.2	Saturn	1
2.2.1	Deep Atmospheric Circulation	1
2.2.2	Tropospheric Meteorology	4
2.2.3	Stratospheric Thermal Structure	6
2.2.4	Stratospheric Photochemistry	6
2.2.5	Formation/Evolution	8
2.3	Titan Atmospheric Processes	8
2.3.1	Chemical Evolution and Methane Depletion	8
2.3.2	Formation/Evolution	9
2.3.3	Detection of Aerosols/New Species	9
2.3.4	Distribution of Oceans on Titan	10
2.3.5	Clouds and Aerosol Distributions	10
2.3.6	Atmospheric Circulation and Dynamics	10
2.4	Saturn's Rings	11
2.5	Summary	11
3	ANTICIPATED RESULTS	12
3.1	Results Anticipated	12
3.2	Scientific Context	12
4	APPROACH	13
4.1	Introduction	13
4.2	Instrument Approach	13
4.2.1	Wavelength Sampling Requirements	13
4.2.2	Spatial Sampling Requirements	16
4.2.3	Integration Time Requirements	16
4.2.4	The ACM Approach	16
4.3	Observational Approach	19
4.3.1	Data Acquisition	19
4.3.2	Calibration and Reduction	19
4.4	Data Analysis	20
4.4.1	Solar Occultations	20
4.4.2	Thermal Emission Spectrophotometry	21
4.4.3	Reflectance Spectrophotometry	22
4.5	Relationship of ACM to Other Prospective Orbiter Instrumentation	23
4.5.1	Complementarity	23
4.5.2	Comparison	24
5	INSTRUMENTATION	25
5.1	Instrument Selection	25
5.2	Instrument Description	25
5.2.1	System Design	25
5.2.2	Instrument Heritage	28
5.2.3	Detector	28
5.2.4	Radiometric Analysis	29

5.2.5	Optical Design	30
5.2.6	Thermal Design	31
5.2.7	Electrical Design	31
5.2.8	Mechanical Design	32
5.3	Calibration	32
5.4	Data Collection, Analysis and Archiving	32
5.4.1	Observing Modes	32
5.4.2	Calibration Methods	33
5.5	Mission Operations and Data Management Plan	34
5.5.1	ACM Mission Operations Plan	34
5.5.2	ACM Data Plan	35
5.5.3	Housekeeping	35
5.5.4	Camera Control	35
5.5.5	Calibration Data and Photometric Corrections	35
5.5.6	Spatial Registration	35
5.5.7	Spectral Information for Data Interpretation	35
5.5.8	Interpretation of Data	35
5.5.9	Data Product	36
6	Responsibilities and Commitments of Scientific Investigators	36
6.1	Principal Investigator, Dr. William Hayden Smith	36
6.2	Co-Investigators	36
7	RELEVANT SCIENTIFIC EXPERIENCE	37
7.1	BIBLIOGRAPHICAL INFORMATION	38
8	INSTITUTIONAL SUPPORT	38
8.1	PI Support	38
A	DIGITAL ARRAY SCANNED INTERFEROMETERS	1
A.1	Theory of Operation	1
A.2	Heterodyning	3
A.3	Laboratory Results for ACM	3
B	SELECTED BIBLIOGRAPHIES OF INVESTIGATOR TEAM	7
B.1	Dr. William Hayden Smith	7
B.2	Dr. Kevin H. Baines	7
B.3	Dr. Gordon L. Bjoraker	7
B.4	Dr. Pierre Drossart	7
B.5	Dr. M. Bruce Fegley	7
B.6	Dr. Keith S. Noll	7
B.7	Dr. Glenn S. Orton	9
B.8	Dr. Harold J. Reitsema	9

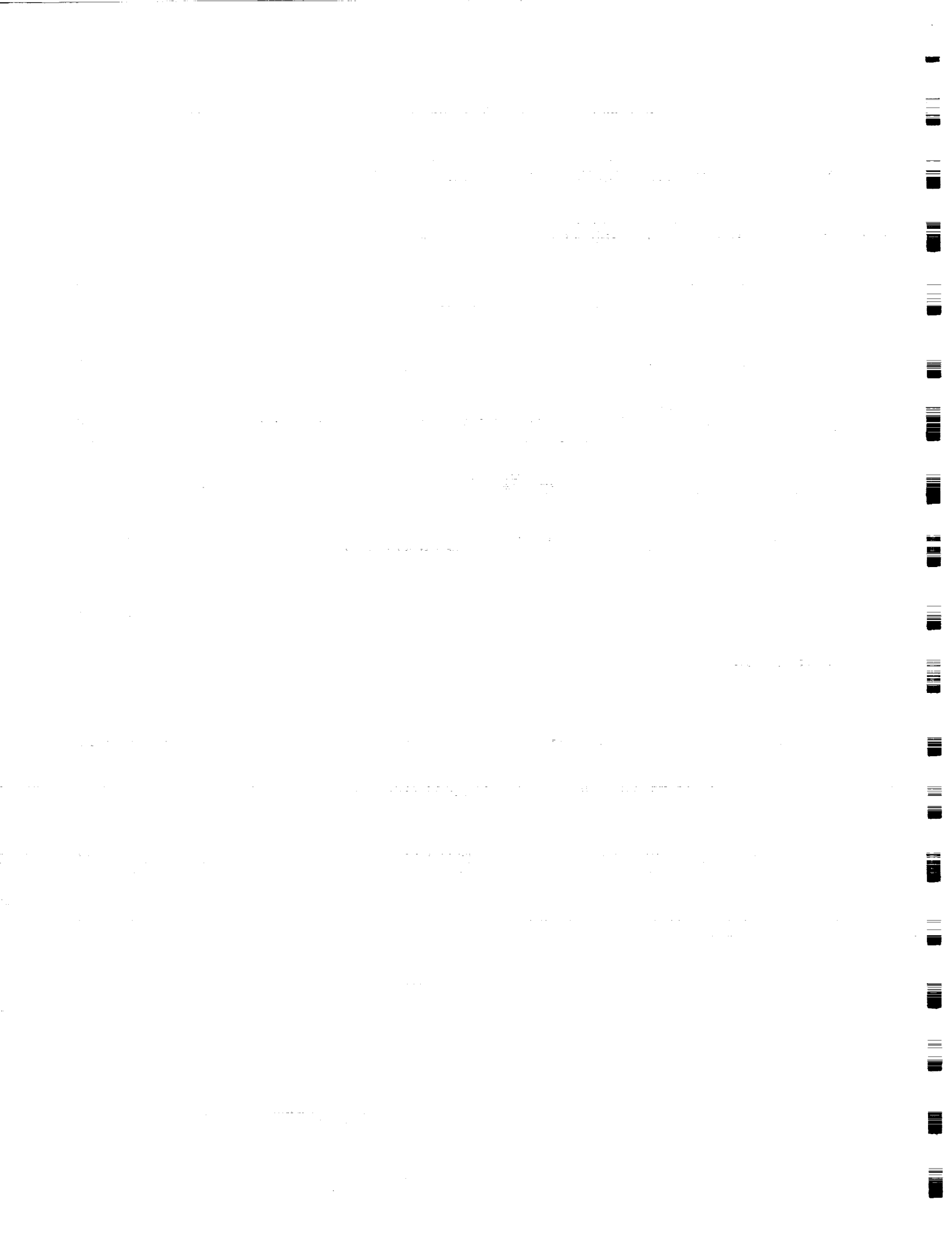
List of Figures

1	Saturn Disequilibrium Trace Gases	3
2	Saturn's CO Abundance	3
3	HCN Abundance	3
4	Vertical Distributions for Tropospheric Gases	3
5	Predicted Latitudinal Variation of CO	3

6	Disequilibrium Species Abundance for Convective Storm systems	5
7	Pressure Levels for Localized Storm Systems	5
8	Model of Moist Convection and the Abundance of Water Vapor	5
9	Water, Ammonia and Methane Spectrum Near 5.2 μm	5
10	Model Profiles for Titan Solar Occultation	7
11	Schematic Model for the Ocean-Atmosphere Evolution	7
12	Volume Mixing Ratios of Selected Species	7
13	Simulated Reconstruction of Spectral Features	7
14	4.7- μm Spectra of Important Saturn Constituents	15
15	Channel 2: Synthetic Saturn Spectra	18
16	Channel 3: Titan Solar Occultation Spectra	18
17	Near-Limb Synthetic Spectra	23
18	ACM Optical Layout	26
19	ACM Functional Diagram	27
20	ACM Hardware Block Diagram	27
21	Detector Dark Current	29
22	ACM Radiometric Calibration Schematic	33
23	Laboratory results, White Light Interferogram	5
24	Laboratory Results, White Light Spectrum	5
25	Laboratory Results, Mercury Spectrum	5
26	Laboratory Results, Narrow Band Continuum Interferogram	6
27	Laboratory Results, Narrow Band Continuum Spectrum	6
28	Laboratory results, Narrow Band Continuum Spectrum	6
29	Laboratory Results, ACM High Resolution Spectrum	6
30	Laboratory Results, Infrared Interferogram	8

List of Tables

1	ACM Instrument Configuration Summary Table	iv
2	Summary of ACM Scientific Objectives	14
3	Summary of Selected Channels	15
4	Spectroscopic Features	17
5	Signal-to-Noise vs Altitude for Titan Solar Occultations	20
6	Channel 2 Uncertainties for Titan Occultations	21
7	Channel 3 Uncertainties For Titan Occultations	21
8	Uncertainties from Saturn Nightside Observations	22
9	Instrument Requirements Derived From Science Objectives	26
10	Typical Integration Times	28
11	Focal Plane Array Requirements	29
12	ACM Radiometric Parameters	30

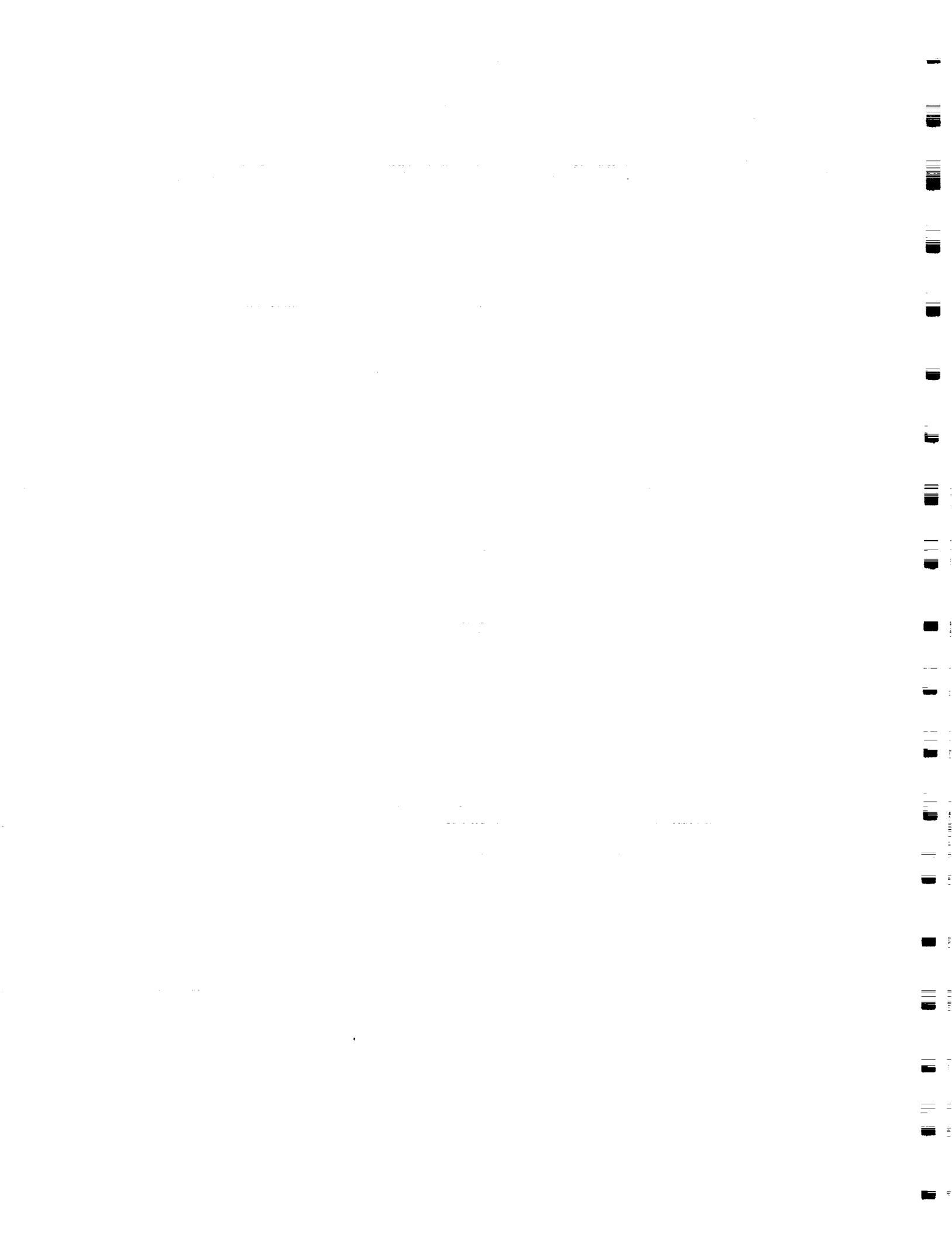


1 Instrument Summary

The Atmospheric Chemistry Mapper (ACM) is a simple, compact, reliable high resolution mapping three channel 3 - 5 μm infrared spectrometer. It has no moving parts and takes maximum advantage of existing space flight hardware and hardware concepts wherever possible. It is mounted on the High Precision Scan Platform (HPSP), co-aligned with the other optical instruments. It makes nadir and off-nadir atmospheric observations through a telescope and solar occultation observations through an auxiliary port dedicated to that purpose.

Table 1: ACM Instrument Configuration Summary Table

Location:	HPSP
Moving parts:	None
Covers:	None required, dust insensitive
Main aperture:	100 mm diameter, f/2, achromat
Auxiliary aperture:	1.5 mm window slit
Contamination:	Main and auxiliary element heaters Sealed optics, insensitive radiators
FOV, total:	1.2×102 mrad
FOV, ea. channel:	1.2×34 mrad
IFOV:	1.2×0.4 mrad
Number of spectral channels:	3
Spectral resolution:	0.25 cm^{-1} , nominal
Channel 1, "H ₂ O"	$\sigma = 1885 - 1940 \text{ cm}^{-1}$, nominal
Channel 2, "CO"	$\sigma = 2123 - 2168 \text{ cm}^{-1}$, nominal
Channel 3, "3 μm "	$\sigma = 3255 - 3300 \text{ cm}^{-1}$, nominal
Exposure time for:	
SNR = 25	50 secs. (5 exp. of 10 secs)
SNR = 100	800 secs. (80 exp. of 10 secs)
Interferometer:	Michelson with grating
Detector:	256x256 staring 3.0-5.3 μm HgCdTe array
Detector temperature:	60K
Detector cooling:	Passive radiator, 400cm ²
Instrument cooling:	Passive radiator, 400cm ²
Radiator surfaces:	$\epsilon \geq 0.85$, $\alpha \approx 0.9$ (black)
Instrument/telescope temperature:	110K
Mass:	<5.5Kg, including electronics
Dimensions:	40cmx28cmx12cm, excluding electronics 15cmx15cmx9cm, electronics
Power requirements:	<5 Watts average, instrument +8 Watts, heater, when energized
Processor:	SA3300
Commanded data:	Detector control parameters
Housekeeping data:	Temperatures, time of observation
Output data:	Raw detector image data
Data rates:	<200 Kbps peak, <20 Kbps mean, typ.
EMI sources; receptors:	DC/DC converter ; A/D converter



2 SCIENTIFIC OBJECTIVES

2.1 Introduction/ Scientific Rationale

The demanding science objectives of the forthcoming exploration of Saturn and Titan during the Cassini mission impose a strong challenge on our ingenuity to devise equally capable instrumentation. Saturn and Titan are among the most important planets in the solar system for detailed study. Saturn is in the second position, after Jupiter, in the hierarchy of planetary dimensions but is without peer in terms of its atmospheric dynamical and circulation activity and has the unique influence of the rings which may participate in the formation of molecules such as CO and H₂O in Saturn's atmosphere. Titan, Saturn's giant satellite, is the only solar system satellite with a massive atmosphere. The mixed reducing/oxidizing nature of Titan's atmosphere is unique and has the potential to shed light on the early history of the Earth's atmosphere. This fact lends an unusual urgency to the detailed study and understanding of Titan's atmosphere. Our goals are to understand the structure, chemistry, dynamics, and evolution of Saturn and Titan, as well as the distribution, composition, and evolution of ring particles. Attainment of these science goals would be well beyond the capability of the previous generation of spacecraft instruments. Consequently, a low cost, high spectral resolution spatial mapping spectrometer has been designed for the attainment of the atmospheric science goals of Cassini at Saturn and Titan.

2.2 Saturn

2.2.1 Deep Atmospheric Circulation

Like Jupiter, the atmosphere of Saturn exhibits dynamical structures on scales ranging from a scale height (approximately 60 km) up to the planetary radius (60,000 km). Most prominent is the zonal jet structure, similar to Jupiter's belt/zone pattern, but incorporating winds up to four times greater than its jovian counterpart. Long-lived oval spots, dynamic vortex streets, and active convective regions, having scales of a few hundreds to thousands of kilometers, are just a few of the wide range of cloud morphologies observed by the fleeting Voyager flybys. The nature of each of these dynamical features, (for example, the causes of the stability, equatorial symmetry, large velocities, and axisymmetry of the zonal structure,) as well as dynamical processes within the convective and vortex street features, are poorly understood. Specifically, connections between the observed circulation at the 1-bar level "cloud surface" imaged by the Voyager visible-wavelength cameras and deep-rooted circulation at the kilobar level are tenuous. In particular, the depth of all dynamical features - from planetwide zonal flows to localized convective regions - is quite uncertain.

As noted by Allison (1985), Hunt (1985), Ingersoll *et al.*, (1984), and others, two extreme pictures of the gross atmospheric dynamics of both Saturn and Jupiter have emerged from the Voyager observations. At one extreme, derived from first-order implications of the large zonal winds and the observed small equator-to-pole temperature gradient (Smith, 1982), and further supported by the observed stability of the zonal velocity profile against visible changes in the belt/zone structure (Smith and Hunt, 1976), the jet streams extend deep into the interior. In the other extreme, the observed flow is confined to a thin layer, powered by thermodynamic phase changes (e.g., latent heat of condensation, ortho/para hydrogen conversion). The first view implies convection is so inefficient that the transport of the observed internal heat flux to the top of the atmosphere is difficult to explain. The latter view, because of the observed large wind speeds, requires large horizontal temperature gradients which should break down under the influence of large convective processes.

The discovery in recent years of significant abundances of a number of disequilibrium trace gases in the observable atmosphere (e.g., CO by Noll *et al.*, 1986; GeH₄ by Noll *et al.*, 1988, AsH₃ by Noll *et al.*, 1988b, and PH₃ by Larson *et al.*, 1980 and Bezard *et al.*, 1989) affords a means

of probing deep atmospheric circulation. The observed presence of these disequilibrium species is linked to vertical mixing which has the effect of quenching chemical reactions that would otherwise decrease their abundances far below detectable levels (Fegley and Prinn, 1985). Sufficiently fast vertical mixing transports molecules such as CO upward from deeper atmospheric levels (where their abundances are larger) on timescales shorter than the chemical timescales for destroying these species.

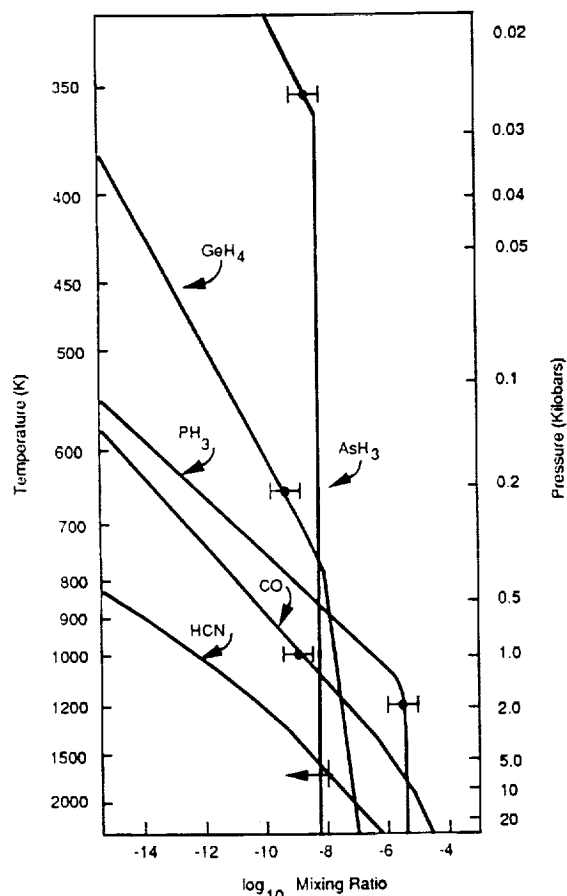
As an example, the observed CO mixing ratio of 2.0 ± 0.7 ppb (Noll *et al.*, 1986) is approximately 45 orders of magnitude larger than the thermochemical equilibrium CO abundance in Saturn's upper troposphere ($T = 190\text{K}$) where CO is observed. From Fig. 1, it can be seen that the observed CO abundance in Saturn's upper troposphere is the same as the CO abundance at approximately the 1000K, 1 kilobar level. Sufficiently rapid vertical mixing, which is parameterized using the vertical eddy diffusion coefficient, K_{eddy} , in Fig. 2 is able to transport CO from the 1000K, 1 kilobar level upward to the observable atmosphere before the CO can be converted back into CH_4 via the net thermochemical reaction $\text{CO} + 3\text{H}_2 \rightarrow \text{CH}_4 + \text{H}_2\text{O}$.

Mathematically, this situation is described by the equalities $t_{\text{conv}} = t_{\text{chem}}$ at $T = T_Q$, where $t_{\text{conv}} = H^2/K_{\text{eddy}}$ is the convective mixing time over one scale height H , and t_{chem} is the chemical destruction time for CO at the quench temperature T_Q . At the 1000K level in Saturn's deep atmosphere, the pressure scale height H is approximately 350 km and the CO chemical destruction time is about 1.7×10^6 seconds (20 days). Thus, the corresponding vertical eddy diffusion coefficient $K_{\text{eddy}} = H^2/t_{\text{conv}} = H^2/t_{\text{chem}} = 7 \times 10^8 \text{ cm}^2 \text{ s}^{-1}$. As shown in Fig. 2, this value is consistent with the range of K_{eddy} values of $10^7 - 10^9 \text{ cm}^2 \text{ s}^{-1}$ independently estimated from free convection theory and the observed heat flux emitted by Saturn (e.g., see Stone, 1976; Flasar and Gierasch, 1977; Prinn *et al.*, 1984). Less rapid vertical mixing, corresponding to smaller K_{eddy} values, transports air parcels upward at a slower rate. Thus the $\text{CO} \rightarrow \text{CH}_4$ conversion has more time to proceed and is not quenched until higher levels (lower temperatures) in Saturn's deep atmosphere, resulting in less CO in the detectable atmosphere. Conversely, faster vertical mixing, represented by larger K_{eddy} values, transports air parcels upward at a faster rate, resulting in more CO in the detectable atmosphere.

The observed mixing ratio of disequilibrium species in the troposphere, then, is directly connected to the rate of vertical mixing in the deep atmosphere. CO and HCN are particularly good "dynamical tracers", having the strongest abundance/ K_{eddy} relationships, as illustrated in Figs. 2 and 3.

Other processes may somewhat enhance abundances of disequilibrium species in the observable atmosphere as well. These include (1) injection of icy material from satellites, meteorites, or rings for CO (Prather *et al.*, 1978; Strobel and Yung, 1979; Noll *et al.*, 1986), (2) the combined photolysis of NH_3 and C_2H_2 for HCN (Kaye and Strobel, 1983), and (3) thunderstorm activity for both CO and HCN (Bar Nun and Podolak, 1985). Except possibly for the rings, the contribution of each of these sources is negligible compared to the upwelling component. Noll *et al.* 1986 find that the meteoritic contribution to CO on Saturn is insignificant, contributing nothing to the observed spectral features. Lewis (1980) concludes that the production of CO and HCN from lightning discharges on Jupiter is unimportant when compared to photochemical and deep-atmospheric sources. From this, Prinn *et al.* (1984) conclude that lightning should be unimportant for CO and HCN on Saturn as well. Moreover, as the photochemical upper limit in Fig. 3 indicates, the amount of HCN predicted to be produced by NH_3 photochemistry (Kaye and Strobel, 1984) is insignificant relative to HCN produced by rapid vertical mixing (e.g., see Fegley and Prinn 1985, 1988). Finally, if ring material were the primary CO source, then ring lifetimes of $10^7 - 10^8$ years would be implied (Noll *et al.* 1986), much shorter than that of the solar system, but nevertheless consistent with recent theories of ring dynamics. Each of these mechanisms enhance abundances in distinct atmospheric levels: while the upwelling component is uniformly distributed throughout the troposphere, extraplanetary sources and photochemical processes would enhance

FOLDOUT FRAME



11070357.028

Figure 1: Comparison of the observed and theoretically predicted abundances of disequilibrium trace gases on Saturn. The observed abundances of arsine (AsH_3 ; Bezdard *et al.*, 1989), germane (GeH_4 ; Noll *et al.*, 1988), carbon monoxide (CO , Noll *et al.*, 1986), and phosphine (PH_3 , Drossart, private communication) found in the 160-210K region of Saturn's upper troposphere correspond to the predicted abundances of these gases at chemical equilibrium in the 350 to 1200K region of Saturn's deep atmosphere. The upper limit on HCN (Tokunaga *et al.*, 1981) corresponds to the predicted HCN equilibrium abundance of approximately 1600K. These species are chemical probes of the deep, unobservable regions of Saturn's atmosphere. The chemical equilibrium calculations presented here are for a chemical model of Saturn's atmosphere enriched in all elements heavier than H and He by 7.5 times solar composition (Cameron, 1982). The pressure scale shown on the figure is a dry adiabat calculated by taking $T = 136\text{K}$ at 1 bar (Prinn *et al.*, 1984), H_2 and the He mixing ratios of 0.963 for H_2 and 0.037 for He (Conrath *et al.*, 1984), and temperature dependent heat capacity (C_P) data for H_2 from the JANAF Tables.

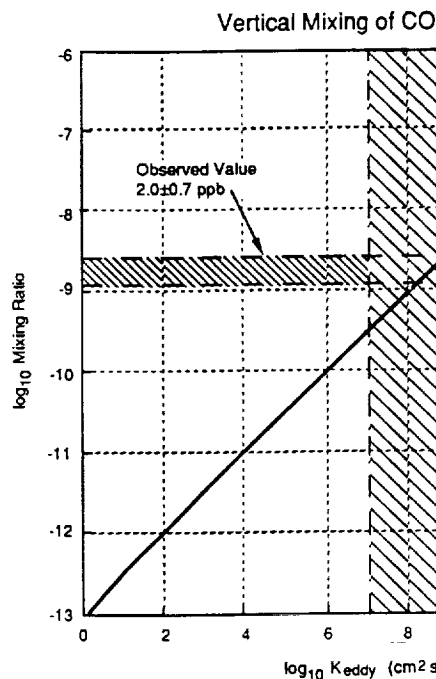
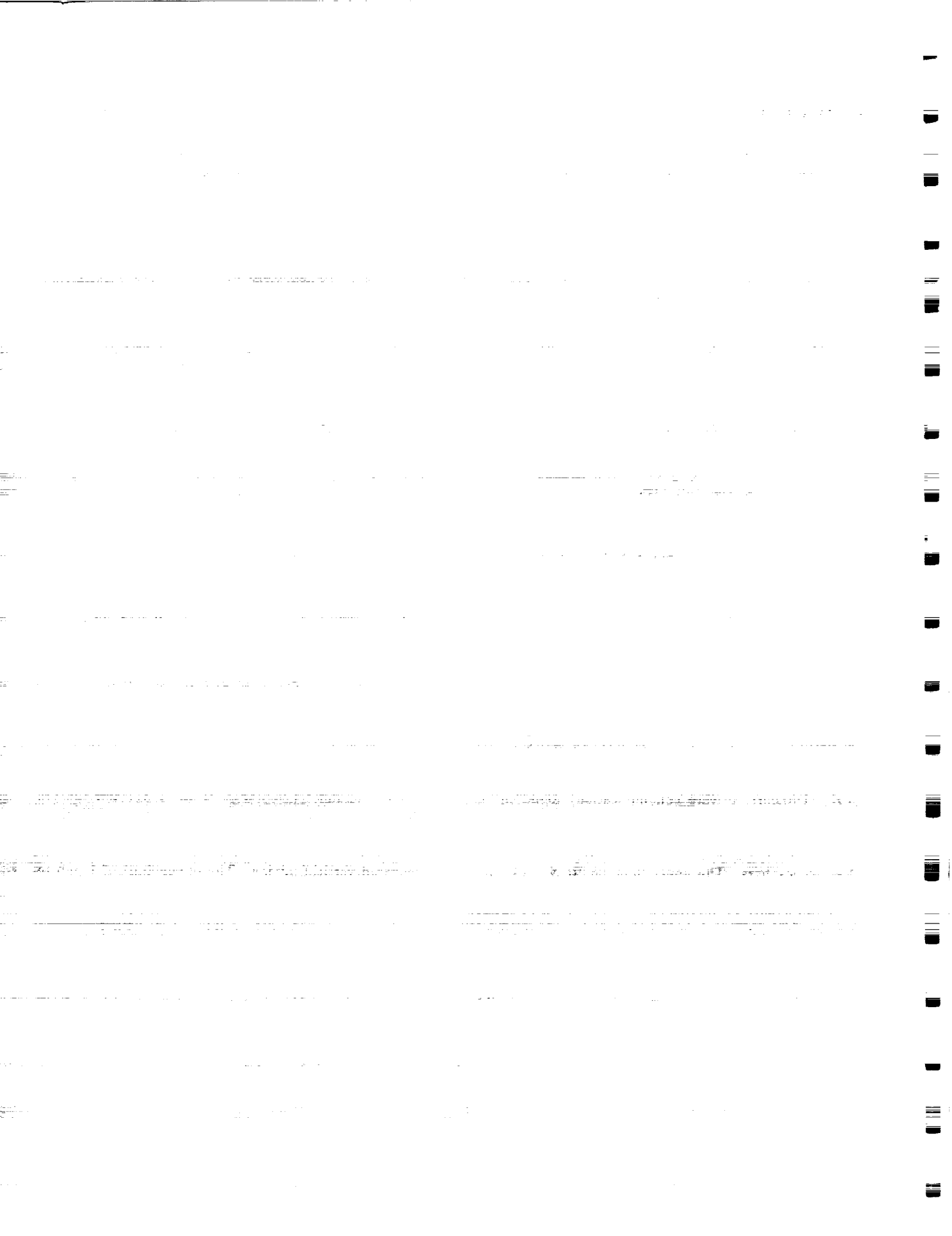
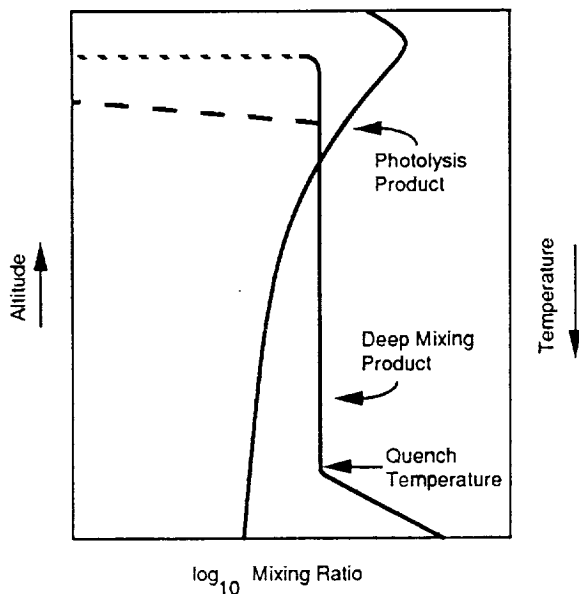


Figure 2: Comparison of the amount of the observable regions of Saturn's vertical mixing with the observed (Tokunaga *et al.*, 1986). Theoretical prediction is consistent with the range of K_{eddy} values from convection theory and the observed Saturn. (e.g., see Stone, 1976; Flasar *et al.*, 1984).

Figure 3: Comparison of the HCN abundance (Tokunaga *et al.*, 1986) with the predicted HCN abundance from stratification (Kaye and Strobel, 1984) with delivered to the observable regions of Saturn by rapid vertical mixing. The upper limit to HCN, given by $K_{\text{eddy}} = 10^2$ is 30 to 3,000 times more vigorous than required to support Saturn's internal heat flux. The upper limit to HCN, given by $K_{\text{eddy}} = 10^2$ is 2 ppb, or about 3.5 times smaller than the amount of HCN predicted to be produced by rapid vertical mixing. Furthermore, as the photochemical production of HCN is small relative to HCN produced by rapid vertical mixing (see Fegley and Prinn 1985, 1988).





11070/357.030

Figure 4: Schematic vertical distributions for quenched lower-troposphere gases and photolysis products. At altitudes above the quench temperature level, the chemical lifetime of the disequilibrium species is longer than the characteristic time for vertical mixing, thus yielding an essentially constant mixing ratio up to where solar UV photolysis (dashed-dot extension) or condensation (dashed) may occur. Photolysis products are enhanced in the stratosphere, relatively depleted in the troposphere.

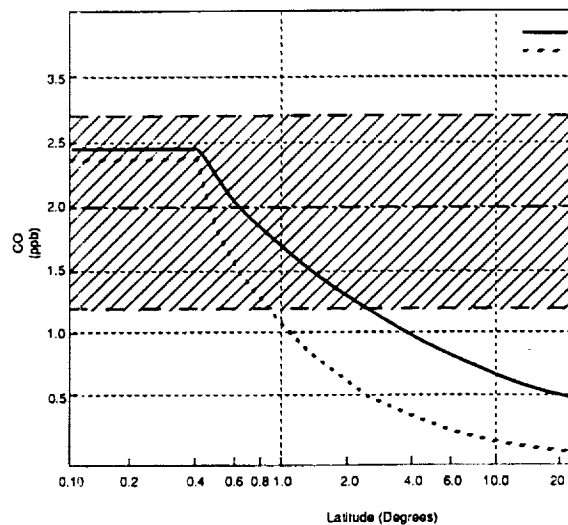
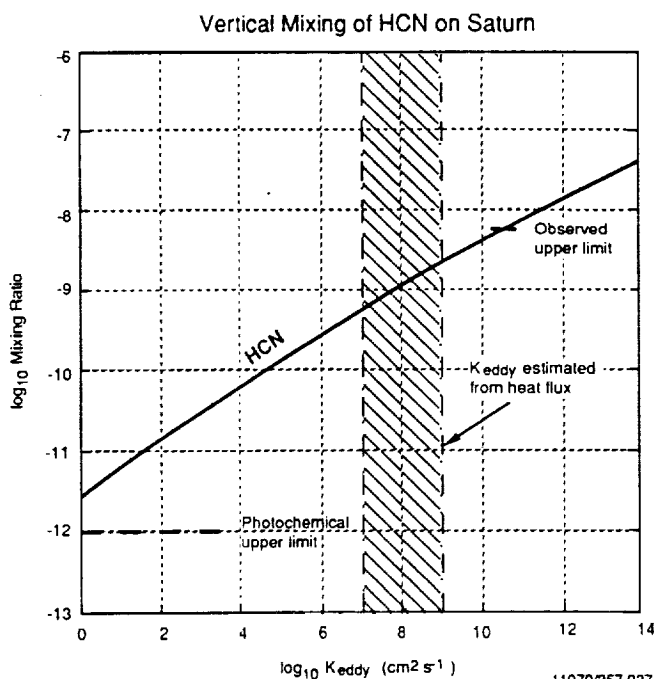


Figure 5: Schematic illustration of the meridional variation of CO on Saturn, calculated assuming that the latitudinal dependence of K_{eddy} is similar to that on Jupiter (Flasar and Gierasch, 1977). The solid line shows the variation in the CO mixing ratio (Fig. 2) and the dashed line shows the variation at the 1000 bar level (taken from Flasar and Gierasch, 1977) in Saturn's deep atmosphere where the $\text{CO} \rightarrow \text{CH}_4$ conversion occurs (Fegley, 1985). The horizontal shaded region shows the global value of (2.0 ± 0.7) ppb CO determined by Fegley (1986). Only ACM observations are capable of measuring the predicted variation in CO; Earth-based and Earth-orbiting observations do not have the required spatial resolution.



11070/357.027

stratospheric abundances, while lightning would locally enhance abundances near the of strongest discharge activity. Finally, as shown in Fig. 4, the convectively-upwelled from the deep interior would be uniformly distributed throughout the troposphere, and the stratosphere. Consequently, while these species are more diagnostic of disequilibrium in general than just dynamical activity, the major tropospheric component is undoubtedly upwelling from Saturn's deep interior. Thus, a properly-designed experiment, as being here, will separate the effects of the various processes to quantify accurately the component desired for analysis of Saturn's deep circulation.

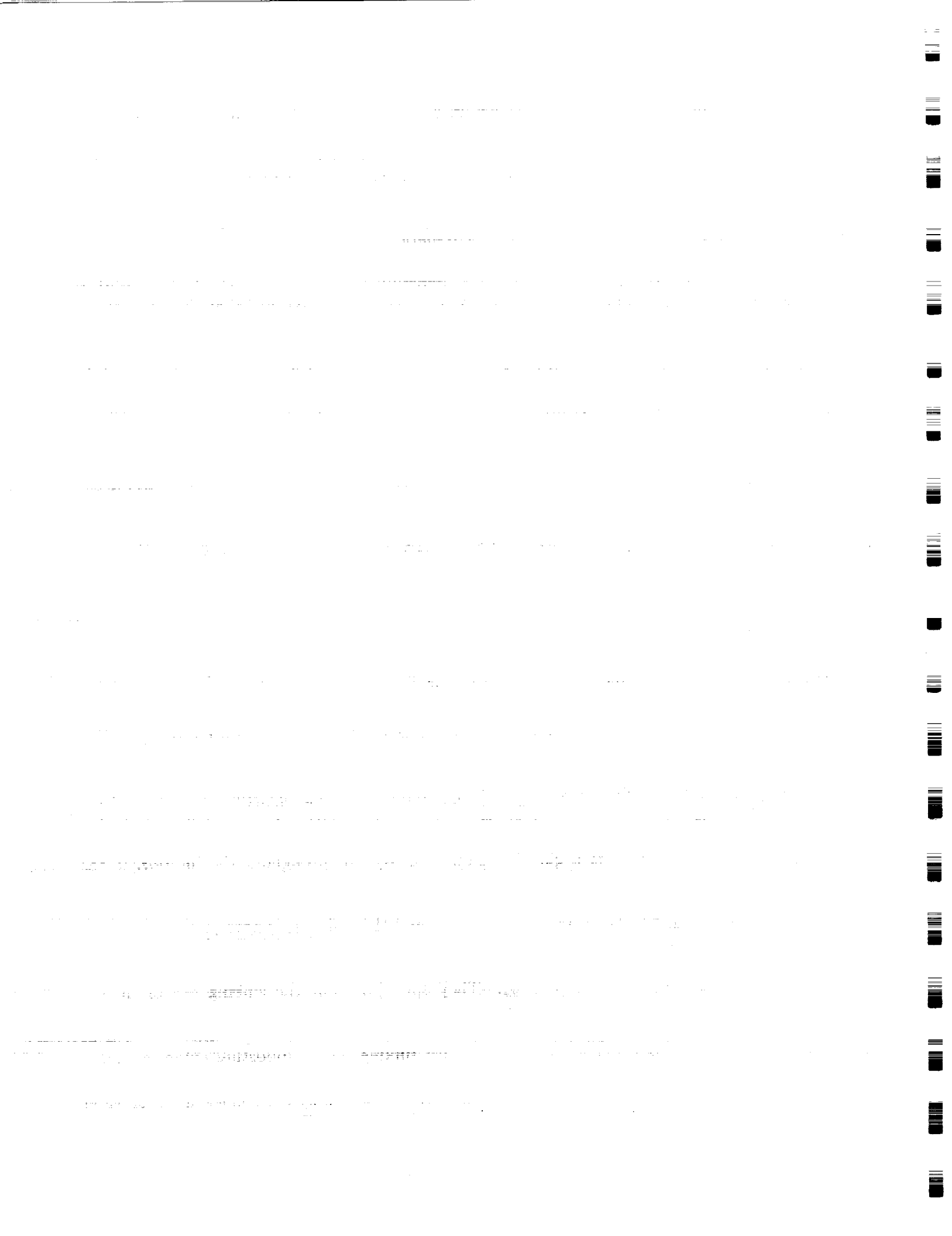
As an example of the power of disequilibrium species abundances to test theories of atmospheric circulation, the predicted latitudinal dependence of CO from the free theory of Flasar and Gierasch (1977) is shown in Fig. 5, where it is assumed that the K_{eddy} for Saturn is the same as that predicted by Flasar and Gierasch (1977) for Jupiter. Jupiter-based observations are not inconsistent with the theory, given the large error bars and the spatial region (essentially the visible disk) sampled. However, to test the predicted variation in CO, high spatial resolution (~ 400 km) observations are required, particularly at the equator where the expected CO abundance drops by a factor of two in 1 degree (1000 km).

These "dynamical tracers" can be used as well to constrain the depths of the basic convective structures. Upwellings which originate at relatively shallow depths above the atmospheric source of these tracers will incorporate the same trace gas abundances as their surroundings. However, as shown in Fig. 6, upwellings which originate deeper in the atmosphere than their surroundings may be enhanced in particular species. As depicted in Fig. 6, the probable pressure levels range from tens of bars for AsH_3 , several hundreds of bars for CH_4 , and several thousands of bars for CO.

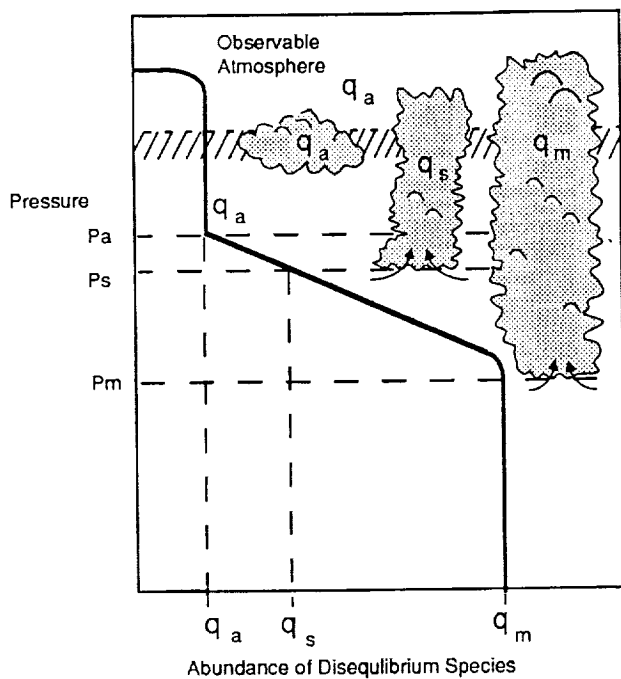
2.2.2 Tropospheric Meteorology

Despite the search for its infrared absorption signature, no observational evidence has been obtained yet for Saturn. This is not surprising, given the water condensation level is far below the reach of the 4-bar depth of the atmosphere accessible to near-infrared observations. Telluric water vapor absorption also renders the search quite difficult. The limited observations have been interpreted as an undersaturation of water vapor around 2 bars (Vandenberg *et al.*, 1984).

In the case of Jupiter, such a depletion of water vapor has been reported by Voyager and airborne investigations (Bjoraker 1985; Bjoraker *et al.*, 1986). As shown in Fig. 7, the measured jovian water vapor profile is well below the saturated profile up to the 4-bar level. If the suspected depletion reflects a global depletion of oxygen throughout the interior, it has profound implications for planetary formation processes. In particular, as shown by Prinn (1988b) for Jupiter this will be difficult to reconcile with generally accepted models of nebular chemistry and giant planet accretion. Lunine and Hunten (1987) have proposed that the apparent depletion of water reflects the nature of convective systems on Jupiter. If convection, driven by condensation of water, is restricted to narrow plumes, encompassing only 1% of the surface area of the disk (Fig. 8). They speculate that the sinking dry air in intervening regions between convective plumes dominates the $5\text{-}\mu\text{m}$ emission, and that the solar-composition water mixing ratio below the 6-bar condensation level is consistently less than 1% (at least 98% of the atmosphere being comprised of dry sinking air). Supporting evidence comes from Gierasch and Conrath (1985), who argue that narrow, high-velocity plumes are a direct response of the convecting troposphere to buoyancy effects induced by the condensation of water vapor.



FOLDOUT FRAME

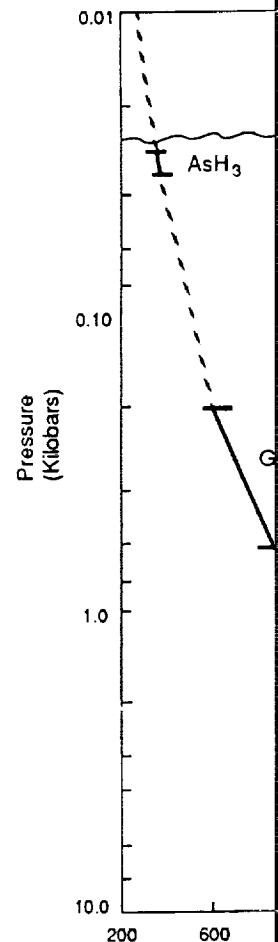


11070/357.026

Figure 6: Schematic of disequilibrium species abundance variations expected for various convective storm systems. Relatively quiescent atmosphere has abundance α_A as determined by large-scale (zonal or global) upwelling from depth P_a . Relatively shallow storm systems, with base pressure less than P_a , will have an abundance α_a as well. A deep-level storm system originating at a pressure $P_s > P_a$ will incorporate larger abundances due to the higher quench temperatures accessible to the dynamic storm system. Storms which originate deeper than a maximum pressure, P_m , will incorporate the "deep-mixed" equilibrium molar fraction. Some species, such as CO and HCN, vary to great depths (exceeding 20 kilobars, c.f. Fig. 1), allowing the depth of a storm system to be accessed over many tens of kilobars from the observed abundances in the < 4 bar region of the atmosphere.

Figure 7: Measurable pressure levels for localized storm systems from AsH_3 , GeH_4 , and CO abundance measurements by ACM. Each constituent yields a specific pressure regime over which pressure can be accurately determined (solid portion), with a typical precision of $\pm 10\%$. Dashed portions indicate regions in which pressure can only be crudely estimated as lying somewhere between the bounds of the solid curves. For each species, the minimum measurable pressure is here taken to be that dictated by the ground-based abundance measurements shown in Fig. 1. In general, these minimum pressures depend on the mean upwelling depth of the quiescent region surrounding the localized upwellings.

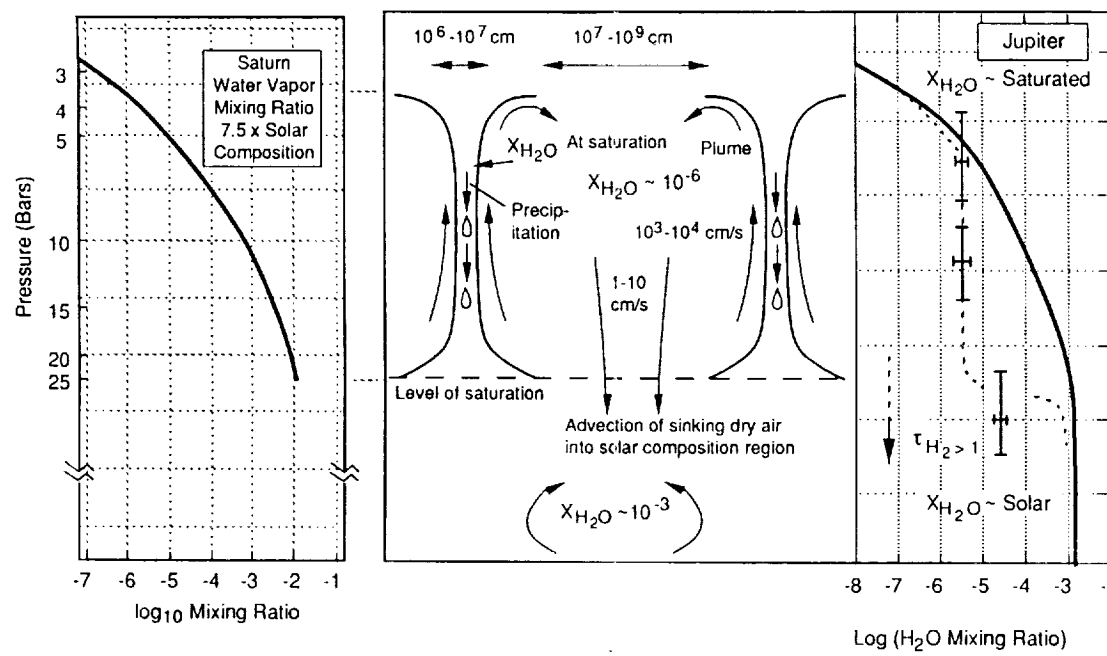
Figure 8: Lunine and... convection, adapted from... of water vapor in... tion of water observ... global saturation le... explained by conce... within broader reg... the saturated profi... out the rising air o... plied to the broad... tion of water in the... spatial resolution o... abundances at < 2 ... such upwelling and





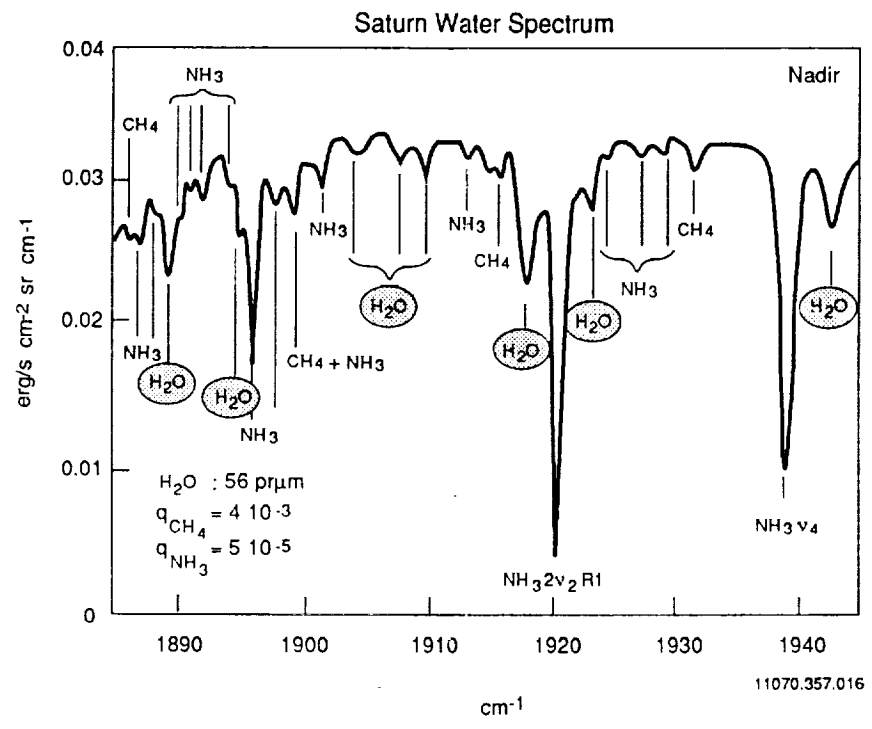


moist con-
abundance
rved deple-
) above the
anel, can be
e upwelling
lings follow
tation dries
s then sup-
ng a deple-
tions. High
btain water
ification of
turn.



11070.357.02

Cloud Base



11070.357.016

Figure 9: High-resolution (0.3 cm^{-1} apodized resolution) water, ammonia and methane spectrum near $5.2 \mu\text{m}$. This is a typical spectrum expected from ACM in Channel 1.

11070/357.024

A similar convective plume model may be plausible for Saturn as well, as it with the non-detection of water in the low spatial resolution observations thus far. An additional similarity is the presence of apparently enhanced localized regions of activity within a narrow latitude band, (39° N latitude vs the equatorial region on Jupiter). Spatial resolution near-infrared mapping in the $5\text{-}\mu\text{m}$ band (see Fig. 9) would test as the water vapor content of various plume regions - presumably incorporating the water vapor curve shown in the left-hand panel of Fig. 8 - would be measured against presumably much drier adjoining regions.

Such convective plumes could extend to the ammonia condensation region lying though the much smaller heat of condensation of ammonia compared to water means powerful convective cells are expected, resulting in less contrast between wet and dry. These differences should be measurable at $5\text{ }\mu\text{m}$, particularly in the strong $2\nu_2$ R1 ammonia band (see Fig. 9).

Another indicator of meteorological activity is the formation and dissipation of clouds. Observations of their vertical velocity, temporal variations in their areal extent and mass to elucidate thermodynamic processes which power them, and concurrently the surrounding environment. Observations of the equivalent widths of uniformly-distributed absorption gas features (e.g., CH_3D at $4.7\text{ }\mu\text{m}$) can reveal the convective velocity, while temporal and spatial mapping of the $5\text{-}\mu\text{m}$ flux emitted from the 4-bar level would elucidate higher-altitude variations in temperature and aerial extent.

2.2.3 Stratospheric Thermal Structure

Temperature profiles for Saturn's atmosphere are fundamental to the establishment of the structure of the atmosphere. There exists an information gap in the middle atmosphere where radio science, thermal infrared nor ultraviolet experiments are sensitive (Atreya *et al.*). Within less than 700 km in vertical extent, this gap extends from 1 mbar to $10\text{ }\mu\text{bar}$. Absorption measurements of C_2H_2 , CO, and PH_3 obtained via solar occultations provide the means to bridge this gap. The solar disk occulted by Saturn's atmosphere results in a spatial resolution of 300 km . Thus, many spectral samples across this region will easily be obtained, considering spacecraft motion of $5\text{-}6\text{ km/sec}$. The temperature is determined from the numerous lines of C_2H_2 and the spectral profiles of other species obtained simultaneously. To obtain spectral profiles can yield a temperature profile accurate to within 2 K .

Generally, temperature and abundances in the stratosphere are irretrievably covered by thermal infrared measurements of features seen in emission. On the other hand, solar occultation absorption measurements at $3\text{ and }5\text{ }\mu\text{m}$ provide a means of separating mixing ratios and temperature information, thus providing an essential datum required for the unambiguous interpretation of thermal infrared measurements of other species.

2.2.4 Stratospheric Photochemistry

Solar occultations provide an opportunity to seek new molecular absorption features in the stratosphere of Saturn. The chord representing the path of solar flux through Saturn's atmosphere will present an immense column density of gas so that species will, in effect, find their features enhanced by as much as $10\text{ - }100$ times in apparent strength. For spectral regions in the $5.2\text{-}\mu\text{m}$ band, where the spectral features are relatively sparse, spectral features of very low abundance species may become evident. For example, features due to isotopes which have features falling in the same bandpass may become detectable, leading to isotopic information. A similar effect is shown in Fig. 12 for a Titan occultation where, as the distance decreases, the features due to isotopes become easily measurable.

FOLDOUT FRAME

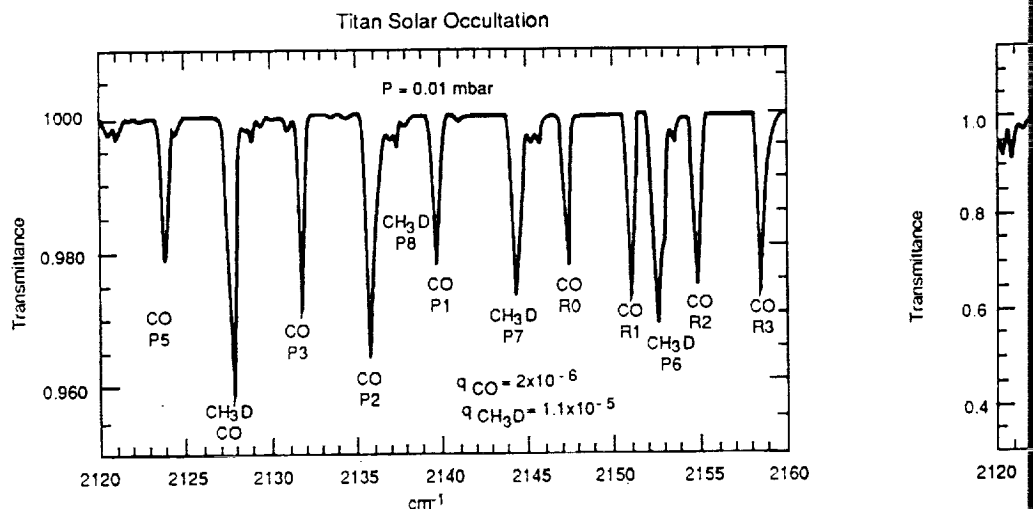


Figure 10: Model profiles for solar occultation profiles for Titan in the 4.7- μ m region. At 10 mbar, the strong CO and CH₃D lines are readily measurable 3-4 % and C and O isotopic features reach as much as five percent absorption depth and

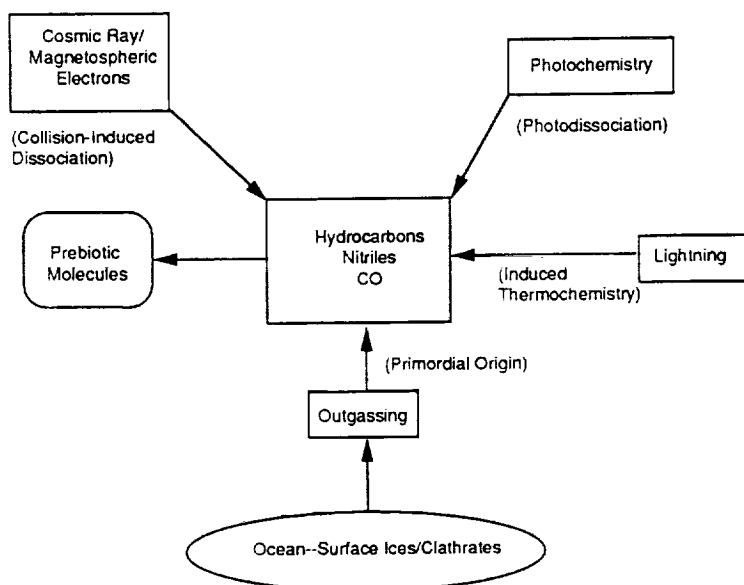


Figure 11: Schematic model for the ocean-atmosphere evolution due to methane photolysis (adapted from Lunine, 1985). Methane evaporated from the ocean is photolyzed in the stratosphere to form predominantly ethane, acetylene, and propane, with the escape of H₂. These products are indicated as hydrocarbons in the figure. The products condense and fall to the surface. N₂ is evolved from the ocean and is collisionally dissociated in the stratosphere and the nitrogen atom fragments enter the chemical cycle, producing nitriles which also condense and fall to the surface ultimately. The result of these processes is that methane is depleted and N₂ dominates the atmosphere even further, altering the radiative balance.

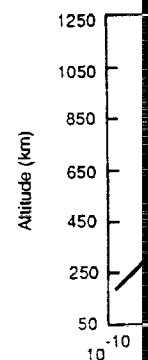
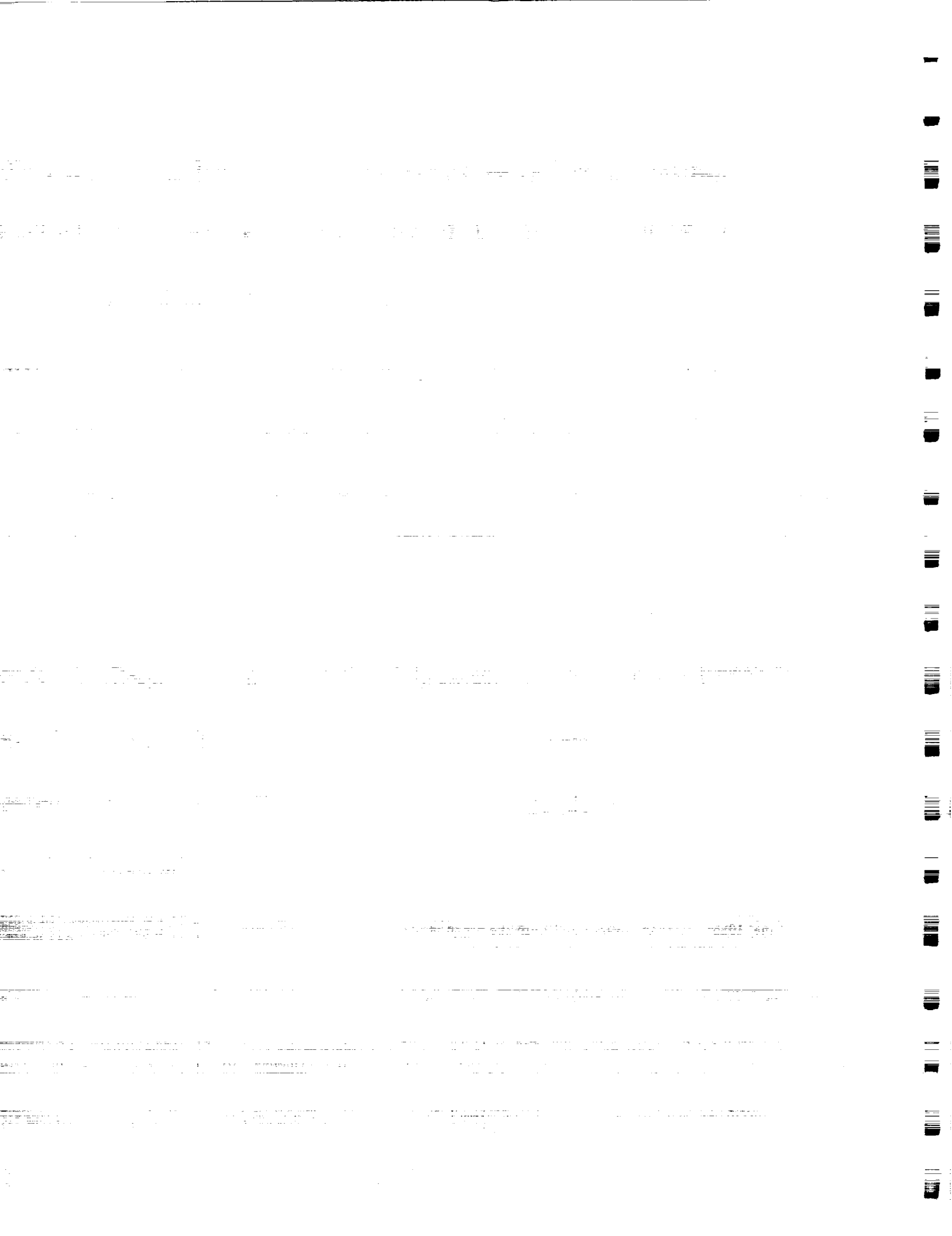
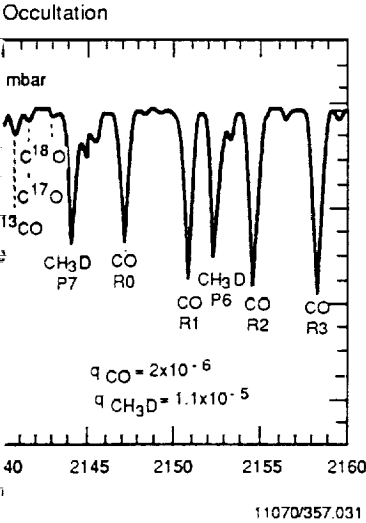
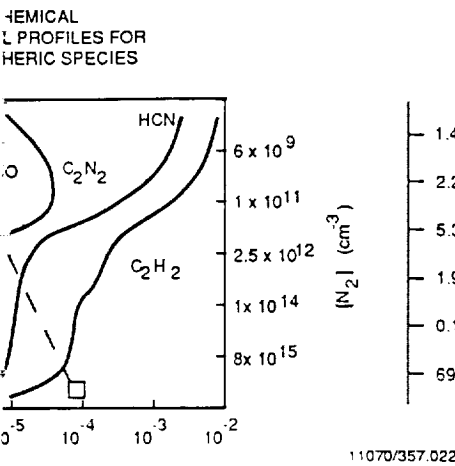


Figure 13: Synthetic Saturnian-to-noise ratios. (a). "H₂O" channel. (b). The Fourier transform is 25. (c). The Fourier transform is 100. (d). As in (b) but with a ratio (100), even minor features are visible.



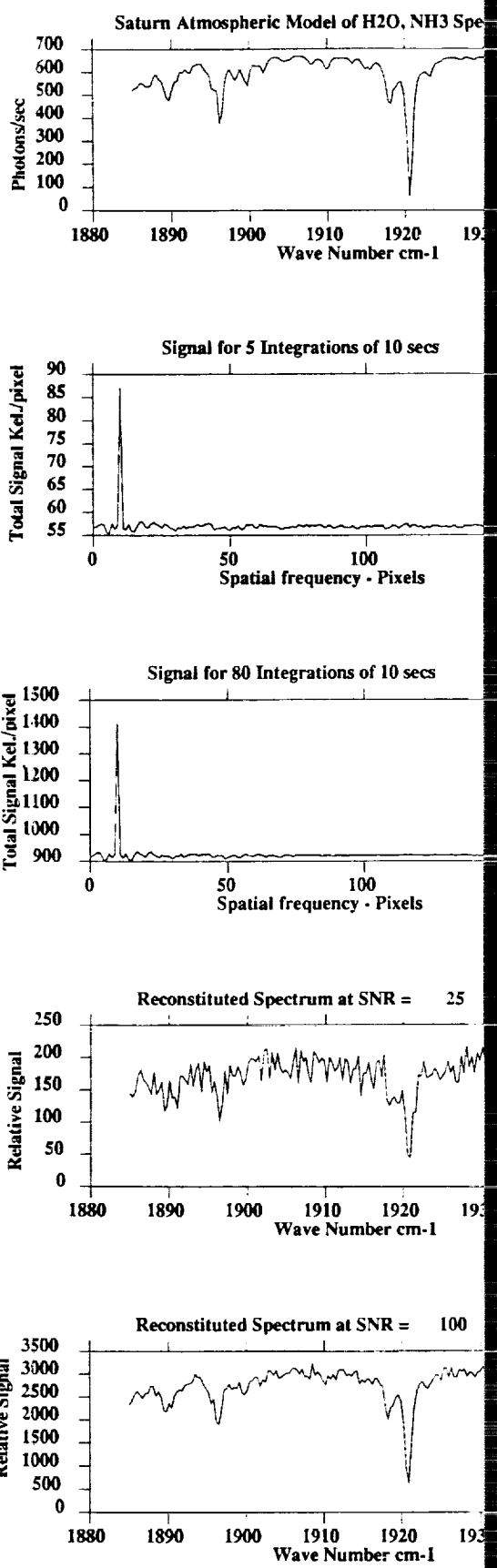


se ratio of
mbar, the



ratios of selected species
nd Gautier,1985). The oc-
1 Fig. 12 are derived from
. The CO profile is taken
s (Lutz *et al.*,1983, Muhle-
derived from models.

terferogram and the resulting observational data for two sig-
responding to the dayside observation of Saturn by ACM in
1g from (a) with noise corresponding to a 50-second integration.
pectrum as observed by ACM. Signal-to-noise ratio in the spec-
ion. (e). The Fourier transform of (d). At this signal-to-noise
recovered from the interferogram.



2.2.5 Formation/Evolution

Water is expected to be the third most abundant gas in Saturn's atmosphere on the solar abundance of oxygen ($O/H \sim 1.4 \times 10^{-3}$), as well as its presence within rings and satellites. Moreover, recent theories of planetary formation, including the of planetesimals scenario of Pollack *et al.*, (1986), predicts an enhancement of water compared to the solar abundance. This particular theory has been found to be consistent with observed enhancements of methane in Uranus and Neptune (Baines and Smith, 1990). Earlier, a depletion of water in Saturn then would greatly impact current theories of formation and evolution.

The D/H ratio of Saturn may reflect chemical fractionation within the atmosphere at the time of its formation as well as the primordial D/H ratio. The initial D/H abundance depends on the D/H ratio within the icy component of the solar nebulae, which is probably isotopically enriched (Hubbard and MacFarlane, 1980). Thus the observed D/H ratio is an indicator of the magnitude of the icy component originally incorporated in Saturn.

Phosphorus, germanium, and arsenic are the heaviest elements thus far observed in Saturn's atmosphere. Accurate determinations of their abundances would improve understanding of the composition of Saturn. Thus far, accurate determinations of elemental abundances from the analysis of disequilibrium species has been hampered by uncertainties in modeling the sunlit atmosphere. High-resolution $5\text{-}\mu\text{m}$ spectral observations of Saturn's nightside, illuminated by scattered sunlight, would significantly improve constraints on the nonvolatile composition of Saturn.

2.3 Titan Atmospheric Processes

2.3.1 Chemical Evolution and Methane Depletion

Titan's unique aspect is its massive, chemically-evolving atmosphere comprised of a mixture of hydrocarbons, nitriles, and inorganic species. In recent years, a scenario for the evolution of Titan's atmosphere, based on this complex mixture, as depicted in Figure 2.3.1.

Methane is released from Titan's inventory of volatile materials (Lunine, 1985) either from the surface ices or clathrates or from the putative ethane/methane/nitrogen ocean. Methane is photodissociated to yield hydrocarbon radicals that initiate a hydrocarbon chemistry leading to the formation of complex hydrocarbon species, such as C_2H_2 . Alternatively, the free radicals may react to form nitriles with the active nitrogen atoms formed via the dissociation of outgassed N_2 by magnetospheric electrons. Then, even more complex chemical species, referred to as "prebiotic" molecules in speculative discussions, may be synthesized. This coupled set of reactions, initiated high in Titan's stratosphere, then, yields the molecules that may have accumulated on the surface or dissolved in the oceans of Titan over geologic time. The formation of the complex chemical species from the reactive fragments of the dissociated CH_4 molecules are key components in modeling the eventual depletion of methane from the ocean. The depletion of the methane inventory heralds the time when the ability to maintain its methane-rich, cloudy, potentially "prebiotic" atmosphere is terminated. Further modeling of these processes can become possible when the vertical mixing coefficient is determined for HCN, C_2H_2 , C_2H_4 , C_2H_6 , and C_2N_2 .

A specific example of the mechanisms which eventually produce the chemical composition of the surface is found in the most abundant gas in Titan's atmosphere, N_2 . N_2 dissociates into atomic nitrogen ($N(^4S)$), primarily via collisions with magnetospheric electrons precipitated into the atmosphere. A series of reactions (Strobel, D.F., 1985, Yung, Y. L. *et al.*, 1984) form in the stratosphere followed by transport to the lower atmosphere and subsequent reaction

other observed nitrile species. Alternative explanations involving radiolysis-dominated syntheses of HCN and other complex molecular species have been offered by Thompson *et al.*, (1990).

Fig. 11 plots theoretical mixing ratios for nitriles and hydrocarbons that are formed subsequent to charged particle collisional dissociation of N_2 and photodissociation of CH_4 . The nitriles and hydrocarbons have a profound effect on the nature of the surface and ocean of Titan by accumulating irreversibly on the surface and increasingly concentrating in the ocean. The variations of the mixing ratios with altitude are very large for many of these species. The mixing ratio of HCN, for example, may vary by over three orders of magnitude over a range of 1000 km in altitude. These predictions are not yet quantitative, requiring a presently unavailable input of vertical distribution profiles and latitudinal and longitudinal variations to permit quantitative modeling. The quantitative interpretation of the entire vertical transport process depends upon acquiring an accurate knowledge of the vertical profiles for these species.

One of the most stable of chemical species, CO, may arise from Titan's surface by release from ices/clathrates, through lightning-induced thermochemistry, and meteoritic infall, or a combination of these processes. Like N_2 , CO should be evenly mixed up to the diffusive separation region and can then be efficiently dissociated by collisions with magnetospheric electrons. However, recent evidence implies that CO is not evenly mixed in Titan's atmosphere. The CO mixing ratio is reported to be 7×10^{-5} in the lower atmosphere of Titan (Lutz, *et al.*, 1983), while Muhleman *et al.*, (1984) determined an upper atmosphere mixing ratio near 10^{-6} . Under the assumption that both measurements are accurate, the measured variable mixing ratio for CO is an unresolved puzzle. The key measurement, then, is the determination of the vertical mixing ratio profile for CO, as may be accomplished near Titan via a high spectral resolution occultation measurement. The CO spectral profiles, shown in Fig. 12, would provide the data to derive vertical mixing ratio profiles for quantitative models of the reaction sequence.

Associated with the CO puzzle is the detection of CO_2 by Voyager IRIS. CO_2 is clearly present at the equatorial limb but undetectable at the north polar limb. The most plausible scenario for the formation of CO_2 is the reaction $CO + OH \rightarrow CO_2 + H$, where the OH is formed from photodissociated water.

While H_2O has not been detected in Titan's atmosphere, its presence is expected on the basis of meteoritic infall. In this picture, the photolysis of H_2O in the upper atmosphere provides the source of the oxygen needed to form the observed concentrations of CO and CO_2 (Yung *et al.*, 1984). The detection of H_2O in the upper atmosphere of Titan would elucidate the atmospheric chemistry of oxygen in Titan (Gautier, 1985) and is marginally feasible for ACM.

2.3.2 Formation/Evolution

Isotopic enhancement by chemical fractionation is effective at low temperatures i.e., in primordial sources, while high temperature processes tend to homogenize the isotopic distributions i.e., thermochemistry. Investigations which provide isotopic ratios can provide a direct determination of the sources for CO, HCN, and the other detectable atmospheric molecules. In Fig. 12, profiles computed at 0.01 mbar and 5 mbar for Titan/solar occultations clearly demonstrate the great sensitivity for the isotopes of oxygen and carbon. The abundant isotopes are measured at higher altitudes while the lesser abundant isotopes emerge as the altitude decreases. Isotopic signatures not observed at $4.7 \mu m$ can then differentiate between a primordial (Prinn and Fegley, 1981) and a thermochemical origin (Yung *et al.*, 1984).

2.3.3 Detection of Aerosols/New Species

The $5.2\text{-}\mu m$ region of the spectrum has essentially no absorption for the known Titan molecular species. Hence that channel is very sensitive to aerosol opacity and very low abundance molecules due to the long path lengths attainable during occultations.

2.3.4 Distribution of Oceans on Titan

Spatial information on the locations of oceans is obtained directly by seeking the enhanced abundances over the oceans compared with the dry air over continental masses. The measurement of ethane, the primary ocean fluid (Lunine, 1985) may be accomplished in both the 5.2- μm band reflected spectrum where strong C_2H_6 spectral bands lie.

2.3.5 Clouds and Aerosol Distributions

Voyager observation of Titan clearly showed the presence of detached atmospheric features. Opacities measured in the visible by Voyager imply that 5- μm photons will sample the atmosphere below 100 km. Titan's cloud structure appears to consist of three basic components: a stratospheric photochemical aerosol between 40 and 150 km, a mixture of condensed hydrocarbons and nitriles between 50 and 80 km, and methane clouds between 10 and 35 km (Samuelson, 1985). Recent models based on Voyager data (Toon *et al.*, 1988) predict a liquid CH_4 condensation cloud in the upper troposphere which is cumulus-like in nature and composed of large particles. This cloud should be inhomogeneously distributed in the troposphere, analogous to terrestrial cumulus clouds in the presence of any circulation system in the first few kilometers above the surface.

Understanding the characteristics of these clouds is important for providing clues to the climate (along with Huygens Probe results). Samuelson (1985) reports the identification of HC_3N condensates in Titan's atmosphere. The vertical and horizontal distribution of these species are important considerations in determining the deposition of solar energy in the atmosphere. By virtue of this effect, they may exert considerable control over Titan's meteorology, much as H_2O clouds do in the terrestrial atmosphere.

2.3.6 Atmospheric Circulation and Dynamics

Methane controls much of the radiative heating and cooling of Titan's atmosphere. Seasonal and temporal variability in the stratosphere may be modulated to an unknown extent by seasonally driven variations of the tropopause temperature, which defines the saturation vapor pressure and concentration in the stratosphere. Verifying this variability, together with information on the location of the local temperature minimum, will determine quantitatively the role of meridional transport in the seasonally driven stratospheric circulation system. The abundance of CH_4 in the troposphere and its meridional and zonal variability will also determine whether it is inhomogeneously distributed (i.e. in "lakes" of liquid C_2H_2 - CH_4 mixtures) or more globally distributed, and it will place bounds on the efficiency of horizontal tropospheric transport (e.g. if CH_4 abundance is found to be uniform, but the source material at and below the surface is not).

Acetylene and ethane are the most abundant of the photochemical products of methane. The distribution of these species is a fundamental problem, since the formation of more complex species depends on the reaction mechanisms of the C_2 species. As the most predominant of the hydrocarbons, their vertical and meridional distribution will be keys to the proper characterization of Titan's photochemistry and transport.

The most abundant and primitive of all the nitriles observed in Titan's atmosphere is hydrogen cyanide, the precursor to the formation of all other important nitrile species, as discussed above. IRIS data clearly show that nitriles were far more abundant near the north polar region than at the equator. This may be explained, in the context of a concentration of unsaturated hydrocarbons at the poles, as an effect of the solstice polar night preceeding the Voyager encounter. Future observations with ACM at a different season will determine whether this model is correct. The data will reveal the time scales relevant to chemical production rates of various segments of the atmosphere involving nitrogen.

2.4 Saturn's Rings

The stability of the ring system over the age of the solar system has been taken as an obvious fact derived from their existence. This has, however, lately been called into question, and processes which should be acting to modify the rings have been discussed eg. in Morfill *et al.* (1983) and Northrup and Connerney (1987), who show that the expected age of the rings against meteorite bombardment depletion is less than 100 myr. Collisions with other ring particles will increase the number of smaller particles over time, unless processes are acting to remove them.

The radial variation of ring particle composition and size is not well known. Although radio occultation data from Voyager show that several regions in the ring system have similar size distributions for cm and greater particle sizes, significant radial variations may exist in ring particle size distributions within the constraints of current data. Cuzzi *et al.* (1980) have shown that a broad inverse-third power size distribution is expected from ring reflectivity and emissivity observations, and Marouf *et al.* (1983) have confirmed this for large particles. A large component of small particles is evident in Voyager images at large phase angles (Smith *et al.*, 1982).

Observations of size and compositional distribution for small particles will lead to further understanding of ring formation and evolution. ACM observations of the rings in transmission, obtained during solar occultations, can be combined with High Speed Photometer visible and ultraviolet data to determine the distribution, abundance, and scattering properties of micrometer-sized ring particles. This will lead to a determination of radial variations in these parameters, with implications for ring evolution and particle migration.

If the meteorite bombardment scenario is correct, the rings are a very dynamic system and neutral gas emission is predicted to be as high as 10^9 molecules $\text{cm}^{-2} \text{sec}^{-1}$ (Connerney and Waite, 1984). Erosion of the rings has been related to observations of CO in the atmosphere of Saturn and to the ultraviolet observations of the hydrogen torus surrounding the ring and satellite orbits (Broadfoot, 1981). Observations which can identify the signatures of an evolving ring are needed to investigate these issues. For water absorption features in solar occultation mode, ACM has a minimum-detectable column density of 10^{15-16} molecules cm^{-2} , or one-two orders of magnitude above the expected column density but within the uncertainties of water production and distribution.

2.5 Summary

ACM directly supports the following Science Objectives listed in the Saturn Orbiter Announcement of Opportunity:

Titan:

Determine abundances of atmospheric constituents, establish isotope ratios for abundant elements, constrain scenarios of formation and evolution of Titan and its atmosphere.

Observe vertical and horizontal distributions of trace gases, search for more complex organic molecules, investigate energy sources for atmospheric chemistry, model the photochemistry of the stratosphere.

Measure winds and global temperatures, investigate cloud physics, general circulation, and seasonal effects in Titan's atmosphere.

Saturn:

Determine temperature field, cloud properties, and atmospheric composition.

Observe synoptic cloud features and processes.

Infer the internal structure and rotation of the deep atmosphere.

Provide observational constraints (gas composition, isotope ratios, heat flux) on scenarios for the formation and evolution of Saturn.

Measure temperatures above the 1-mbar level.

Rings:

Study configuration of the rings and dynamical processes responsible for ring structure.
Map composition and size distribution of ring material.

Jupiter Flyby:

Extend the time for studies of atmospheric dynamics beyond the period accessible to the Galileo nominal mission.

Infer global composition with instrumentation not carried by the Galileo Orbiter, combining the local *in situ* measurements of the Galileo probe.

3 ANTICIPATED RESULTS

3.1 Results Anticipated

Specific results anticipated from the Atmospheric Chemistry Mapper include:

- For Saturn:

1. Depth of vertical transport over latitude and the associated deep-atmospheric processes.
2. The spatial distributions, depths, lifetimes and strengths of localized convective systems.
3. Low vertical-resolution thermal profiles in the "information gap" above the troposphere.
4. Abundances of minor constituents useful in the interpretation of disequilibrium species, planetary origin, formation, and evolution scenarios, including H_2 , AsH_3 , GeH_4 , PH_3 , CH_3D , and NH_3 .

- For Titan:

1. Vertical mixing ratio profiles, at $\sim 1/6$ scale height resolution of chemically active species (CO , HCN , C_2H_2 , C_2H_4 , C_2H_6 , CH_3D , C_2N_2) from 0.01 to 10 mbar.
2. Vertical temperature profiles at $\sim 1/6$ scale height from 0.01 to 10 mbar.
3. Abundances of minor constituents useful in the interpretation of planetary origin, including C^{17}O , C^{18}O , $\text{C}^{12}\text{C}^{13}\text{H}_2$, ^{13}CO , CH_3D .

- For Saturn's Rings:

1. 3-5 μm IR radial profile of optical thickness and composition.
2. Detection or upper limit determination of neutral H_2O in ring system.

3.2 Scientific Context

The attainment of ACM's primary scientific objectives - to understand various physical and dynamical processes in Saturn's and Titan's atmosphere - anticipates specific measurements and results.

Investigations of Saturn's deep atmospheric processes is based on a measurement of the meridional variation of depth of vertical transport processes by specifying the variation of atmospheric K_{eddy} coefficients as determined from measurements of the tropospheric profiles of disequilibrium species, primarily CO and HCN . Meteorology anticipates coupled processes by specifying spatio-temporal dependences that reflect energetics, lifetimes, and vertical transport in convective systems. Stratospheric thermal structure is defined by vertically resolved temperature profiles. The above investigations are brought into perspective by the unifying scientific theme of Saturnian atmospheric processes. These processes undergo transitions

and importance as attention is focussed from the deep atmosphere to the stratosphere to emphasize the continuity of the atmosphere.

Similarly, Titan's atmospheric processes unify photochemistry, circulation and dynamics with the determination of the sources of observed atmospheric species. Vertical profiling of temporal distributions of photochemical species are anticipated results that reflect the nature of Titan's atmosphere and determine the sources of the measured components. The distribution of hazes, observed through occultations and the motions of clouds and hazes in reflected light, couple circulation and dynamics to photochemical processing.

Measurements of ring particle size distributions and compositional inhomogeneities are necessary to study the formation and dynamical evolution of the rings. Observation of neutrons in the ring region is needed to establish the erosion rate of the rings due to meteoroid bombardment.

Investigations of Saturn and Titan's formation and evolution investigations utilizing minor photochemical and/or isotopically differentiated constituents, specifically predictions of atomic abundances and isotopic ratios.

4 APPROACH

4.1 Introduction

As summarized in the ACM overview (Table 2), the science goals and expected results in the preceding Sections lead naturally to the requirement for spatially resolved molecular absorptions at about $0.30 - 0.40 \text{ cm}^{-1}$ spectral resolution. Three channels, covering $0.30 - 0.40 \text{ cm}^{-1}$ each, are required, centered near 3.0 , 4.7 , and $5.2 \text{ }\mu\text{m}$. ACM allows observation of the Saturn condensable H_2O and NH_3 (for meteorology and planetary formation), disequilibrium trace gases CO , HCN , PH_3 , GeH_4 , AsH_3 , (for deep atmospheric circulation and additional planetary formation studies), the hydrocarbons C_2H_2 , C_2H_6 , CH_4 , C_2H_4 , and the nitriles HCN and C_2N_2 (for studies of Titan's complex chemistry), and CH_3I isotopes of C and O for planetary formation and evolution studies.

4.2 Instrument Approach

4.2.1 Wavelength Sampling Requirements

The infrared spectrum beyond $2\text{ }\mu\text{m}$ contains strong fundamental transitions for trace gases present in the atmospheres of Saturn and Titan. High spectral resolution is required to resolve the individual molecular lines in relatively crowded spectral regions.

Near $5 \text{ }\mu\text{m}$, the low absorption cross-sections of the abundant gases in the atmosphere of Saturn produce a "spectral window" into the troposphere to detect thermochemical disequilibrium trace gases originating from deep within Saturn's atmosphere. Spectral observations in this window are an essential feature of the science goals established above.

Fig. 14 shows that the spectral region near $4.7 \text{ }\mu\text{m}$ contains numerous spectral features for various disequilibrium species desired for investigation. This circumstance points to the choice of spectral range which enables all the desired species to be observed simultaneously. A similar choice is made for the 3.0 and the $5.2\text{-}\mu\text{m}$ intervals.

The spectral resolution must be sufficient to separate individual lines throughout the troposphere and troposphere, and to resolve tropospheric water and CO lines in Saturn. In the hydrocarbon bands near $3.0 \text{ }\mu\text{m}$, as well as in the rich disequilibrium species window near $4.7 \text{ }\mu\text{m}$, this requirement leads to a 0.3 cm^{-1} spectral resolution. The $5.2\text{-}\mu$ region is less crowded and predominantly samples condensable species (H_2O and NH_3) below the 1 bar level in Saturn. In this region the spectral resolution is relaxed to 0.40 cm^{-1} sampling.

ACM's spectral characteristics are summarized below in Table 3. A compendium

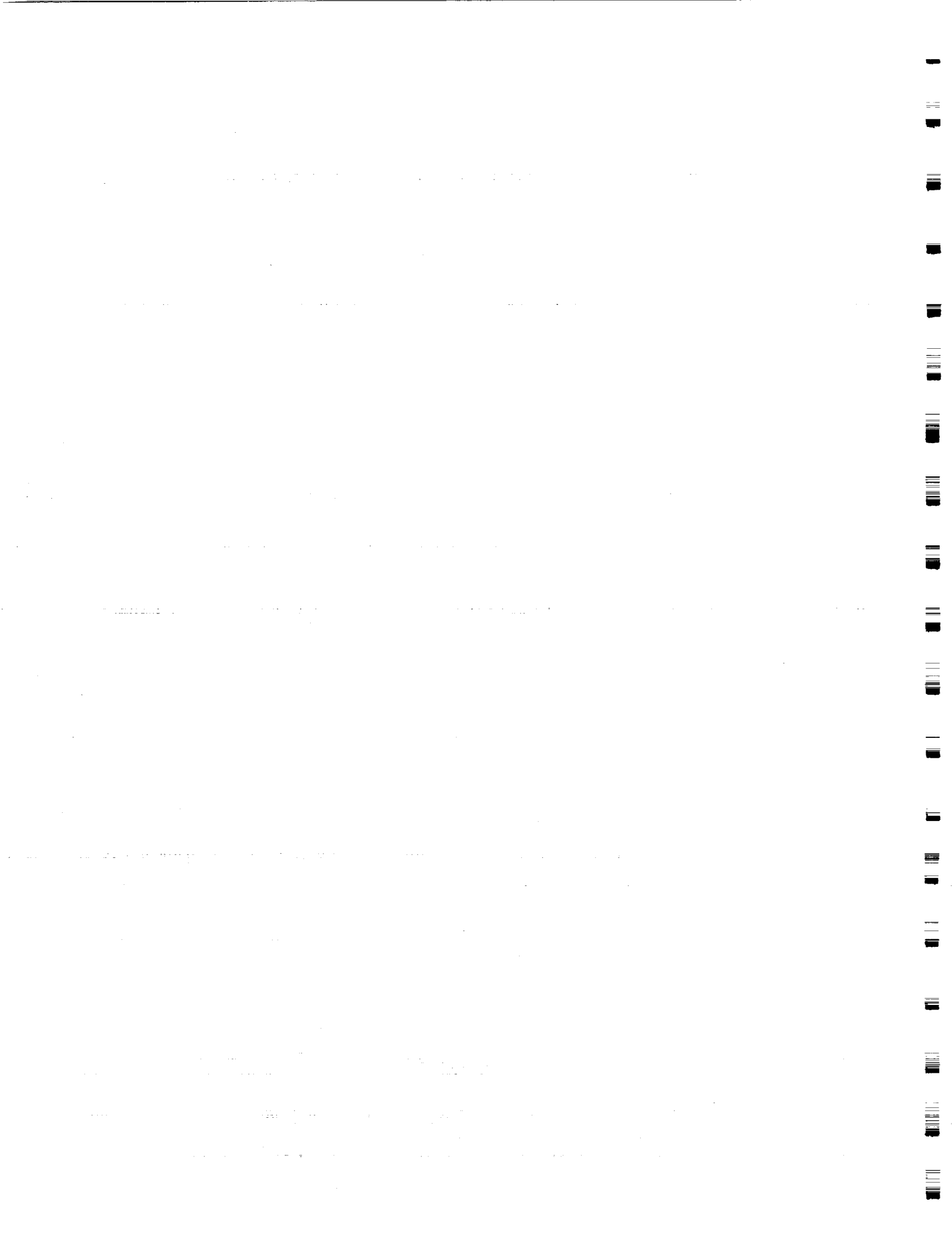
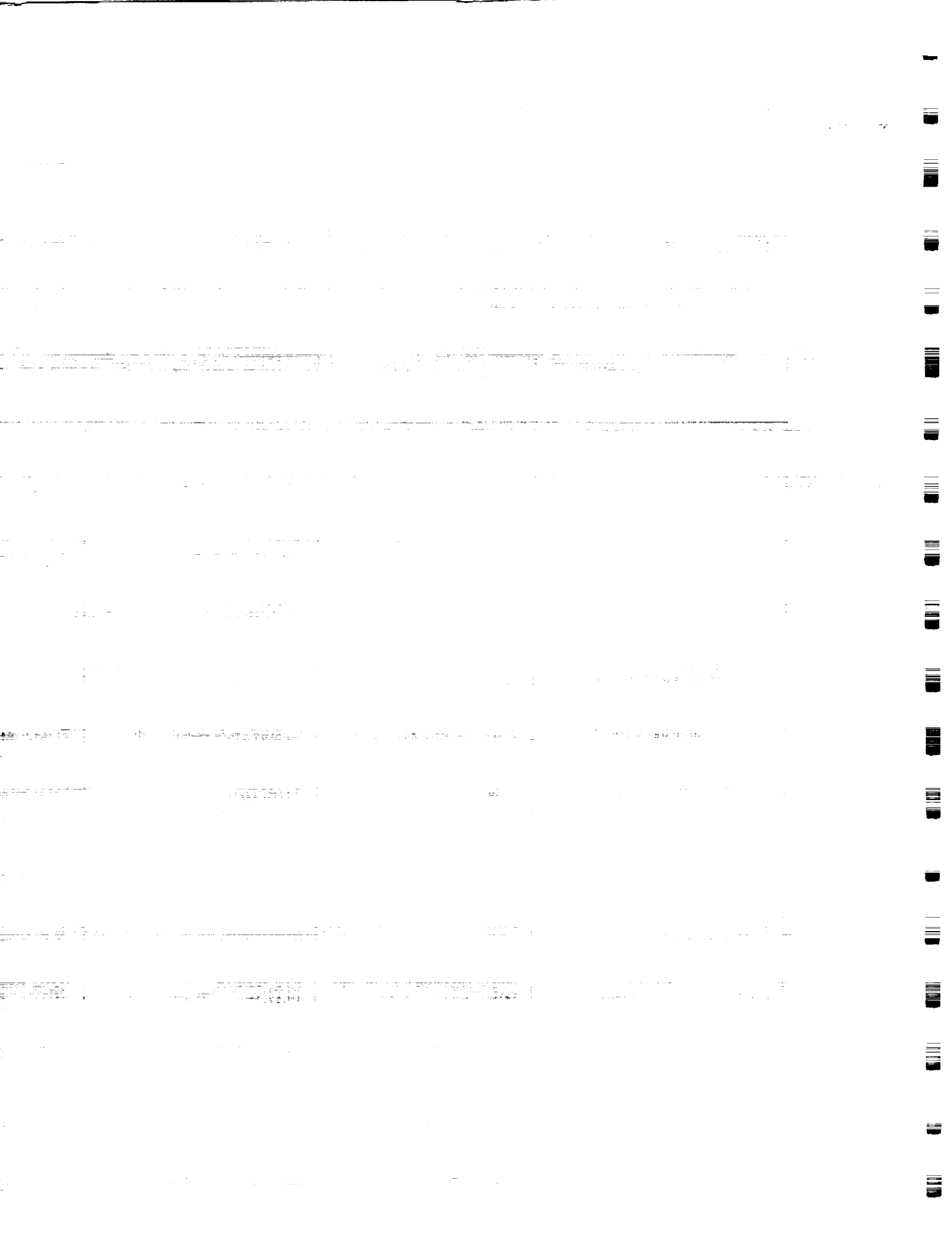


Table 2: ACM SCIENCE, MEASUREMENT OBJECTIVES AND REQUIREMENTS OVERVIEW. The "roadmap" may be utilized to follow ACM's approach to the study of Titan. The first column at the left to locate a step-by-step listing of ACM's measurements, approach, and its role in the elucidation of photochemical processes in Saturn or Titan may be determined by entries containing CO. Then, the rows with CO entries will relate the science goals, where ACM science are specified in the final column.

SCIENCE OBJECTIVES Processes in the Saturnian System	SCIENCE GOALS Broadbrush Anticipated Results	OBJECTIVES
		Specific Anticipated Results
1. Saturn Atmospheric Processes A. Circulation/Dynamics 1. Deep Atmosphere 2. Meteorology B. Stratospheric Structure 1. Thermal Structure 2. Photochemistry	Depth of vertical transport over latitude Spatial distribution, depth, lifetime, strength of localized convective storm systems Thermal profiles Trace chemical constituents	Latitudinal variations in atmospheric K _{eddy} 1. Spatial/temporal of H ₂ O/NH ₃ vapor ratios 2. Depth of convection over time 3. Lower/NH ₃ variations over latitude, time 4. Cloud "patchiness" over time Temperatures in the "ion gap region" and Identify trace constituents
2. Planetary origin, Formation/Evolution	Composition: Abundances of minor constituents, isotopic ratio	C/H, O/H, N/H, Ge/H, D/H
3. Titan Atmospheric Processes A. Photochemistry B. Circulation /Dynamics	1. Vertical profiles of temperatures and chemically active species 2. Spatial/temporal distributions of chemically active species Latitudinal winds at CH ₄ cloud level	CO, HCN, C ₂ H ₂ , C ₄ H ₂ , CH ₃ D as a function of latitude + time CO, HCN, C ₂ H ₂ , function of latitude Zonal wind field
4. Titan formation /evolution	Composition: Abundances of minor constituents, isotopic ratio	D/H, ^{12,13} C, ^{16,17,18} O
5. Ring Origin & Evolution	Radial distribution/ particle sizes <5μm	τ at 3.0μm and 5.0μm





2.

FOLDOUT FRAME

oadmap" to relate ACM science goals to the observational Saturn, for example, by looking down the "science goals" nt to Saturn's atmospheric dynamics. Similarly, CO and "Approach" and then "Measurements" and follow down y a role. The numerous measurements that are unique to

MEASUREMENT APPROACH		REQUIREMENTS	UNIQUE ASPECT
Measurement	Technique		
of disequilibrium as function of latitude (HCN)	3 + 5μm, high spectral/spatial resolution nadir mapping day-side/night-side	Two Channels, ("CO", "3μm"); 1000km spatial resolution	Disequilibrium species (HCN)
CH ₃ D, CH ₄ in troposphere as a function of latitude, time	5μm, high spectral/spatial resolution, nadir and limb mapping, dayside/night-side	Two channels ("H ₂ O", "CO"); ~500km spatial resolution	H ₂ O
in troposphere as a function of latitude, longitude, time	3+5μm, high spectral/spatial resolution, nadir and limb mapping, dayside/night-side	Two channels ("CO", "3μm"); ~500km spatial resolution	CO, HCN
bottom cloud	5μm, high spectral/spatial resolution, nadir and limb mapping, dayside/night-side	One channel, ("CO")	CH ₃ D absorption map
CH ₄ hot band	3 + 5μm high spectral/spatial resolution, nadir dayside/night-side	Three channels, ("H ₂ O", "CO", "3μm"); ~500km spatial resolution	
equal 1-16 line absorption (HCN)	3μm, high spectral resolution, solar occultations	One channel (3μm); ~300km vertical resolution	C ₂ H ₂ ν ₃ absorption photometry in solar occultations
constituents	3 + 5μm high spectral/spatial resolution, solar occultations	Three channels ("CO", "H ₂ O", "3μm"),	High spectral resolution solar occultations
um & volatile condense deep atmosphere. weak constituents,	5μm, high spectral resolution nadir mapping, darkside and solar occultations.	Two channels ("CO", "H ₂ O"), 0.2 cm ⁻¹ sampling	H ₂ O, CO, GeH ₄ , AsH ₃
tion vertical profiles stratosphere	3 + 5μm high spectral resolution, solar occultations	Two channels ("CO", "3μm"); ~5km vertical resolution (~1/6 scale height)	High vertical resolution C ₂ H ₂ , CO, HCN profiles from solar occultations
es derived from the absorptions, CO abundances of desired	3+5μm mapping	Two channels ("CO", "3μm"); ~100km resolution	CO, HCN maps
patchy clouds	3+5μm mapping	Two channels ("H ₂ O", "3μm"); ~30km resolution	Large spatial coverage high spatial resolution
s pe,	5μm high spectral resolution, solar occultations.	One channel ("CO"), 0.2 cm ⁻¹ sampling	16,17,18O
action profile	Solar occultations, mapping	All channels, <50km resolution	

Table 2: Summary of ACM Scientific Objectives, Anticipated Results and Approach.

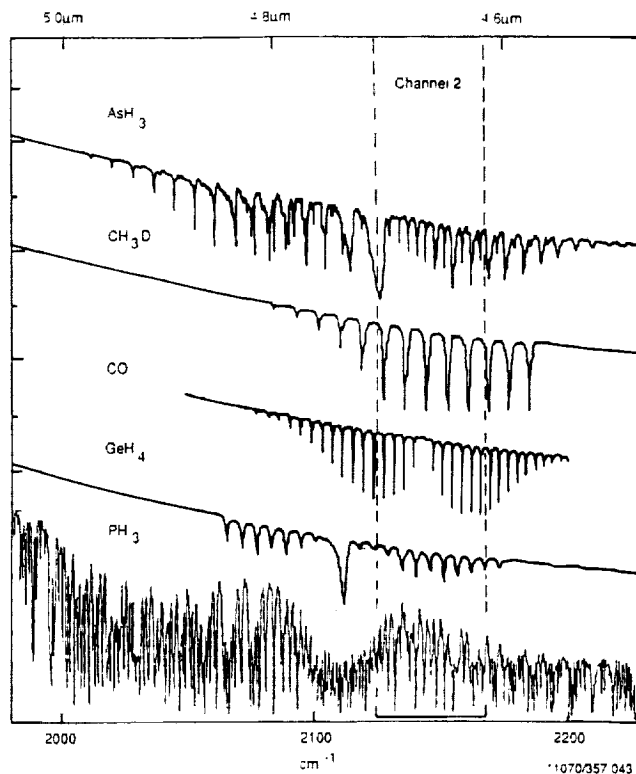


Figure 14: 4.7- μm spectra of important species in Saturn. Phosphine (PH_3) is the primary absorber in the 5- μm methane window. Channel 2 is selected where PH_3 absorption is relatively weak within the region of prominent spectral signatures of the disequilibrium constituents arsine (AsH_3), germane, (GeH_4), and carbon monoxide (CO).

Table 3: Summary of Selected Channels.

Channel	Name	Spectral Range		Spectral Resolution cm^{-1}	Principal Observed Species
		cm^{-1}	μm		
1	H_2O	1885-1940	5.15-5.31	0.40	$\text{H}_2\text{O}, \text{NH}_3, \text{CH}_4, \text{C}_3\text{H}_8$
2	CO	2123-2168	4.61-4.71	0.30	$\text{CO}, \text{CO isotopes}, \text{PH}_3$ $\text{GeH}_4, \text{AsH}_3$ $\text{CH}_3\text{D}, \text{C}_2\text{N}_2$
3	C_2H_2	3255-3300	3.03-3.07	0.30	$\text{C}_2\text{H}_2, \text{C}_2\text{H}_6, \text{HCN}$

spectral lines for Saturn and Titan is shown in Table 4. These features are displayed in modeled spectra for Saturn and Titan in Figs. 9, 15, and 16.

4.2.2 Spatial Sampling Requirements

IFOV: To observe atmospheric features at ~ 1000 km resolution on Saturn, i.e., approximately the size of convective storm systems observed by Voyager, requires a maximum instantaneous field-of-view (IFOV) for Nyquist spatial sampling (two pixels per spatial resolution element) of 2.8 milliradians at $3 R_S$. In order to map the planet over a few Saturn rotations requires 1000 km resolution at $5 R_S$, i.e., 1.7 milliradians.

The desire for resolved limb views at a specific viewing angle for center-to-limb measurements (4.4.3) argues for a pixel size of about 0.5 milliradians in one dimension. The other dimension, oriented perpendicular to the radius, is not so constrained.

Near apoapsis, it is desirable to resolve belt/zone variations in order to study gross dynamics over relatively long periods of time. For a $60 R_S$ apoapsis, this requires 0.7 milliradians resolution along the polar axis. At these scales, zonal spatial variations are expected to be much smaller than meridional variations. Thus a significantly larger IFOV in the East/West direction is acceptable.

These considerations lead to an IFOV of about 0.5×1.7 milliradians, with the larger dimension nominally oriented parallel to the equator. The chosen IFOV of 0.4×1.2 milliradians comfortably exceeds these requirements without impacting other instrument parameters.

Image Size To reduce observational complexity, it is desirable to be able to image simultaneously, at the specified spatial resolution, the full planetary diameter near apoapsis. At $60 R_S$, this leads to an image field-of-view of 33.3 milliradians, or 83 pixels. Thus, to cover the three channels, 249 pixels are needed.

4.2.3 Integration Time Requirements

Occultations and reflectance spectra are powerful probes of Saturn and Titan for 3 and $5\text{-}\mu\text{m}$ absorption spectroscopy required for investigations of vertical mixing ratios and temperatures. Below, (Section 4.4) we describe in more detail analysis techniques and requirements. Here, we relate these requirements to instrument design.

For reflectance and thermal emission spectroscopy of Saturn, the integration time is limited by the planetary rotation, which changes the viewing geometry. (Spacecraft pointing is expected to produce a deviation less than 0.145 milliradians for long duration observations when the star-tracker is used). In ten minutes, Saturn rotates 3.6 degrees. At an airmass of 6 (i.e., at an emission angle of 70.5 degrees), a 3.6 degree variation corresponds to a 1.07, or 18%, variation in airmass. This is near the maximum acceptable for effective center-to-limb analyses, and places a useful upper limit on most integrations.

Solar occultation measurements require three orders of magnitude shorter integration times than reflectance/thermal spectroscopy in order to obtain vertical profiles at better than half-scale-height resolution. Specifically, at a spacecraft tangential velocity of 5 km/sec, one second integrations yield 1/6 scale-height vertical samples on Titan. In order to prevent opacity variations from producing pseudo spectral features within a spectrum, the occultation technique further require that the spectral data be acquired simultaneously for all observed interferogram elements, rather than sequentially, as for a Michelson interferometer.

4.2.4 The ACM Approach

The above discussion specifies the instrument requirements needed to attain the selected science goals. To obtain the required simultaneous spectral and spatial coverage at the desired

Table 4: Cassini/ACM Line List of Most Important Spectroscopic Features

Chemical Family	Species	cm ⁻¹	Line Assignment	Saturn	Titan
Oxygen Compounds	H ₂ O	1942.2	ν_2 , rotational lines	x	
		1923.2	"	x	
		1918.0	"	x	
		1910.2	"	x	
		1895.2	"	x	
		1889.6	"	x	
	CO	2165.6	1-0 R5	x	x
		2162.0	1-0 R4	x	x
		2158.3	1-0 R3	x	x
		2154.6	1-0 R2	x	x
		2150.9	1-0 R1		x
		2147.1	1-0 R0	x	x
		2139.4	1-0 P1		x
		2135.5	1-0 P2		x
		2131.6	1-0 P3		x
		2127.7	1-0 P4		x
		2123.7	1-0 P5	x	x
Disequilibrium Hydride Molecules	GeH ₄	2111.0	ν_3 Q	x	
		2139.2	ν_3 R4	x	
		2150.0	ν_3 R6	x	
		2155.4	ν_3 R7	x	
		2165.8	ν_3 R9	x	
	AsH ₃	2126.	ν_3 Q	x	
Isotopes	¹³ CO	2134.3	1-0 R10		x
		2138.0	1-0 R11		x
		2140.8	1-0 R12		x
	C ¹⁸ O	2133.5	1-0 R11		x
		2143.0	1-0 R14		x
	C ¹⁷ O	2141.6	1-0 R16		x
	CH ₃ D	2160.5	ν_3 P5	x	x
		2152.61	ν_3 P6	x	x
		2144.3	ν_3 P7	x	x
		2135.8	ν_3 P8	x	x
	¹³ C ¹² CH ₂	3281.9	ν_3 P1	x	x
		3297.7	ν_3 R5	x	x
Nitriles	HCN	3255-3300	ν_3 P5-P16	x(P5,P8)	x
	C ₂ N ₂	2155.9	ν_3 P6		x
		2164.2	ν_3 R20		x
		2167.0	ν_3 R30		x
		2167.6	ν_3 R32		x
	NH ₃	1920.62	2 ν_2 R1	x	
		1939.	2 ν_2 R2	x	
Hydrocarbons	CH ₄	1915.5	$\nu_3 - \nu_4$ R12	x	x
		1931.3	$\nu_3 - \nu_4$ R13	x	x
	C ₂ H ₂	3255-3300	ν_3 (R0,P1-P16)	x	x
	C ₂ H ₄	1890.	$\nu_2 + \nu_4 + \nu_5$		
	CH ₂ =C=CH ₂	1930-1940	ν_5 P branch	x	x
	C ₂ H ₆	3254.	$\nu_3 + \nu_9 + \nu_{11}$	x	x
		1900-1920	$\nu_9 + \nu_{12}$	x	x
	C ₃ H ₈	1936.	$\nu_{21} + \nu_{21}$	x	x

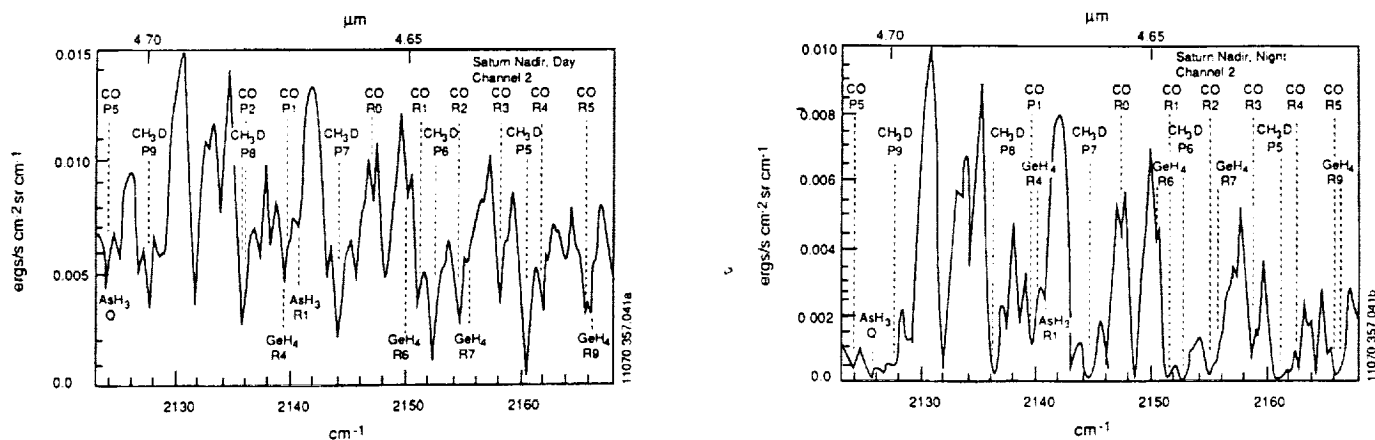


Figure 15: Channel 2: synthetic Saturn spectra. Day (left) and night (right) synthetic spectra of Saturn under nadir viewing conditions, based on the analysis of Noll *et al.* (1986) and Bezard *et al.* (1989). The model assumes mean molar fractions $q_{PH_3} = 4.5 \cdot 10^{-6}$, $q_{CO} = 2.0 \cdot 10^{-9}$, $q_{GeH_4} = 5.0 \cdot 10^{-10}$, $q_{AsH_3} = 2.5 \cdot 10^{-9}$, and $q_{CH_3D} = 3.2 \cdot 10^{-7}$. A $\tau = 0.15$ haze is assumed located at 0.300 mbars, and a thermally-emitting 205 K cloud deck is assumed present at 4 bars. Daytime observations are useful for interpreting abundances above the haze layer which, due to scattering of sunlight, obscures the atmosphere below. Nighttime observations of thermal planetary emission allows unobstructed views of the troposphere down to the cloud deck.

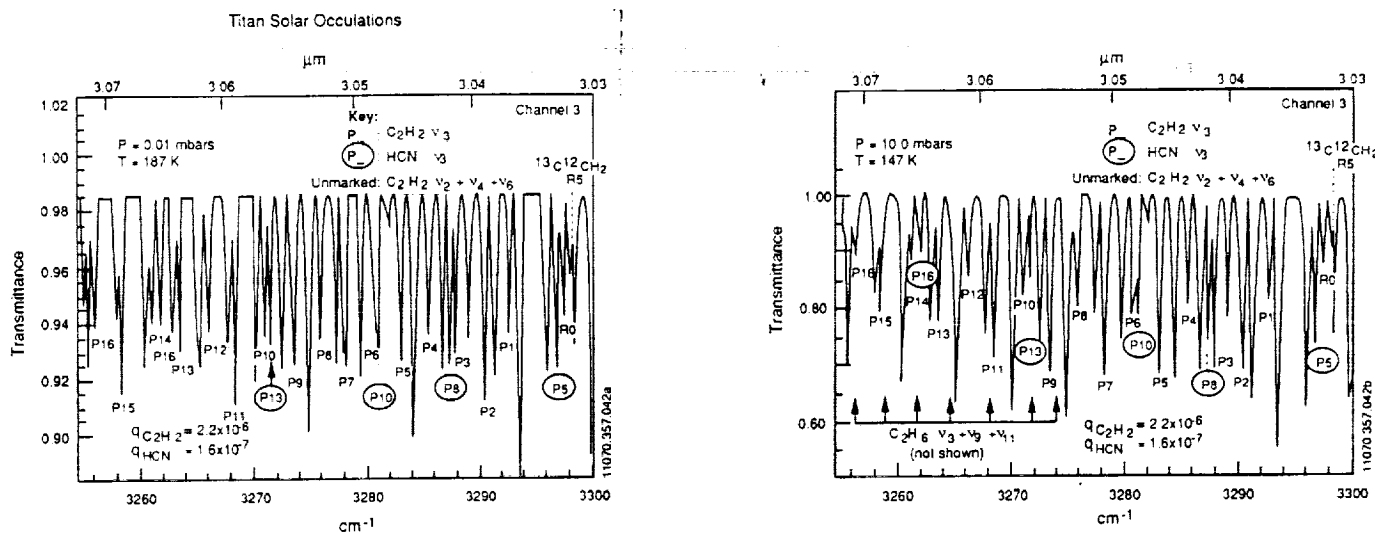


Figure 16: Channel 3: Titan solar occultation spectra for 0.01 and 10.0 mbars tangent pressure levels. Three molecular bands are prominent: the ν_3 bands of HCN and C_2H_6 and the $\nu_2 + \nu_4 + \nu_5$ band of C_2H_2 . Also depicted schematically are the locations of strong C_2H_2 lines. Differences in relative absorptions of various lines between 0.01 and 10 mbars are indicative of temperature effects at 187K (left) and 147K (right).

spectral and spatial resolution, ACM incorporates a digital array scanned interferometer (Appendix A). ACM utilizes the vertical dimension of the detector array - 256 pixels in one-dimensional imaging of Saturn, Titan, or the rings while simultaneously acquiring elements (using 256 pixels in the orthogonal direction) as required for the solar occultations. Two-dimensional maps are, in general, constructed by raster scanning in the same (horizontal) direction of the detector array, utilizing the HPSP scanning capability. The scan rate is set at 0.4 milliradians in the vertical (one-dimensional imaging) direction, and 1.2 mrad in the horizontal (raster scanning) direction, thus meeting the requirements established in Section 4.2.2. Efficient acquisition of only the spectral regions of interest - the three distinct regions described above - is accomplished at the desired high spectral resolution through the use of fixed blocking filters, each covering one-third of the array. Filters for channels 1, 2, 3, 4, 5, 45, and 45 cm^{-1} wide respectively, leading to spectral sampling intervals for the 220 spectral elements of 0.27, 0.20 and 0.20 cm^{-1} . Use of the appropriate Hamming function yields the desired apodized spectral resolutions of 0.4 and 0.3 cm^{-1} . Thus ACM acquires high-resolution spectra in three channels with 85 spatial pixels in each channel, as described in the preceding Sections 4.2.1-4.2.3.

ACM with its digital-array scanned interferometer system has additional operational advantages, including 1) no moving parts, 2) compact/lightweight design, 3) low power requirement, and 4) low data rate. These enable reliable and efficient acquisition of high-spectral-resolution maps at low cost in both spacecraft and project resources.

To summarize, ACM meets all the requirements for the science goals and measurements within the specified approach for high spectral resolution spatial mapping and observations of the atmospheres of Saturn and Titan. In view of the no-moving parts design, ACM and the economy of choice of selected spectral channels, ACM produces an element that meets a wide range of science requirements.

4.3 Observational Approach

4.3.1 Data Acquisition

ACM observations include nadir and center-to-limb observational studies of 5- μm spectra for the day and night side of Saturn and 3- μm absorption spectra for the day and night side of Saturn and Titan. Solar occultations of both planets are obtained for all three spectral regions simultaneously. Solar occultations use an off-axis illumination to ensure that no light enters the instrument. The instrument fact sheets provide details for specific modes of operation and the observational requirements.

The observational data are interferograms for the spatial elements filling the entrance pupil. The interferogram contains the spectral information within the spectral bandpass selected by the selection filter. The integrations for each interferogram will vary from less than 1 second (for solar occultations) to over 100 seconds (for thermal emission spectra of Saturn's atmosphere and characterizing Titan at 5 μm). Interferograms can be co-added to reach very high S/N ratios as shown below.

4.3.2 Calibration and Reduction

Calibration: The detector array response is radiometrically calibrated pixel-by-pixel before launch as a function of signal level, bias, and temperature. The ACM blocking-filters have bandwidths of 45-60 cm^{-1} , resulting in a pixel quantum efficiency that is constant and independent of the spectral distribution within the bandpass. The detector response calibration is checked and maintained by periodic observations of the Radiometric Calibration Target (RCS) before launch and for the duration of the mission. As a secondary calibration, ACM utilizes the

observations of the solar spectrum acquired in Solar Occultation Mode. Additional details of calibration procedures are described in Section 5.4.

Reduction: The reduction of interferograms is well defined. First, deep space images provide a dark current and read noise measurement. Next, images of the RCT provide an absolute photometry reference and flatfield calibration. The dark frame is subtracted from the measured interferogram to remove dark current and bias and the interferograms are co-added, as required, and transmitted to the Earth for further processing. Conventional FFT methods, transform symmetrization, apodization, spectral enhancement processing and other techniques will be applied to the interferograms to produce the required spectral maps of Saturn and Titan. The data processing methods we have used for interferometric spectra are described in Appendix A. These are similar to those found in Hanel (1983). These methods are the result of more than three decades of development. The error sources and their character are well understood. A detailed discussion of the radiometry specifically for attained S/N in the spectral data is provided in the instrument section.

4.4 Data Analysis

4.4.1 Solar Occultations

Solar occultations are the primary mode for Titan observations. Primary use will be made of the "CO" channel (channel 2) at $4.7\ \mu\text{m}$ and the " $3.0\text{-}\mu\text{m}$ " channel (channel 3) to derive vertical mole fraction profiles of CO, HCN, C_2H_2 , C_2H_6 , and CH_3D from $10\ \mu\text{bars}$ to $10\ \text{mbars}$. In addition, temperature profiles will be obtained from the relative absorptions observed in P1 - P16 lines of the $\text{C}_2\text{H}_2\ \nu_3$ band, as well as the HCN and CO bands.

At $3.0\ \mu\text{m}$ and $4.7\ \mu\text{m}$, the ACM optical system provides a S/N of 2190 and 970, respectively, in one second integrations above $200\ \text{km}$ altitude, corresponding to $\sim 1\ \text{mbar}$. This calculation is based on the measured visible extinction coefficient of Rages and Pollack (1983) above the 200-km level and a conservative inverse relationship between wavelength and optical depth. Specifically, we find integrated particle extinctions of ~ 0.16 and ~ 0.1 at $200\ \text{km}$ for these two channels. Given an extinction scale height of $25\ \text{km}$ (Rages and Pollack, 1983), we obtain the S/N ratio as a function of altitude shown in Table 5. Thus vertical profiles are useful in both channels down to approximately the 10-mbar level.

Table 5: Signal-to-noise vs altitude for Titan solar occultations.

Altitude	Pressure (mbars)	S/N Channel 2 ($4.7\ \mu\text{m}$)	S/N Channel 3 ($3\ \mu\text{m}$)
≥ 200	≤ 1.0	970	2190
150	2.5	671	1253
130	5.0	426	590
100	10.0	63	28
90	15.0	16	4
80	25.0	2	0.1

Figs. 12 and 16 show synthetic solar occultation transmission spectra in Channels 2 and 3. Uncertainties derived from these models utilizing the above S/N estimates, are shown in Tables 6 and 7, calculated for one of the stronger individual lines, assuming a constant mole fraction with altitude. Including all of the observed lines for each species reduces the estimated uncertainties in S/N by factors of 2.0, 2.5, and 5 for CH_3D , CO, and C_2H_2 , respectively.

Table 6: Channel 2 mole fraction vertical profile uncertainties from Titan solar occultations. Nominal and precision of mole fraction derived from nightside observations of a single absorption feature for each species listed.

Species	Altitude	Pressure (mbar)	Nominal mole fraction (ppm)	Mole fraction uncertainty (ppm) (3σ)
CO	405	0.01	2.0	0.18
	130	5.00	2.0	0.03
	100	10.0	2.0	0.17
	90	15.0	2.0	0.63
CH ₃ D	405	0.01	11.0	0.85
	130	5.00	11.0	0.17
	100	10.0	11.0	0.95
	90	15.0	11.0	3.44

Table 7: Channel 3 mole fraction uncertainties from Titan solar occultations.

Species	altitude	pressure (mbar)	nominal mole fraction (ppm)	mole fraction uncertainty (ppm) (3σ)
C ₂ H ₂	405	0.01	2.2	0.06
	100	10.0	2.2	0.68
HCN	405	0.01	0.17	0.004
	100	10.0	0.17	0.052

We have simulated the ACM spectrum retrieval using the Saturn model atmosphere for signal to noise ratios of 25 and 100 (see Fig. 13). From experience with this simulation we estimate that thermal profiles from 10 μ bar to 10 mbar can be determined with uncertainties better than ± 2 K.

Data analysis proceeds according to established inversion techniques used successfully in the ATMOS experiment (Farmer and Raper, 1985).

Channel 1 is not predicted to show absorptions of any known constituent, except weak temperature-sensitive, methane features. This channel will be used to measure aerosols at 5.2 μ m and to search for trace constituents.

Analysis of ring occultations will proceed as for Channel 1. Apparent solar diameter is 1.6 km at 3 R_S. At 6 km/sec, the sun takes 30 seconds to traverse a point in the sky. The thirty observations acquired during this time may be differentiated to obtain spatial resolution significantly better than 180 km. Particle sizes are derived from occultation transits as well as measurement of forward scattering efficiency at several wavelengths observed at nightside with ACM and in visible wavelengths by other Cassini instruments. Super-resolution techniques (e.g., maximum entropy) will improve resolution by a factor of ~ 5 , to ~ 36 km resolution. The known profile of the sun and the estimate of the IR ring profile from the visible profile from e.g. the ISS or the High Speed Photometer will facilitate this effort.

4.4.2 Thermal Emission Spectrophotometry

Thermal emission spectrophotometry will be used on the darkside of Saturn to derive column abundances and mean molar fractions in Saturn's visible troposphere. Species include the condensates H₂O and NH₃, the disequilibrium species CO, GeH₄, and AsH₃, and

CH₃D. Absorptions of individual features yield integrated column abundances. The depth of the atmosphere will be determined from (1) the CH₃D absorption, and (2) the temperature derived from the broadband thermal fluxes observed at 4.7 and 5.2 μ m. CH₃D mimics CH₄ in its spatial and vertical distribution. Except for high in the photochemically-active stratosphere, the CH₃D molar fraction is fixed. Given the CH₃D/CH₄ ratio derived from ACM, as well as from other experiments, and the excellent CH₄ vertical profile expected to be derived by various Cassini instruments, CH₃D absorption will be an excellent yardstick to measure depths in the Saturnian atmosphere. As a second method, brightness temperatures of the \sim 4-bar source, as defined by the flux gradient at 4.7 μ m and 5.2 μ m, will be used to determine the altitude of the bottom cloud, given excellent pressure/temperature profiles expected from other experiments.

Tropospheric molar fractions derived from ground-based observations have been hampered by significant but uncertain amounts of sunlight reflected from high-level clouds. Recent ground-based studies indicate that the reflected sunlight comprises 30 - 40% of the 5- μ m flux emitted by the atmosphere, and is largely responsible for ground-based mole fraction uncertainties of \pm 30%. Observations of Saturn's darkside will mitigate this uncertainty. The effect of the upper-level cloud on thermal emission is readily handled in darkside observations as it only attenuates the outgoing thermal flux without acting as an additional source of light (being relatively cold, it's thermal emission is unimportant as well). The CH₃D-derived pressure is thus easier to evaluate as the observed absorption is not "filled in" by high-altitude reflected sunlight as on the day-side. Evaluation of the temperature (and hence pressure) of the bottom cloud emission source is made easier to derive as well due to the purely-sampled flux gradient between 4.7 and 5.2 μ m uncontaminated by reflected sunlight.

Expected uncertainties for various constituents can be estimated from synthetic spectra (e.g., Fig. 9 and 15), given our expected maximum spectral-average S/N of 100 for 10-minute integrations (corresponding to an NESR of 3×10^{-5} ergs sec⁻¹ cm⁻² sr cm⁻¹). Uncertainties for the best spectral feature for each species are listed in Table 8.

Table 8: Mole fraction uncertainties from Saturn nightside observations.

Species	line	mole fraction	
		Nominal value	Uncertainty (3 σ)
CO	R0	2 ppb	0.18 ppb
GeH ₄	R6	0.5 ppb	0.15 ppb
AsH ₃	R1	0.25 ppb	0.09 ppb
PH ₃		4.5 ppm	0.22 ppm
CH ₃ D	P6	0.32 ppm	0.03 ppm
H ₂ O		56 pr μ m	6 pr μ m
NH ₃	R1	500 ppm*	18 ppm*

*Below NH₃ condensation level.

4.4.3 Reflectance Spectrophotometry

Reflectance spectrophotometry will be used on the daysides of Saturn and Titan to determine stratospheric abundances and aid in constraining the tropospheric component. Center-to-limb observations will enable aerosol properties to be derived as well, particularly of the ammonia cloud residing near the 1-bar level. Observations of well-mixed constituents (such as CH₃D and, perhaps, a relatively weak hot band of CH₄ at 5.2 μ m), will enable cloud-top pressures and cloud opacities to be derived as well from center-to-limb observations.

In Fig. 17, we show the power of center-to-limb observations to distinguish stratospheric from

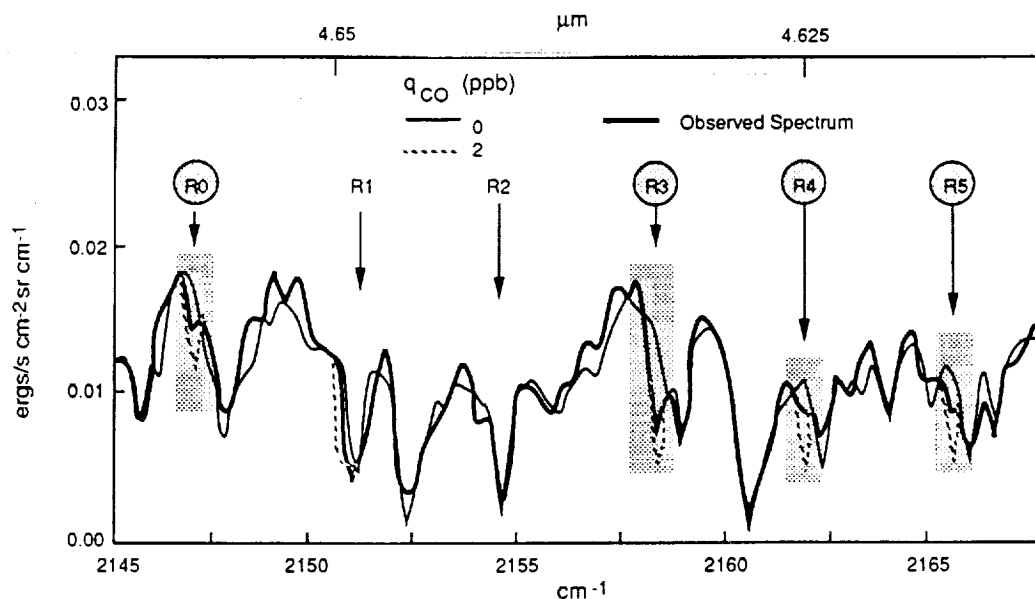


Figure 17: Near-limb synthetic spectra for two degenerate CO models of Noll et al (1986). Models, which segregate CO in the stratosphere and troposphere, both satisfy the center-of-disk, low-spatial-resolution observations of Noll et al. (1986). Near-limb, high-spatial-resolution observations easily distinguish between the

tropospheric sources of CO. While the Noll *et al.*, (1986) full-disk observations could not distinguish between two alternative models restricting CO to either the stratosphere or troposphere, observations near the limb readily separate the two degenerate solutions.

From a combined analysis of center-to-limb observations in all three bands, a picture of deep-atmospheric circulation has been derived, thus aiding in understanding deep-atmospheric circulation. Analysis of cloud characteristics will place in context the integrated water and ammonia abundances and contribute to the understanding of meteorology.

4.5 Relationship of ACM to Other Prospective Orbiter Instrumentation

4.5.1 Complementarity

ACM affords strong complementarity to other proposed orbiter instruments, including MISTI, and MSAR. It also complements the localized Huygen Probe measurements. The following aspects:

Huygens Probe: Instruments on the Huygens probe of Titan's atmosphere will measure temperature, gas composition, and aerosol structure at one location. ACM will provide global measurements of CO, CH₃D, C₂N₂, C₂H₆, C₂H₂, and HCN in Titan's stratosphere which will provide measurements in a global context. Aerosol opacity in the stratosphere will be derived from solar occultations for many locations on Titan using ACM's 5.2-μm channel.

CIRS, MISTI: The Composite Infrared Spectrometer (CIRS) and the Cassini Infrared Spectrometer (MISTI) are both designed to measure stratospheric temperatures on Saturn using thermal emission from the ν₄ band of CH₄ at 7.7 μm. In addition, CIRS will measure CH₃D at 8.6 μm. Thermal emission from both molecules depends on both temperature and mole fraction. On Titan, ACM solar occultation measurements of multiple CH₃D lines provide a means of uniquely determining the vertical mole fraction profiles of substituted methane between 1 μbar and the tropopause. Since the CH₃D/CH₄ ratio is expected to be constant, ACM measurements combined with CIRS or MISTI will provide temperature profiles for Saturn and Titan. In addition, ACM's own localized 1/6

temperature profiles derived from C_2H_2 solar occultation measurements will serve as a verification check, thus complementing the global measurements.

ISS: The Imaging Subsystem will provide visible images of cloud features in Saturn's upper troposphere. ACM will provide maps of disequilibrium species brought up from great depth (CO , HCN , GeH_4 , AsH_3 , PH_3). Correlation of visible cloud features with K_{eddy} derived from the transport rate of disequilibrium species will elucidate the respective roles of internal energy and sunlight in driving Saturn's atmospheric dynamics.

MSAR: This instrument is designed to measure CO and HCN emission on Titan using limb sounding at millimeter wavelengths. The emission is a function of temperature and gas abundance. ACM will independently measure the vertical profile of CO and HCN in absorption during solar occultations. The altitude coverage is from 10 μ bar to the tropopause with better than 1/6 scale height sample. Together the two instruments will provide temperature profiles over 5 decades in pressure in Titan's upper atmosphere. This will help fill in the gap between ultraviolet and infrared temperature measurements from Voyager. MSAR will also measure the continuum brightness temperature of Saturn at centimeter wavelengths. The opacity between 2 and 13 cm is dominated by gaseous NH_3 in the 1 to 10 bar region, but H_2O may also be important. ACM will provide maps of H_2O and NH_3 abundances at the 4 bar level. The combined data will permit the separation of spatial variations in temperature, NH_3 abundance, and aerosol opacity in Saturn's deep troposphere.

Radio Science: The radio occultation experiment measures the atmospheric scale height or T/μ , where T is temperature and μ is the mean molecular weight. ACM will measure the stratospheric temperatures of Titan and Saturn determined by solar occultation measurements of CH_3D at 4.7 μm and C_2H_2 at 3.1 μm . When combined with radio data, both T and μ will be determined.

4.5.2 Comparison

The ACM experiment will, to our knowledge, be the ONLY instrument capable of addressing the abundance and spatial and temporal distributions of H_2O and disequilibrium constituents GeH_4 and AsH_3 in Saturn's deep (~ 3 bar) atmosphere. (The SAM experiment will explore its sensitivity to H_2O cloud absorption at depths of 8 - 10 bars pressure at wavelengths of 12 cm, however.) By virtue of its sensitivity to the 5- μm atmospheric window, it is the only instrument able to probe the abundance of CO at this depth (CIRS is sensitive to CO absorption near the 200- to 400-mbar level). ACM and SAM will both be sensitive to the abundance of NH_3 near the 1- to 5-bar level, although ACM's spatial resolution will be 30-90 times better. VIMS will be able to detect PH_3 and CH_3D absorption in Saturn at this depth, and the CO and CH_3D absorption in Titan's reflected spectrum. However, its poorer spectral resolution (by a factor of 40) will create severe limitations on (1) the extent to which particulate and gaseous absorption can be distinguished from one another and (2) the vertical range over which they can be retrieved. The CIRS experiment will be able to detect PH_3 , NH_3 and CO tropospheric absorption features and retrieve their abundances near the 0.1 - 0.5 bars, although the absorption by CO will be rather weak at the CIRS spectral resolution in the far infrared. For NH_3 and CO , ACM's spatial resolution will be a factor of 4-10 times better.

At higher levels in the atmosphere, MSAR and CIRS are sensitive to temperatures and various gaseous constituents from limb sensing. In one important sense, ACM occultation mode observations of temperature and gaseous constituents is superior (although more limited in sampling) because of its implicit ability to separate the effects of temperature and gaseous abundance. This is important for temperature sounding in Titan, where MSAR assumes that CO is vertically

uniform and CIRS assumes that the CH_4 abundance can be constrained from one or more profiles at the base of the stratosphere.

UVSI occultation measurements, in principle, may be similar to the ACM capabilities depending on the particular configuration of the instrument design. These capabilities, demonstrated already by the Voyager UVS occultation results, include determining the temperature, mixing ratio near the $1\text{-}\mu\text{bar}$ level in Saturn (Festou and Atreya, 1982). With sufficient sensitivity and stability and spectral range, similar results may be possible for C_2H_2 and C_2H_6 .

5 INSTRUMENTATION

5.1 Instrument Selection

The science goal of studying atmospheric chemistry using individual line profiles has been an unattainable goal within the weight, volume, and power constraints of outer solar system missions. The ACM is an innovative, no-moving parts Fourier Transform Spectrometer based on the heritage of optical, electronic, and cryogenic heritage which meets these requirements. As defined by the Planetary Instrument Design and Definition Program (PIDDP), the ACM will weigh $\sim 2\text{ Kg}$ and requires $\sim 5\text{ Watts}$ average power.

It is characteristic of Fourier Transform Spectrometers (FTS) that superposition of spectral elements onto the detector occurs simultaneously (Fellgett, 1951). Spectral measurements using FTS, including DASIs, in the domain where the signal-to-noise ratio (S/N) in the instrument approaches the photon noise limitations, should be used with a passband limited to the elements of interest. The DASI enables high spectral resolution within the weight, volume, and power constraints for the Cassini mission because of its throughput advantage and its valuable instrument profile advantage.

5.2 Instrument Description

5.2.1 System Design

ACM's specifications are shown in Table 9. No cover is required, since minor condensation by solid aerosols will not affect instrument performance. Water, a by-product of condensation, will condense on the primary and must be driven off by heat applied at infrequent and short intervals.

There are two radiators, one at 50K for the detector, and one at 100K for the instrument. They are black, rendering them insensitive to contamination, but requiring that they point toward the sun for optimum operation. They are co-planar, the innermost bonded by a flexible strap to the detector, the outermost one thermally bonded by structure to the instrument.

ACM is shown in Figs. 18 and 19. An $f/2$ 10 cm aperture telescope of three elements focuses light on a slit 1.2 mrad wide and 102 mrad long, the long axis out of the plane of the paper. The long axis is nominally parallel to Saturn's axis. As the instrument is scanned in the direction of the axis, the spectrum from a given point on the planet will move across the slit, passing through several spectrometer channels.

The interferometer portion of ACM is discussed in detail in Appendix A and is further described in Section 5.2.5 below. Fringes, suitably spatially magnified and filtered to remove unwanted wavenumbers, form at the detector. Fig. 20 shows a block diagram of this process.

The detector is a 256^2 array of pixel size $40\text{ }\mu\text{m}$. Under control of a microprocessor, the detector is photocharged for a programmable length of time. Table 10 lists typical integration times for various observations. Dark current constitutes a sizeable fraction of signal, but can be accurately measured and cancelled. Due to finite well depth, longer integration

Table 9: Instrument Requirements Derived From Science Objectives

FOV, total:	1.2×102 mrad
FOV, ea. channel:	1.2×34 mrad
IFOV:	1.2×0.4 mrad
Number of spectral channels:	3
Spectral sample:	0.25 cm ⁻¹ , nominal
Channel 1, H ₂ O	$\sigma = 1885 - 1940$ cm ⁻¹ , nominal
Channel 2, CO	$\sigma = 2123 - 2168$ cm ⁻¹ , nominal
Channel 3, C ₂ H ₂	$\sigma = 3255 - 3300$ cm ⁻¹ , nominal
Number of spectral channels:	3
Spectral resolution:	0.25 cm ⁻¹ , nominal
Channel 1, "H ₂ O"	$\sigma = 1885 - 1940$ cm ⁻¹ , nominal
Channel 2, "CO"	$\sigma = 2123 - 2168$ cm ⁻¹ , nominal
Channel 3, "3 μ m"	$\sigma = 3255 - 3300$ cm ⁻¹ , nominal
Main aperture:	100 mm diameter, f/2, achromat
Auxiliary aperture:	15×1.5 mm slit
Contamination:	Main and aux element heaters
Interferometer:	Michelson with grating
Detector:	256×256 staring 3.0-5.3- μ m HgCdTe array
Detector temperature:	60K
Detector cooling:	Passive radiator, 400cm ²
Instrument cooling:	Passive radiator, 400cm ²
Radiator surfaces:	$\epsilon=0.85$, $\alpha \approx 0.9$ (black)
Instrument/telescope temperature:	110K
Mass:	<5.5Kg, including electronics
Dimensions:	40cmx28cmx12cm, excluding electronics 15cmx15cmx9cm, electronics
Power requirements:	<5 Watts average, instrument +8 Watts, heaters, when energized
Processor:	SA3300
Data rates:	<200 Kbps peak, <20 Kbps mean, typ.

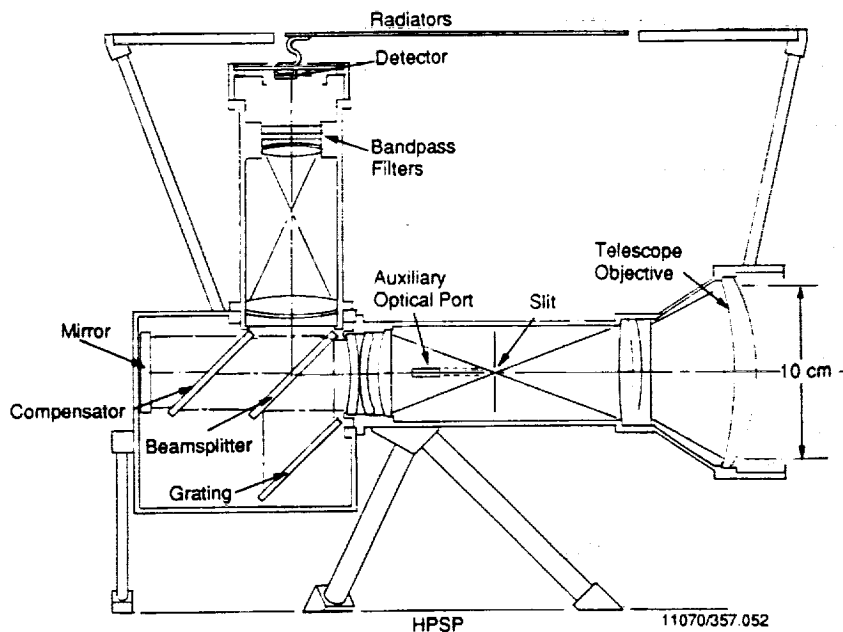


Figure 18: Optical layout shows the simplicity of ACM

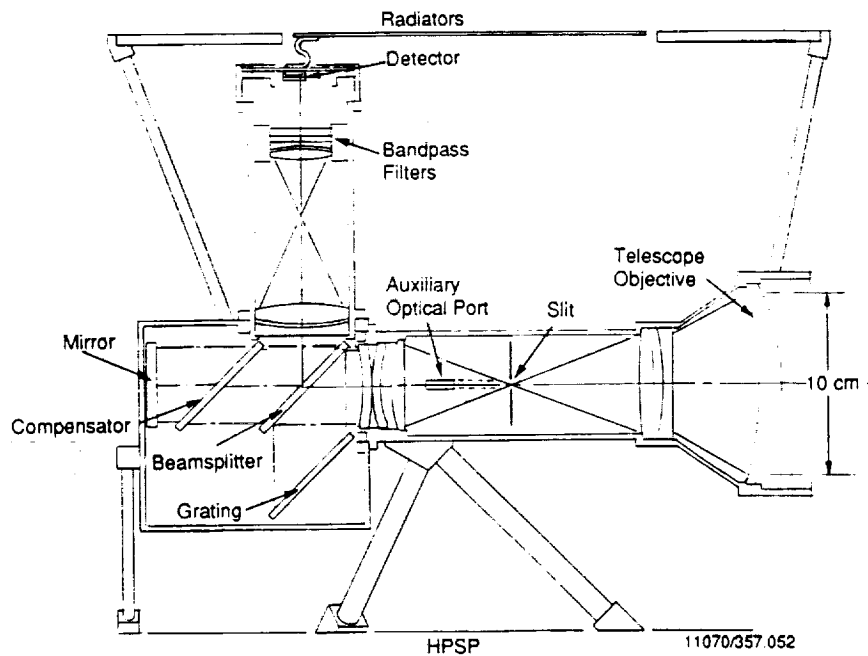


Figure 19: ACM consists of a photon collecting telescope, followed by a heterodyning interferometer array, and processing electronics.

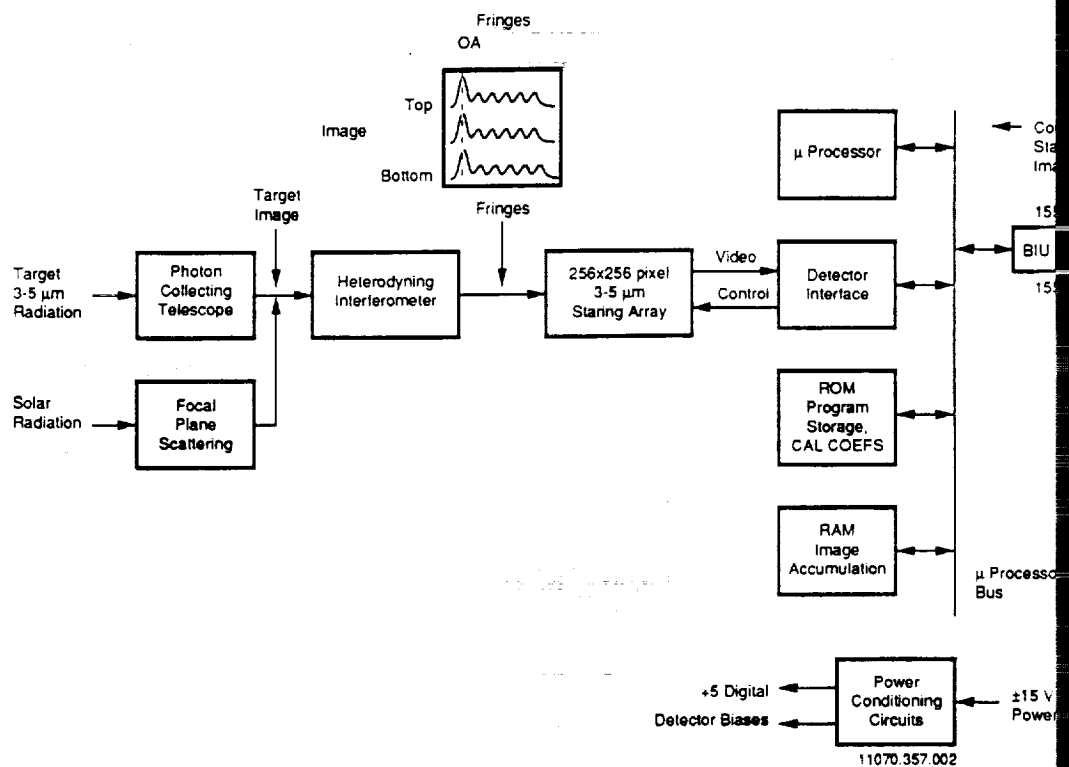


Figure 20: ACM block diagram showing hardware elements and their relationships

accomplished by multiple readouts and summation. Since each pixel has a unique volts/photon gain, correction for gain is required.

Table 10: Typical Integration Times

	Typical Integration Times	
	snr=100	snr=50
Saturn nightside 2150 cm^{-1} :	1524 seconds	383 seconds
Saturn dayside 2150 cm^{-1} :	440 seconds,	111 seconds
Titan solar occultation 2150 cm^{-1} :	2 seconds	0.5 seconds

To observe limb occultations of the sun, ACM is pointed to allow the sun to enter the auxiliary optical port. Sunlight falls on pinhead spherical reflectors aligned at the rear of the entrance slit. A cylindrical mirror spreads the light across the full width of the grating to fill the interferometer optics and to illuminate the detector fully. To control stray light, the auxiliary line of sight is at greater than 30° with respect to ACM's optical axis.

5.2.2 Instrument Heritage

ACM is a Fourier Transform Spectrometer (FTS) equivalent in principle to the interferometers which have been previously successfully utilized in spacebased remote sensing, eg. Nimbus and IRIS (Voyager)(Hanel, 1983) and ATMOS (Farmer *et al.*, 1985). ACM is, however, a simplified FTS design.

Thermal, mechanical and electronic designs and components of ACM are readily available in spaceflight hardware precedence at Ball (and other flight hardware vendors). Two areas which are specifically addressed here are the passive radiator and the IR focal plane array.

Passive radiators for space hardware are required on nearly every mission, and numerous successful designs exist. Ball has flown low-temperature passive radiators on many missions, including the Coastal Zone Color Scanner and the IRAS multi-stage dewar radiator. Passive radiators are also used for Gamma Ray Spectrometers for both the Mars Observer and CRAF missions. Ball can design an appropriate radiator for Cassini ACM, or utilize a common design with other CRAF/Cassini instruments.

The IR focal plane array to be used for ACM uses the array fabrication technology developed by Rockwell for the HST IR Near Infrared Camera and MultiObject Spectrograph (NICMOS) instrument. Modifications required for ACM will be minor, requiring only that the HgCdTe alloy have a $5.2\text{-}\mu\text{m}$ cutoff wavelength rather than $2.5\mu\text{m}$. Fortunately, ACM does not require a perfect detector as defective pixels cause only a slight reduction in S/N as information is contained in the frequency domain. Detectors that are totally unacceptable for other flight programs can give very satisfactory results for ACM. The key parameter of concern is dark current, followed by quantum efficiency at $5.3\text{ }\mu\text{m}$, readout noise and defects, in that order. The development of processing techniques, multiplexing readout and detector electronics is carried by the HST program, with significant progress having been made already. No risk to the Cassini program is envisioned, since the resources of the HST program are committed to producing useable arrays. We have made arrangements with RI for receipt of a test device, and have already received the NICMOS multiplexer (with shortwavelength detector material) and the long wavelength detector material (on a different multiplexer).

5.2.3 Detector

ACM uses a two-dimensional array similar to the array currently under development for the NICMOS program. Table 11 summarized its characteristics. A figure showing construction of the

Table 11: Focal Plane Array Requirements

type:	256 × 256 Rockwell Science Center array
spatial sampling:	0.4 × 1.2 mrad FOV/pixel 102 × 1.2 mrad FOV/array
quantum efficiency:	70% min at 5.3 μm
dark current:	<1 femtoamps at 60K
read noise:	<100 electrons/pixel
well depth:	>1 × 10 ⁵ electrons for 500 mV bias
pixel size:	40 μm at 85% fill factor
temperature:	60K, passive cooler

hybrid array may be found in the fact sheets. A pixel size of 40 μm permits the use of substrates without concern of breakage of the indium bump bonds.

Dark current is of critical importance. Fig. 21 shows dark current data for a Rockwell device with 60- μm pixels extensively tested at Ball. In this region dark current is dominated by gain-recombination current. The proposed 40 μm pixel-pitch device will have comparable dark current, since the pixels are smaller but the material has a lower bandgap energy at longer wavelength.

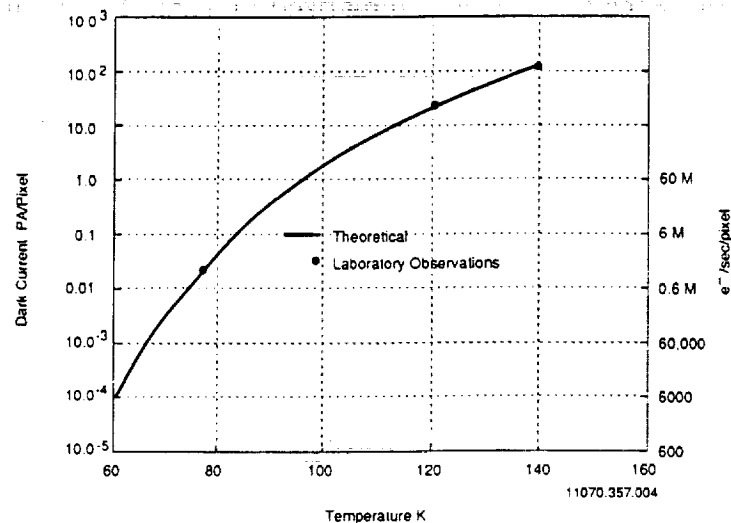


Figure 21: Dark current data for Rockwell 4.7 μm 60- μm -pixel HgCdTe 128² array under nominal conditions. Also shown is the expected behaviour with temperature. Dark currents for 40 μm -pixels are expected to be comparable.

The detector is operated at 60K and is thermally bonded via a cold finger and metal strap to a 50K radiator. Short wire bonds are brought from the detector case to the PWB also at 60K. Manganin wires provide thermal insulation to the instrument case. Relatively long manganin wires provide thermal insulation between the case and the package at 20°C. A figure in the fact sheets shows the detector system.

5.2.4 Radiometric Analysis

Instrumental efficiency is the product of the effective transmittance of the elements in the instrument with the detector response as a function of wavelength. ACM contains efficient optical elements and makes effective use of the incident radiation. ACM parameters are listed in Table 12.

Table 12: Radiometric Parameters

Parameter	Symbol	Value
Source brightness	B_s	3×10^4 to 3×10^5 Photons/cm ² /sec/sr
Telescope Focal length mm	F	200
Telescope f/no	f	2
Telescope Transmission	T_T	0.94
Entrance aperture slit		8 μ m by 240 μ m
Spectrometer Magnification spatial	m	2:1
Spectrometer Resolution	S	0.2cm ⁻¹
Spectrometer Transmission	T_s	0.43
Filter Transmission	T_F	0.67
Detector Array Size	N_p by N_l	256 by 256
Detector Pixel Size	p_x	40 μ m
Quantum Efficiency (including fill factor)	QE	70%
Line Irregularity Factor (lost pixels etc)	LIF	TDS
Dark Current	DC	< 10 ³ electrons/sec
Readout Noise	RN	< 100 electrons
Total Integration time	t	1 to 600 seconds
Number of integrations/exposure	n_{it}	1 to 100

The radiometric performance of ACM is summarized in Table 12. A flux of $3\text{--}4 \times 10^4$ photons per sec from Saturn is detected at 4.7 μ m, and about ten times that flux is seen near 5.3 μ m. Of this flux, about one half is reflected sunlight and one half is due to thermal emission from the planet. The nominal Rockwell MWIR detector array is expected to have a dark current of less than 10 femtoamp at 65K. Presently available arrays (see Fig. 21 detector section) indicate that this is a conservative estimate of the dark current for the detectors for ACM, with the possibility that the dark current will be as low as 1 femtoamp.

5.2.5 Optical Design

The ACM optical train consists of a silicon-germanium-silicon, 200 mm EFL, f/2 objective lens, a Michelson interferometer with a grating in one arm, an anamorphic relay telescope and imager, and a filter plate near the array detector. The optical layout is shown in Fig. 18. (ACM's optical design is discussed in more detail in the Instrument Fact Sheets.)

The objective lens forms an image on the entrance slit, whose width is 1.2 mrad and length 102 mrad. Following the slit, the light is recollimated and passes to a beamsplitter. The recollimation lens also projects a pupil onto the grating. This constrains all of the light passing through the slit to the active grating surface. The grating is composed of three sections. Each is ruled for Littrow operation at the central wavelength of one of the three science spectral bands, and the width of each sub-grating is inversely proportional to the expected flux from Saturn in that band in order to produce uniform S/N in the interferogram. The wavelengths, grating periods and sub-grating widths are listed in the Instrument Fact Sheets.

The recombined beams from the beamsplitter pass through an anamorphic relay telescope and imager. This sub-system acts as a terrestrial telescope in the plane perpendicular to the slit, and as a reimager in the perpendicular plane, yielding a one dimensional image of the slit on the detector, with the light spread out in the perpendicular direction containing the spectral information. In the imaging direction, each 40- μ m pixel row corresponds to 0.4-mrad. The last element of the optical system is the filter plate. Each is a strip filter, covering several rows of pixels and limiting these rows to a specific spectral region.

Because the DASI interference pattern is symmetrical across the center of the pupil, it is not necessary to record both sides. The detector is placed to gather a maximum of data from one of the two redundant halves of the pattern. Accordingly, the pupil is sized to fill the detector when

the optical axis of the system is placed in the middle of the 25th column of detector 10% of detector width.

Solar occultation observations use an auxiliary 1.5-mm aperture, located to the back of the entrance slit. Cylindrical reflector segments scatter light into the internal acceptance cone. This system is discussed in detail in the Instrument Fact Sheets.

Since ACM is optically simple and rugged, and operation at $5\text{ }\mu\text{m}$ imposes an order of magnitude lower stability requirements than in the visible, maintenance of the optical alignment is relatively easy.

5.2.6 Thermal Design

ACM uses radiators and a high degree of thermal isolation from the HPSP. The detector is cooled to 60K to minimize dark current, and the optics at 110K to minimize parasitic flux and conduction from the detector. The detector is cooled with a simple flat plate radiator at 50K, and the optics with a similar radiator at 100K. Thermal design is discussed in detail in the Instrument Fact Sheets. A system thermal diagram may be found there.

At the heliocentric distance of Saturn, a radiator measuring $20\text{cm} \times 20\text{cm}$ and with an emissivity of 0.85 can radiate 17.6mW at 50K. This gives a 23% margin over the total detector dissipation, radiative loading from the instrument, radiative loading from the HPSP, the MLI, and conduction from lead wires and support structures. The instrument radiator at 100K can radiate 195mW with an area of 406 cm^2 and an emissivity of 0.85. The radiator is hard-mounted to the optics box, and the whole assembly is covered with multilayer insulation (MLI). This radiator is sized to give a 9% margin over the total load from HPSP radiation, the MLI, and conduction in wires and support structures. Preliminary analysis indicates a 2° rise in detector temperature for every 10° rise in HPSP temperature.

In order to remove water deposited on the telescope aperture due to contamination from the instrument exhausts, ACM will have heaters to raise these surfaces to 200K. Preliminary analysis indicates about 7 W heater power are required if the radiators, intentionally black for this purpose, are pointed towards the sun.

The electronics module is covered with MLI and hard mounted to the HPSP. Heat is lost through the MLI. The bulk of the 5 Watts average power dissipation is conducted to the HPSP or radiated to space by removing a portion of the MLI. An adiabatic interface is easily achieved.

5.2.7 Electrical Design

The electronics module, shown in detail in the fact sheets, has several functions:

- Control and readout of the detector. Control is simple, basically three clock lines, three horizontal and three in the vertical direction, to select a particular row and column. Correlated double or triple sampling is accomplished in software. Bias voltages are provided for flexibility in operation. Since integration times are typically one second or longer, readout speed is not a concern.

- Command, status, and data to the BIU and S/C telemetry. Microprocessor-based buffering RAM provides any desired protocol, data rates, and housekeeping data. Real-time channels are implemented.

- Control of the primary lens and auxiliary window heaters via telemetry and control switches.

As for any outer solar system mission, reliability is a key issue for the Cassini mission. Backup supplies and watchdog timers are fully redundant. Radiation and single-event-upset resistant parts and designs are used. The recommended SA3300 processor is proposed.

The electronics are packaged on three multi-layer PCBs in a 6"x6"x3" aluminum enclosure, so that the BIU and electronics form a 6"x6"x3.5" package with a mass of ~1.6 Kg. Both are thermally coupled to the HPSP and insulated so that operating temperatures coincide with HPSP temperatures.

5.2.8 Mechanical Design

ACM's mechanical outline is detailed in the fact sheets. The radiators are co-planar with other instrument radiators to avoid FOV conflicts. ACM is designed to be narrow, that it may easily be fit between two other instruments. No cover is required, as described in Section 5.2.1. The electronics module fits under the instrument case against the HPSP mounting surface.

The instrument is composed of three subassemblies: telescope, interferometer, and detector optics. The telescope materials and optical structure will be designed to passively compensate for thermally induced defocus passively.

Structural support and thermal isolation between the instrument and HPSP is achieved by a quasi-kinematic mount system using thin wall, fiberglass struts. The mounting system accommodates differential thermal expansion between the instrument and HPSP by (quasi-kinematic) flexure of the fiberglass struts in their respective low load directions.

The 100K thermal radiator is rigidly attached to the instrument. During ground handling and launch environment, thermally actuated latches will couple the two radiators together to provide structural support for the 50K unit. The latches will automatically release during on-orbit cooldown.

The instrument hardware has a mass of 3.5 kg (7.63 lb) (without the electronics) The fact sheets give a detailed weight breakdown.

5.3 Calibration

Fig. 22 summarizes the radiometric performance of ACM and identifies key parameters and elements which influence calibration. The critical radiometric calibration is dark current cancellation, which is easily accomplished by pointing towards an area free from IR sources. Dark current and detector fixed-pattern noise contributions can be separated by varying the integration time. Radiometric gain is calibrated using the 300K Radiometric Calibration Target (RCT). Alternatively, Saturn's rings will be viewed in solar illumination or the solar occultation mode will be used as a calibration stability check. ACM will be spectrally calibrated by observing known discrete lines.

5.4 Data Collection, Analysis and Archiving

ACM records data as two-dimensional interferograms. These are read into a data acquisition buffer as a raw data image. The detector integration time and the portion of the array to be read out are electronically selectable and are tailored to the specific observation being taken.

5.4.1 Observing Modes

ACM operation follows two basic observing modes: Limb occultation spectroscopy and nadir and off-nadir imaging spectrophotometry. Unique observations, such as calibration or ring studies, utilize minor variants of these two basic modes.

Limb Occultation Mode Solar occultation limb spectroscopy mode uses a small aperture and a spherical reflectors to fill the full vertical dimension of the array. Since the solar image defines the spatial resolution element, summing over the spatial coordinate does not further degrade

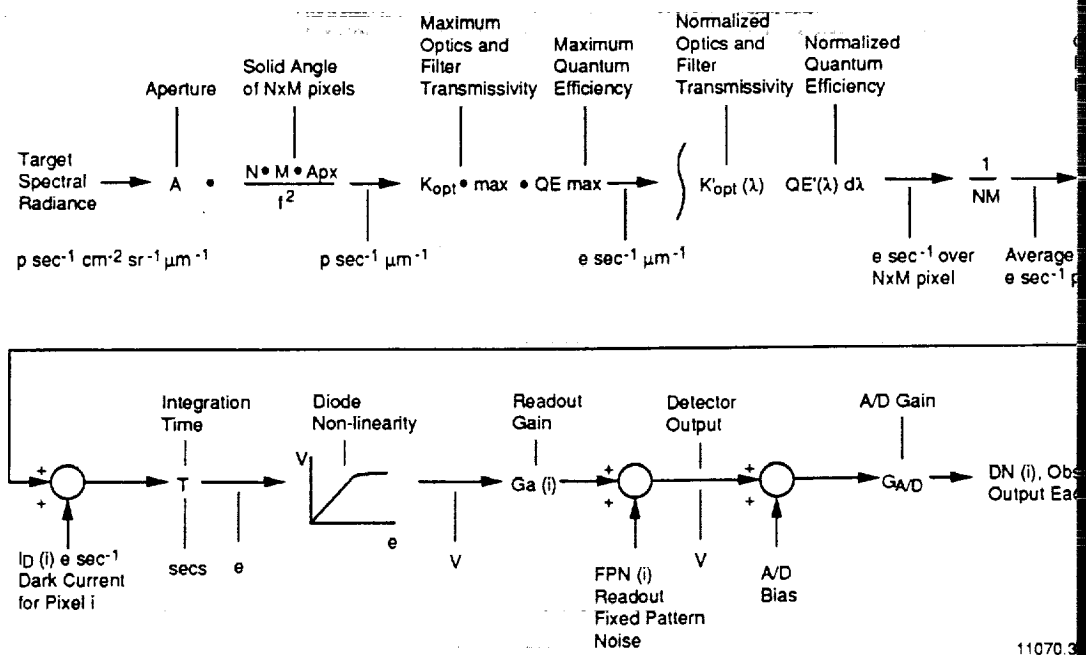


Figure 22: Summary of the radiometric performance of ACM and identification of key parameters and influence calibration. Retrieval of input spectral radiance involves quantifying and removing the effect of this radiometric flow diagram.

resolution and permits the highest possible signal to noise ratio. The data are essentially noise limited. The solar image is reformatted into a line source at the input in order to illuminate the detector array.

Spectral Imaging Mode This observing mode uses the objective lens to collect and reflect light from the planetary atmospheres. Thermal emission and reflected sunlight in this mode require similar integration times, and both require the knowledge of the vertical spatial coordinate. Thermal emission from Saturn dominates the 5.3- μm channel and approximately equals the reflected solar flux at 4.7 μm . At 3 μm for Saturn and 2.2 μm for Titan, the detected flux is essentially reflected sunlight.

5.4.2 Calibration Methods

Preflight calibration will establish a baseline against which potential responsivity of the detector is determined, detected and corrected during the mission.

The important issues are :

Thermal Control: Temperature sensors will measure and report, as required, ACM temperature and array temperatures. The instrumental preflight response will be determined as a function of temperature and maintained by in-flight corrections as a portion of the overall calibration procedure described below.

Radiometric Calibration: ACM will undergo detailed pixel-by-pixel detector calibration before launch to determine the gain and linearity curve over the operating temperature range. The well-defined, narrow ACM spectral passbands. During assembly testing, ACM will

calibration with the Radiometric Calibration Target to transfer ACM's pixel to pixel response from the laboratory standard. At Saturn, drifts in instrumental response can be additionally measured during the solar occultations. This boot strapping process will result in a stable calibration for the duration of the Cassini mission that will periodically be re-established to the initial baseline.

5.5 Mission Operations and Data Management Plan

Mission operations and data management will follow the Cassini Project guidelines. The SOPC (Sequence Operations and Planning Computer) provides the interface for uplink planning and downlink data collection. The ACM Science Coordinator will maintain close attention to the requirements of the Cassini project and constraints on mission operations.

5.5.1 ACM Mission Operations Plan

ACM uses the project-provided SOPC workstation to design observational sequences, which in the case of ACM involves only two modes, as described in Section 5.4.1. These simple modes use electronically selectable readout times. All pointing operations are HPSP controlled.

Data Rates ACM produces an average frame rate for telemetry of one frame each 600 seconds during imaging of Saturn and Titan. At 12 bits per 256 x 256 pixel frame, ACM produces a data rate of 1.3 kbps. Since subsequent frames after the first frame are correlated, simple data editing will reduce the average rate to well below 1 kbps. This data rate does not vary during ACM observational sessions for Saturn or Titan.

ACM will obtain approximately one frame per second in solar occultation mode. The vertical dimension of the array is summed to yield three vectors of 12 bits x 256 pixels each, corresponding to a maximum data rate of 9.2 kbps. This rate is easily accommodated on the real time down link if the data is buffered on the spacecraft memory. Since profiles subsequent to the first are similar, data editing will reduce the actual data rate to below 6.1 kbps after the first data integration. Further, this data rate only occurs for only approximately 300 seconds each during ingress and egress for approximately 30 occultations of Titan and Saturn in the planned mission. Thus, the mean data rate over the mission is entirely negligible, and data recording requirements of 5Mbits per eclipse are manageable.

Instrument Control ACM has simple instrument control modes. Only the detector parameters are varied, since the entire instrument is otherwise passive. Temperature and electronics subsystem measurements are routinely acquired and transmitted for housekeeping purposes.

Science Observation Planning and Design The ACM Science Coordinator will work closely with the ACM PI and Co-Is to integrate ACM objectives into the project timeline of spacecraft activities. Since ACM has uncomplicated observational modes, this is not expected to induce constraining requirements. ACM particularly plans to make observations at low priority times and for solar occultations when other probable spacecraft instruments are not active.

1. Solar Occultations ACM observes the sun through an auxiliary aperture that will safeguard other instruments from any possible accidental exposure to the sun's direct rays. The geometry will also protect the passive coolers from sun exposure.
2. Saturn Thermal and Saturn/Titan Reflectance Measurements Being boresighted, ACM observes Titan during close approaches with other HPSP instruments and has no special requirements. It operates essentially as an infrared camera. For Saturn, the prime mode of

observations for ACM is the spectral mapping mode in which images are acquired of the entire planetary disk. Data acquisition occurs during the long periods when Cassini is at 20 R_S . Although all orbits are valuable, the optimum orbits for nightside observations are from orbits 16 through 34, providing the best relationship between spacecraft position and nightside. The proposed orbits will permit detailed studies of the polar regions of the mission.

3. Rings Occultations of the rings and reflectance mapping are carried out in the manner as described under 1 and 2, above.

5.5.2 ACM Data Plan

ACM will use the SOPC as the prime interface with the Cassini Project and will connect to workstations for data analysis and interpretation with provision for communication with home institution computers. The data will be formatted into standard FITS format and archiving (similar to the Halley Watch standard). Image processing will use standard and standard image processing software, in particular, IRAF.

5.5.3 Housekeeping

Temperature data and detector parameters will be routinely monitored and returned for housekeeping and instrument calibration purposes.

5.5.4 Camera Control

ACM has flexible, electronic camera control. On demand, the controller will read out array areas at specified time intervals. The data packets with suitable identifiers are returned from the SODB by the SOPC and made available to the workstations for processing and interpretation.

5.5.5 Calibration Data and Photometric Corrections

Periodic flat field, solar, and deep space images are required and will be returned in the data stream with the other images. These data are to be applied to each planetary/ring image for normalization according to procedures described above.

5.5.6 Spatial Registration

Reconstruction of spatial maps is determined by well known planetary rotation rates and spacecraft pointing information. Thus, ACM does not impose severe pointing requirements for spatial registration.

5.5.7 Spectral Information for Data Interpretation

Laboratory data for essentially all the expected species are well known. The data base is passed to the ACM science team and will be expanded as new data become available.

5.5.8 Interpretation of Data

The data product will be incorporated into current and revised models for Saturn described in detail in the science goals and approach sections above.

5.5.9 Data Product

The raw, reduced, and reconstructed data (eg. spectral maps for specific species, etc.) will be available at the workstations and will be supplied to the NASA Planetary Data Centers in a form suitable for archiving (eg. WORM). The PDSC at Washington University will provide an easy interface to the NASA system.

6 Responsibilities and Commitments of Scientific Investigators

6.1 Principal Investigator, Dr. William Hayden Smith

Dr. Smith will have overall responsibility for design, development, testing, and implementation of the ACSIS onto the Cassini Orbiter on schedule and within budget. He also is responsible for flight operation and data analysis activities. He will serve as the primary contact for all phases of the investigation, except where he delegates responsibility to other science or engineering team members. He is responsible for defining science requirements, science planning, data acquisition, and science data analysis and reporting. Dr. Smith's primary scientific responsibility is to interpret chemical processes in Titan from maps and vertical profiles of hydrocarbons and nitriles.

6.2 Co-Investigators

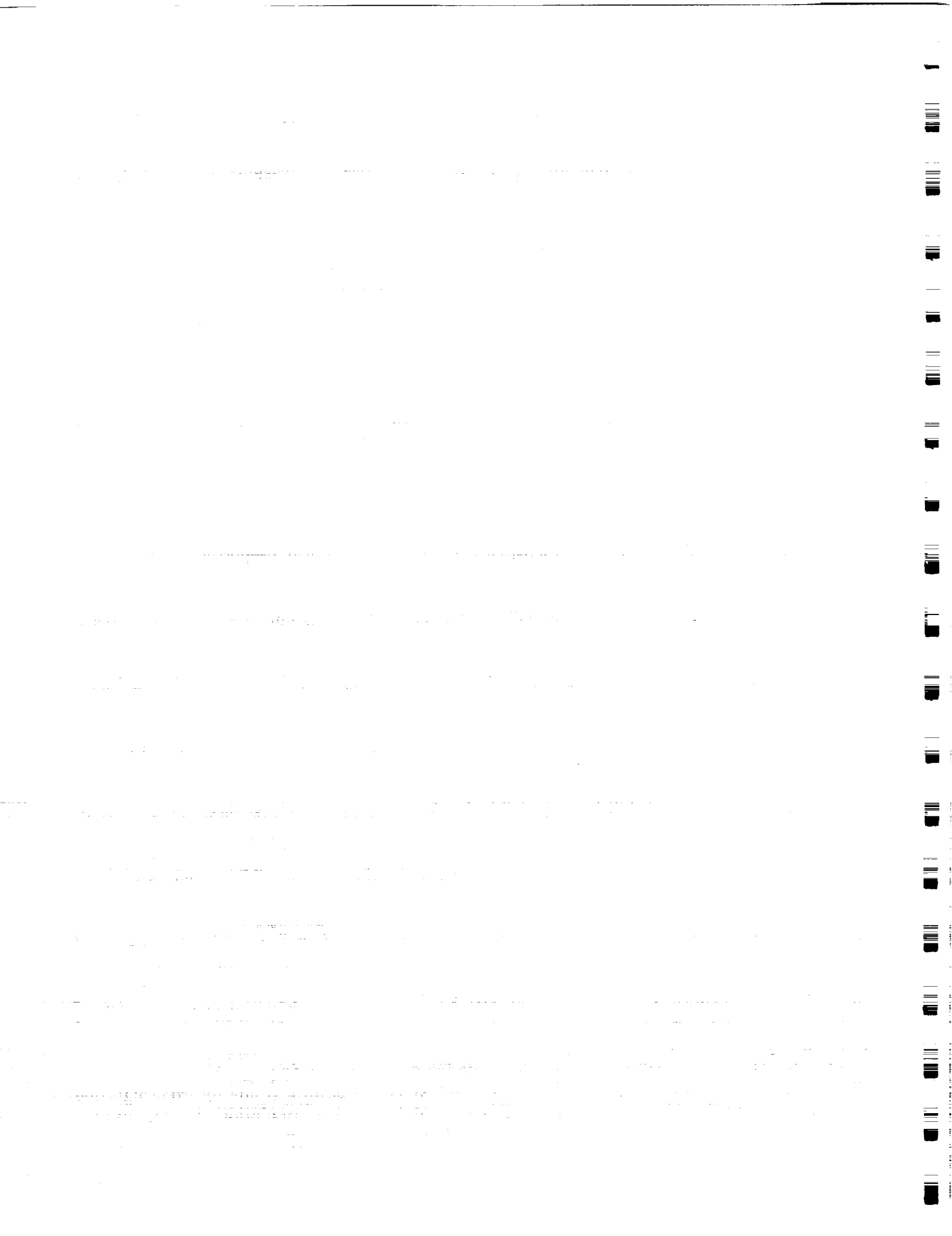
Dr. Kevin H. Baines will be responsible for deriving dynamical properties of stratospheric and tropospheric hazes and clouds in Saturn from the reflective and transmittance measured in 3 and 5 μm maps and from spectral features of condensable and non-condensable gases observed therein. For Titan, he will be responsible for determining spatial distributions of cloud properties and dynamics from occultation data and 3 and 5 μm maps of reflectance. Dr. Baines will be the primary scientific interface with the JPL Cassini Project Office during the pre-launch Science Support phase as well as during the mission, overseeing sequence planning and handling activities at JPL. Dr. Baines is the designated successor to the PI, if required.

Dr. Gordon L. Bjoraker will be responsible for deriving maps of tropospheric hydrocarbons on Saturn from nightside observations, taking advantage of his previous experience in analyzing water from Voyager IRIS. Dr. Bjoraker will also assist in deriving vertical profiles of CH_3D , CO , hydrocarbons and nitriles in Titan's atmosphere from solar occultation data.

Dr. Pierre Drossart will be responsible for determining the spatial distribution of equilibrium species and hydrocarbons in Saturn's upper atmosphere above the NH₂ cloud primarily from center-to-limb dayside observations, utilizing his considerable experience in analyzing groundbased high-resolution 5 μm observations. He will be responsible as well for determining spatial variations of CH_3D , CO , hydrocarbon, and nitriles from dayside 3 and 5 μm maps.

Dr. M. Bruce Fegley will derive dynamical parameters (e.g., K_{eddy} for Saturn's atmosphere from observed maps of disequilibrium constituents). He will assist in the determination of localized convective plume dynamics by, for example, estimating convective cell depth from vertical abundance variations, and by relating observed disequilibrium abundances to deduced dynamical and chemical processes. He will also be responsible for determining isotopic and heavy elemental abundances for scenarios of planetary and satellite formation and evolutionary processes.

Dr. Keith S. Noll will be responsible for deriving maps of the tropospheric and stratospheric disequilibrium species (CO , HCN , PH_3 , GeH_4 , and AsH_3) on Saturn, primarily from ground-based observations, utilizing his experience in analyzing ground-based high-resolution spectra of Saturn. He will be responsible for the analysis of dayside 3 μm reflectance



to determine spatial variations of C_2H_2 and HCN in the troposphere. He will also analysis of CO in Titan from occultation and $5\ \mu m$ dayside observations.

Dr. Glenn S. Orton will assist in deriving cloud properties and will formulate transfer models for recovering gas in the context of realistic atmospheric particulates. He will derive temperature profiles from C_2H_2 lines on Saturn, and HCN, CO, and CH_4 on Titan from occultation observations. He will be responsible for implementing cloud opacity models.

Dr. Harold J. Reitsema will have overall responsibility for design of solar occultations and analysis of solar occultation profiles for Saturn, Titan, and rings and ring imaging, utilizing his considerable experience in planetary and ring occultation observations.

7 RELEVANT SCIENTIFIC EXPERIENCE

Dr. Wm Hayden Smith has more than twenty-five years experience in the development, testing, and scientific use of astronomical instrumentation, both on groundbased telescopes and spacecraft. In the early 1970's, he was responsible for development, testing, and implementation of uv-optical gratings and detectors for the Copernicus experiment. He is the developer of the Spectropolarimetric Imaging Fabry-Perot Interferometer (SPIFI), successfully used in the 1970's and early 1980's to obtain high spectral resolution imagery of Saturn and other planets as well as deep-space sources. Most recently, he has developed acousto-optic based spectropolarimeters and digital array scanned interferometers for astronomical observations.

Dr. Kevin H. Baines has been a member of the Galileo/Near Infrared Imager (NIMS) team since 1984, having primary responsibility for designing and implementing 1-5 μm solar reflectance and thermal emission spectral observations of planetary surfaces, including Venus and Jupiter. He has been an active user of telescopic instrumentation and analysis of outer planet remote sensing data, particularly the International Ultraviolet Explorer satellite and the NASA/Infrared Telescope Facility.

Dr. Gordon L. Bjoraker has considerable experience in the acquisition and analysis of airborne and groundbased 3 and 5 μm observations of Saturn and Jupiter, having been the first to quantify the jovian tropospheric water profile. He has considerable experience in the analysis of 5 μm spectra from spacecraft as well, particularly dayside and nightside observations of Saturn and Jupiter.

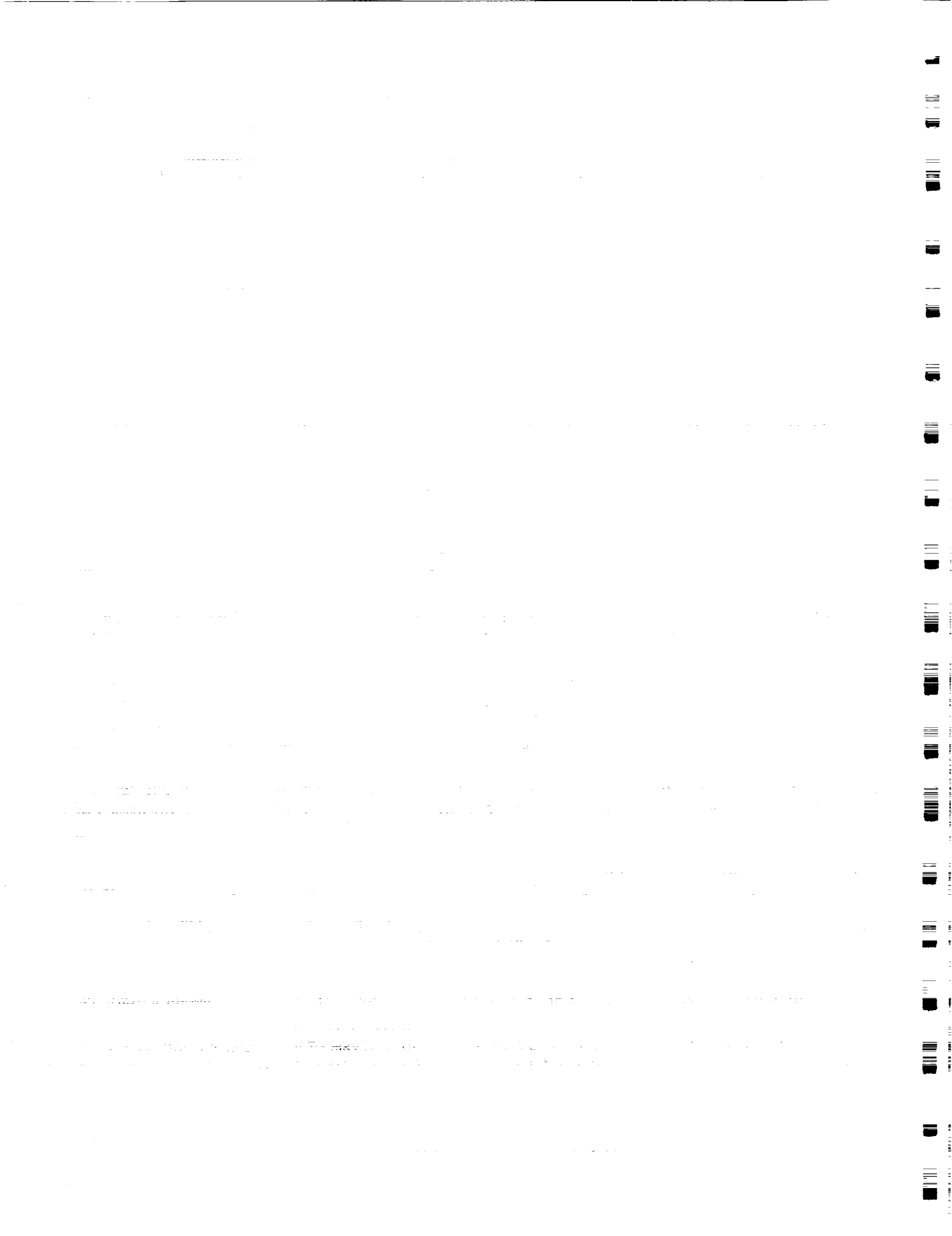
Dr. Pierre Drossart is an experienced observer of 5 μm spectral features in the atmosphere of Saturn, being a co-discover of arsine on Saturn. He was the first to detect spatial variations of H_2O and PH_3 in Jupiter, utilizing both Voyager/IRIS and groundbased observations. He is a member of the Galileo/NIMS team, primarily aiding in the analysis of 5 μm spectra from Jupiter and 2 μm maps of Venus.

Dr. M. Bruce Fegley is an expert on chemical processes in the outer Solar System, especially well-known for his detailed studies of disequilibrium species in the atmospheres of the Major Planets and for his studies of solar nebula chemistry and its implications for the evolution of outer planet satellites.

Dr. Keith S. Noll is an experienced planetary astronomer, having been a co-discover of carbon monoxide, germane, and arsine in Saturn's atmosphere. He has considerable experience in observing hydrocarbons, particularly C_2H_2 and C_2H_6 , on Jupiter and Saturn.

Dr. Glenn S. Orton has considerable experience in analysis of groundbased astronomical spectra, from spectral observations from the ultraviolet to the far infrared, with primary emphasis on the determination of thermal structures of outer planet atmospheres from radiometric inversions. He has been the Principal Investigator of the Pioneer 10 and 11 Infrared Radiometer experiment at Saturn.

Dr. Harold Reitsema has been observing stellar and satellite occultations since 1960. He is a codiscoverer of satellites of Saturn (Telesto, detected through groundbased observations).



and Neptune (Larissa, discovered through stellar occultation). Dr. Reitsema is a Co on the Giotto Halley Multicolour Camera and the Space Infrared Telescope science teams. He has extensive experience in space instrument design at Ball Aerospace.

7.1 BIBLIOGRAPHICAL INFORMATION

Relevant bibliographical information may be found in Appendix B.

8 INSTITUTIONAL SUPPORT

8.1 PI Support

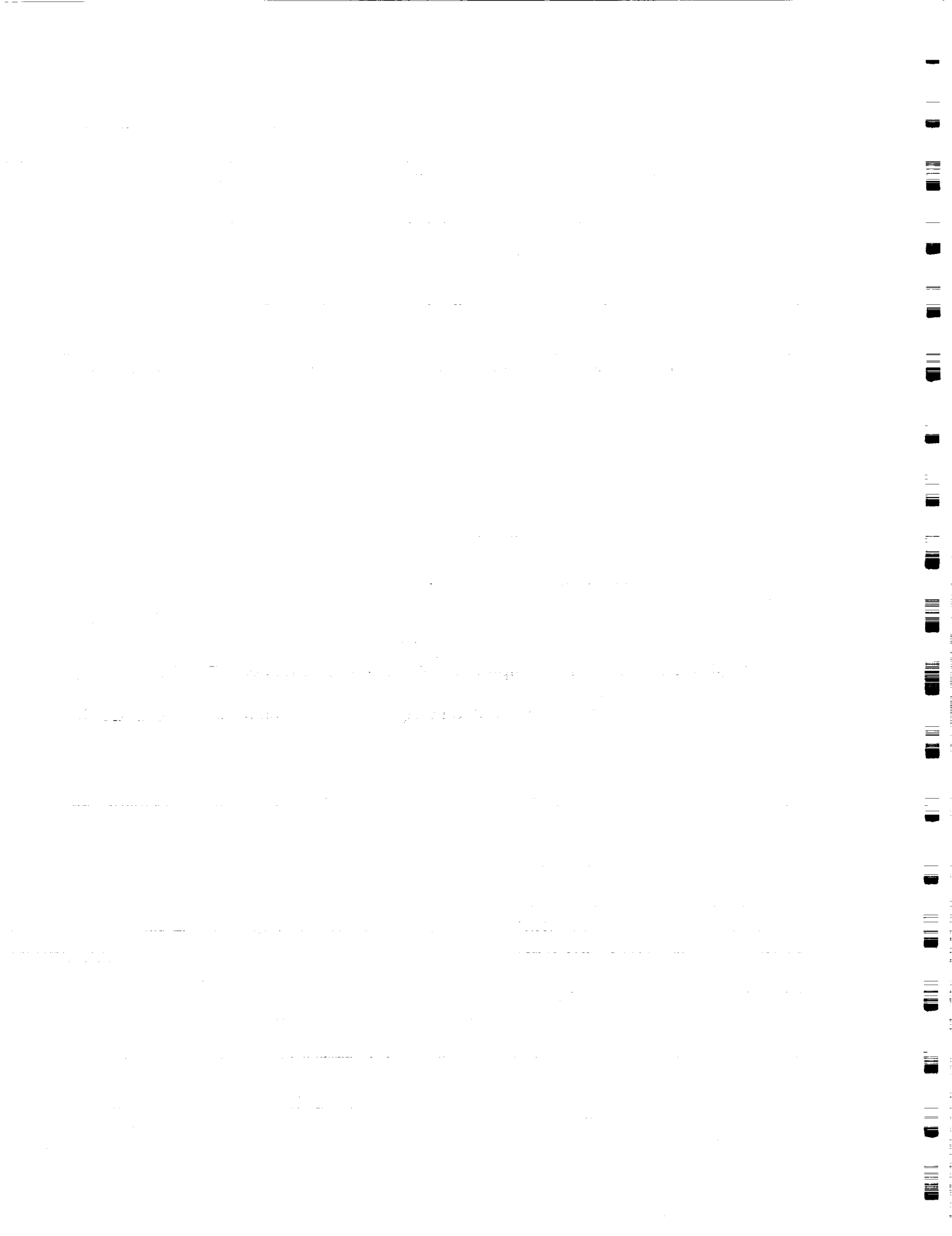
Washington University, St. Louis. Mo., agrees to provide the necessary level of complete satisfactorily and on schedule all aspects of the investigation in this proposal.

References

1. Bar Nunn A. and Podolak N. The contribution by the thunderstorms to the CO, C₂H₂, and HCN on Jupiter. *Icarus*, 64:112-124, 1985.
2. Broadfoot A.J., Sandel D.E., Shemansky J.B., G.R. Holberg, Strobel D.F., Mc Kumar S., and Hunten D.M., Atreya S.K., Dohnahne T.M., Moos H.W., Blamont J.E., Pomphrey R.B., and Linik S. Extreme ultraviolet observations of 1 encounter with Saturn. *Science*, 212:206-211, 1981.
3. M. Allison. Theories for the general circulation of Saturn's atmosphere. In *The of Saturn and Titan*, 1985.
4. Yung Y.L. Photochemistry of the atmosphere of Titan: comparison between observations. *Ap. J. Supp. Ser.*, 55:465-506, 1984.
5. Ingersoll A.P., Beebe R.F., Conrath B.J., and Hunt G.E. *Structure and dynamics atmosphere*, pages 195-238. The University of Arizona, 1984.
6. Bezard B., Drossart P., Lellouch E., Tarrago G., and Maillard J. P. Detection Saturn. *Astrophys. J. Lett.*, 1989. In press.
7. Fegley M. B. and Prinn R. G. Chemical constraints on the water and total oxygen in the deep atmosphere of Jupiter. *Astrophys. J.*, 324:621-625, 1988.
8. Fegley M. B. and Prinn R. G. Equilibrium and non-equilibrium chemistry of atmosphere: implications for the observability of PH₃, N₂, CO and GeH₄. *A* 299:1067-1078, 1985.
9. Fegley M. B. and Prinn R. G. The predicted abundances of deuterium-bearing atmosphere of Jupiter. *Astrophys. J.*, 326:490-508, 1988.
10. Smith B.A. and G.E. Hunt. *Motions and morphology of clouds in the atmosphere* pages 564-585. The University of Arizona, Tucson, 1976.
11. Smith B.A. and *et al.* A new look at the Saturnian system: The Voyager 2 image 215:504-537, 1982.
12. Lutz B.L., de Bergh C., and Owen T. Titan: Discovery of carbon monoxide in its *Science*, 220:1374-1375, 1983.
13. Festou M. C. and Atreya S.K. Voyager ultraviolet stellar occultation measure composition and thermal profiles of the Saturnian upper atmosphere. *Geophys.* 9:1147-1150, 1982.
14. Farmer C.B. and Raper O.F. High resolution infrared spectroscopy from space: report on the results of the Atmospheric Trace Molecule Spectroscopy (ATMOS) on Spacelab 3. In *NASA CP 2429*, 1985.
15. Strobel D.F. Photochemistry of Titan. In *ESA SP-241*, pages 145-148, 1985.

16. Strobel D.F. and Yung Y.L. The Galilean satellites as a source of CO in the Jovian atmosphere. *Icarus*, 37:256-263, 1979.
17. Muhleman D.O., Bergh G.L., and Clancy R.T. Microwave measurements of carbon monoxide on Titan. *Science*, 223:393-396, 1984.
18. Marouf E.A., Tyler G.L., Zebker H.A., Simpson R.A., and Eshleman V.R. Particle size distributions in Saturn's rings from Voyager 1 radio occultation. *Icarus*, 54:189-211, 1983.
19. Bjoraker G. *The gas composition and vertical cloud structure of Jupiter's troposphere derived from five micron spectroscopic observations*. PhD thesis, University of Arizona, Tucson, 1985.
20. Prinn R. G., Larson H. P., Caldwell J. J., and Gautier D. *Composition and chemistry of Saturn's atmosphere*, pages 150-194. University of Arizona Press, 1984.
21. Gautier. The composition of the Titan atmosphere. In *ESA SP-241*, pages 75-81, 1985.
22. Hunt G.E. The meteorology of Saturn. In *ESA SP-241*, pages 33-39, 1985.
23. Morfill G.E., Fechtig H., Grün E., and Goertz C.K. Some consequences of meteroid impacts on Saturn's rings. *Icarus*, 55:439-447, 1983.
24. Bjoraker G.L., Larson H.P., and Kunde V.G. The abundance and distribution of water vapor in Jupiter's atmosphere. *Astrophys. J.*, 311:1058-1072, 1986.
25. Barnes T. H., Eiju T., and Matsuda K. Heterodyned photodiode array Fourier Transform Spectrometer. *Applied Optics*, 25, 1864, 1986.
26. Butcher H., Douglas N., Frandsen S., and Maaswinkel F. A practical non-scanning fts for astronomy, abstracts of OSA topical mtng. on high resolution fourier transform spectroscopy,. Presented in Santa Fe, NM, February 1989.
27. Fizeau H. *Ann. Chim. Phys.*, 66:429, 1862.
28. Caulfield H.J. *Holographic Spectroscopy in Advances in Holography*,. Volume 2, Marcel Dekker, New York, 1976.
29. Larson H.P., Smith H.A. Fink U., and Davis D.S. The middle-infrared spectrum of Saturn: Evidence for phosphine and upper limits to other trace atmospheric constituents. *Astrophys. J.*, 240:327-337, 1984.
30. Hubbard and MacFarlane. Theoretical predictions of deuterium abundances in the Jovian planets. *Icarus*, 676-682, 1980.
31. Lunine J. and Hunten D.M. Moist convection and the abundance of water in the troposphere of Jupiter. *Icarus*, 69:566-570, 1987.
32. Ring J. and Stephens C.L. *Mon. Not. Roy. Astr. Soc.*, 158:5, 1972.
33. Kaye J.A. and Strobel D.F. HCN formation on Jupiter: the coupled photochemistry of ammonia and acetylene. *Icarus*, 54:417-433, 1983.
34. Kaye J.A. and Strobel D.F. Phosphine photochemistry in the atmosphere of Saturn. *Icarus*, 59:314-335, 1984.
35. Pollack J.B., Podolak M., Bodenheimer P., and Christofferson B. Planetsimal dissolution in envelopes of forming giant planets. *Icarus*, 67:409-443, 1986.
36. Connerney J.E.P. and Waite J.H. New model of Saturn's ionosphere with an influx of water from the rings. *Nature*, 312:136-138, 1984.
37. Lunine J.I. Titan's surface: Nature and implications for Cassini. In *ESA SP-241*, pages 83-88, 1985.
38. Cuzzi J.N., Pollack J.B., and Summers A.L. Saturn's rings: Particle composition and size distribution as constrained by observations at microwave wavelengths. II. Radio interferometric observations. *Icarus*, 38:683-705, 1980.
39. Lewis J.S. Electrical discharge synthesis of organic compounds on Jupiter. *Icarus*, 43:85-95, 1980.
40. Kamiya K., Yoshihara K., and Okada K. Holographic spectra obtained with Lloyd's mirror. *Japan. J. Appl. Phys.* 7, 1129, 1968.

41. Rages K. and Pollack J.B. Vertical distribution of scattering hazes in Titan's sphere. *Icarus*, 55:50-62, 1983.
42. Baines K.H. and Smith W.H. The structure of the atmosphere of Neptune. *Icarus*, in press.
43. Flasar M. and Gierasch P.J. Eddy diffusivities within Jupiter. In A. Valance, ed. *Proc. Symposium on Planetary Atmospheres*, pages 85-87, Royal Society of Canada, 1984.
44. Prather M.J., Logan J.A., and McElroy M.B. Carbon monoxide in Jupiter's atmosphere: An extraplanetary source. *Astrophys. J.*, 223:1072-1081, 1978.
45. Douglas N.G., Butcher H.R., and Melis W.A. Heterodyned, holographic spectra of Titan. *Sp. Sci.*, 1990. In press.
46. Toon O.B. and et. al. Methane rain on Titan. *Icarus*, 1988. October.
47. Connes P. Astronomical Fourier spectroscopy. *Ann. Rev. Astron. and Ap.* 8, 1979.
48. Fellgett P. PhD thesis, Univ. Cam., 1951.
49. Jacquinet P. The luminosity of spectrometers with prisms, gratings, or Fabry-Pérot interferometers. *J. Opt. Soc. Am.* 44, 761, 1954.
50. Stone P.H. The meteorology of the Jovian atmosphere. In T. Gehrels, editor, *Jupiter*, page 618, University of Arizona Press, Tucson, 1976.
51. Gierasch P.J. and Conrath B.H. Theoretical predictions of deuterium abundance in the atmospheres of Jovian planets. *Icarus*, 44:676-682, 1985.
52. Courtin R. and et. al. The composition of Saturn's atmosphere at northern latitudes from Voyager IRIS spectra: NH_3 , PH_3 , C_2H_2 , C_2H_6 , CH_3D , CH_4 and D/H isotopic ratio. *Astrophys. J.*, 287:899-916, 1984.
53. Hanel R.A., Conrath B.J., Kunde V.G., Pearl J.C., and Pirraglia J.A. Albedo, flux, and energy balance of Saturn. *Icarus*, 53:262-285, 1983.
54. Samuelson R.E. Clouds and aerosols of Titan's atmosphere. In *ESA SP-241*, 1985.
55. Prinn R.G. and B. Jr Fegley. Kinetic inhibition of CO and N_2 reduction in circumstellar nebulae: Implications for satellite composition. *Astrophys. J.*, 249:308-317, 1986.
56. Noll K. S. Evidence for ash_3 in Saturn. In *Austin DPS*, 1988.
57. Noll K. S., Knacke R.F., Geballe T.R., and Tokunaga A.T. Detection of carbon monoxide in Saturn. *Astrophys. J.*, 309:L91-L94, 1986.
58. Noll K. S., Knacke R.F., Geballe T.R., and Tokunaga A.T. Evidence for germane in Saturn. *Icarus*, 75:409-422, 1988.
59. Atreya S.K. and et. al. *Theory, measurements and models of the upper atmosphere of Saturn*, pages 239-277. The University of Arizona, Tucson, 1984.
60. Dohi T. and Suzuki T. Attainment of high resolution holographic Fourier Transform spectroscopy. *Appl. Opt.* 10, 1137, 1971.
61. Okamoto T., Kawata S., and Minami S. Fourier Transform Spectrometer with a photodiode array. *Appl. Opt.* 23, 269, 1984.
62. Northrup T.G. and Connerney J.E.P. A micrometeorite erosion model and the erosion of Saturn's rings. *Icarus*, 70:124-137, 1987.
63. Barnes T.H. Photodiode array Fourier Transform Spectrometer with improved range. *Appl. Opt.* 24, 3702, 1985.
64. Stroke G. W. and Funkhouser A. T. Fourier transform spectroscopy using holography without computing and with stationary interferometers. *Phys. Letters* 16, 1974.
65. Smith W.H. and Schempp W.V. Digital array scanned interferometers. *Applied Optics*, 1990. In press.
66. Thompson W.R. and et. al. Plasma discharges in $\text{N}_2\text{-CH}_4$ at low pressure: results and application to Titan. *Icarus*, 1990. In press.



A DIGITAL ARRAY SCANNED INTERFEROMETERS

A.1 Theory of Operation

ACM contains an optimized digital array scanned interferometer that provides a high spectral and spatial mapping capability. The incident light collected by the telescope, passes through the beam splitter, transmits to the mirror or grating, returns to the beam splitter, reflects, and is collected by a lens can form the spatial interferogram which is reimaged onto the detector at the correct spatial scale. Since ACM is self-scanned *i.e. it has no moving parts*, a rigid, monolithic construction renders it insensitive to vibrations and thermal effects.

Without moving parts, ACM directly samples a spatially displayed interferogram, providing a faithful representation of the incident spectrum. Digital array scanned interferometers were described more than a century ago by Fizeau (1862). Subsequently, modern digital array scanned interferometers were initiated by Stroke and Funkhouser (1965). Caulfield (1976) reviewed digital array scanned interferometers and their applications in detail, while Kamiya *et al.* (1968), Dohi (1971), Okamoto *et al.*, (1984), Barnes (1985), Barnes *et al.*, (1986), and Smith *et al.* (1990) have demonstrated specific advantages of various forms of self-scanned interferometers. Barnes (1985) has described a source doubling interferometer that uses difference imaging to correct detector pixel-to-pixel response variations for absorption studies against extended sources, an important, key development. Dohi and Suzuki (1971) and Barnes *et al.* (1986) utilized heterodyning methods with digital array scanned interferometers to attain high spectral resolution. Spectral resolving powers of 120,000 have been achieved in a facility using the 3.6 m European Southern Observatory telescope (Butcher *et al.*, 1989). Jet Propulsion Laboratories has developed and patented a self-scanned interferometer (Breckinridge and U.S. Patent No. 4,523,846). Wm. Hayden Smith has an approved patent awaiting issuance. Further, we have now developed specific versions of digital array scanned interferometers with PIDDP support to provide high spectral resolution and high spatial resolution in the 3 to 5.4 μms for the Cassini mission. This long technological history for these systems demonstrates that there is little or no technical risk nor development required for digital array scanned interferometers.

Details of our laboratory research with these instruments is discussed in detail in Smith and Schempp (1989).

The interferogram due to a spectral distribution $S(\sigma)$ is given by (Connes, 1970)

$$I(x) = \int_0^{\infty} S(\sigma)B(\sigma)\{1 + \cos(2\pi\sigma x)\}d\sigma$$

where $B(\sigma)$ includes the instrument transfer functions and the MTF of the array of detectors. The pixel position is measured by x and σ is the spectral frequency (cm^{-1}). In order to perform the Fourier inversion of the interferogram, we extend the frequency to negative values:

$$G(x) = 2I(x) - I(0) = \int_{-\infty}^{\infty} S(\sigma)B(\sigma)e^{2\pi i\sigma x}d\sigma$$

The incident spectrum is computed via the fast Fourier transform from:

$$S(\sigma)B(\sigma) = \int_0^{\infty} G(x)e^{-2\pi i\sigma x}dx$$

In fact, the observed interferogram is a discrete sample of the continuous interferogram. We estimate the spectrum from the observed interferogram:

$$O(\sigma) = F\{[G(x) * II(\frac{x}{b})] III(\frac{x}{a}) II(\frac{x}{c})\}$$

$$O(\sigma) = [S(\sigma) B(\sigma) \text{sinc}(ba)] * III(a\sigma) * \text{sinc}(c\sigma)$$

where we adopt the notation $F[A]$ as the Fourier transform of A , and $*$ is the convolution operator. The top-hat function, $II(\frac{x}{b})$, indicates that the ideal interferogram is integrated over b , the width of a pixel on the CCD. The Shah function or Dirac comb, $III(\frac{x}{a})$, samples the convolved interferogram at a spacing, a , the pitch of the detector array. For many infrared arrays $b < a$. For example, the Rockwell MWIR HgCdTe array we used in our lab studies and are proposing as the detector for ACM has $b = 0.9a$. The sampling of the interferogram with the top hat function rather than a delta function effectively changes the instrument profile from $B(\sigma)$ to $B(\sigma)\text{sinc}(b\sigma)$, so the response of the detector to the interferogram modulation depends upon the width of the pixel, b , compared with the sampling interval, a .

The interferogram cannot be sampled to infinity, but is truncated at a finite value of x , so that the total number, n , of points in a symmetrically sampled interferogram is $(\frac{2\epsilon}{a}) - 1$. We effectively increase the free spectral range for a given spectral resolution by asymmetric sampling. The spectral resolution that is obtained for a wavenumber range between σ_{min} and σ_{max} is equal to the number, N , of elements in the detector for single-sided interferograms. ACM uses a small number of pixels to oversample the highest spatial frequency and to locate the central maximum to symmetrize the interferogram. The number of pixels determining the resolution and bandwidth will be 20% less than the total pixels for the detector length. Spatial sampling of the interferogram divides the incident flux over the N pixels of the detector. The S/N attained in the interferogram is determined by the ratio of the photon flux to the photon, dark, background, and residual detector spatial noise.

ACM has the ideal instrument function, a sinc function, that transmits all frequencies equally up to the cutoff. By comparison, an ideal grating spectrometer's sinc^2 instrument function rapidly attenuates the higher spectral frequencies. Ring and Stevens (1972) showed that spectral profiles measured with two beam Fourier transform spectrometers, such as ACM, achieve a factor of two better effective spectral resolution than grating spectrometers for a given instrumental FWHM or spectral resolving power. In order to achieve the same effective spectral resolution, then, a grating spectrometer must reduce its slit width which decreases its throughput or etendue. Jacquinot (1954) has shown that an interferometer's resolution-luminosity product, $R\Omega$, is several hundred times larger than for an equivalent grating spectrograph, particularly when a long entrance slit as desired here is to be used for a spectral mapping mode. The attained spectral resolution is not constrained by the desired spatial resolution. Therefore, unlike a grating spectrometer, the *spatial* resolution across the aperture of ACM is determined primarily by the imaging, and not the spectral requirements. The ACM design specifically uses this characteristic for the occultation mode.

Fourier Transform Spectrometers (FTS) superimpose all N spectral elements onto the detector simultaneously (Fellgett, 1951). ACM also spatially samples all spectral elements at once and is relatively insensitive to any variations in the incident flux over the integration time. ACM encodes each wavelength so that parasitic and stray light are not reconstructed in the spectrum. This establishes a well defined continuum. Further, all detector pixels are illuminated at a high flux level so that all interferogram pixels are detected at a similarly high S/N. The photometric accuracy is then determined from the photon noise, detector dark current, read noise, background flux, and residual pixel-to-pixel wavelength response variations after photometric correction. ACM efficiency is essentially constant for the selected wavelength bands required for the science goals. The detected quantum efficiency of ACM reaches approximately 10% at $5.2 \mu\text{m}$ providing the efficiency and sensitivity to achieve our high spectral resolution science goals for Cassini.

For photon noise limited interferograms, the S/N for the transformed spectrum is $s(kn)^{-1/2}$, where s is the signal flux, n is the system noise, and k is the number of spectral elements. Because of the Jacquinot advantage, ACM achieves a throughput advantage and thus an increased signal flux, s , equal to hundreds of times that for an equivalent aperture grating monochromator. For ACM, k is near 200, assuming a worst case flat input continuum. (see details of S/N calcula-

tion in radiometry section). The increased throughput compensates for the number of elements so that the physically smaller ACM, compared with an equivalent high resolving monochromator, reaches an equal measured S/N in a given observational time. In addition, the advantage of a simple, no-moving parts instrument design and a super-resolution function. Since ACM is cooled to 100K to reduce its emissivity at 5 μm , its size, weight, and dissipated power and consequent minimal heat load is an important, even advantage.

A.2 Heterodyning

ACM attains high spectral resolution by spectral heterodyning. Heterodyning lowers the frequency of interest into a frequency appropriate for optimal sensing with a HgCdTe MWIR focal plane array. The desired spectral resolution times the number of elements, N , then, equals the number of spectral elements which may be simultaneously sensed without confusion. This method has been developed and demonstrated for over two decades (Dohi and Suzuki(1971), Barnes *et al.*, (1986) and Butcher *et al.*, (1989). Butcher *et al.* constructed a facility instrument for the European Southern Observatory 3.6-m telescope on a heterodyned interferometer like to that proposed here. That instrument routinely achieves a spectral resolution of over 120,000, far in excess of that we require here.

In the spectral heterodyning case, the interferogram becomes :

$$S(\sigma - \sigma')B(\sigma - \sigma') = \int_0^\infty G(y)e^{-2\pi i(\sigma - \sigma')y} dy$$

or

$$O(\sigma - \sigma') = (S(\sigma - \sigma')B(\sigma - \sigma')\text{sinc}(b\sigma - b\sigma')) * III(a\sigma - a\sigma') * \text{sinc}(c\sigma - c\sigma')$$

where σ' is the heterodyning frequency, corresponding to zero frequency on the detector. The fringe frequency on the array is given by (from the grating equation for small angles)

$$f = 2(|\sigma - \sigma'|) \tan \theta$$

where the Littrow wavenumber is σ , and the fringe frequency varies linearly on the detector with increasing wavenumber. This characteristic permits the number of fringes on the array to be controlled by the selection of the correct Littrow angle.

The resolving power in ACM is given simply by (Douglas *et al.*, 1990)

$$R = \frac{\sigma}{\delta\sigma} = \frac{2\sigma(W) \sin(\theta)}{1.2}$$

Thus, ACM attains a spectral resolution equal to essentially the full resolving power of a grating, but retains the throughput advantages of an interferometer.

An interference filter in the optical beam limits the incident optical bandpass to pass only the desired frequency in the interferogram. Filters with 2% bandpasses are required for the high resolution of ACM to match the free spectral range. These elements are strip interference filters deposited on a common substrate with three passbands, at 3.0, 4.7, and 5.2 microns. Such filters have been developed and qualified for space flight.

A.3 Laboratory Results for ACM

Interferometric observations with a lab prototype have substantiated the proposed design of ACM. We have found the instrument to be very stable, easily aligned, and to produce high quality results routinely. Fig. 23 shows an interferogram for a single vertical spatial frequency. The image of the entrance aperture illuminated with a broad band white light source

this interferogram, Fig. 24 shows the expected black body distribution, modified by the quantum efficiency variations of the virtual phase CCD. Fig. 25 shows the spectrum from the Hg lamp interferogram in Fig. 28 and demonstrates the broad wavelength range that can be sensed, from 10,000 cm^{-1} to more than 40,000 cm^{-1} here. Fig. 26 is an interferogram taken from Fig. 28 for a LED source coplanar with the Hg lamp described above. This source is a narrow band continuum, similar to the case of the 3 and 5- μm spectra to be observed with ACM. Fig. 27 is the FFT of the interferogram of the LED, and shows a typical LED profile. Spatial resolution is important in ACM science and is demonstrated here for two sources, a HG lamp and a LED at the focal plane. High spectral resolution is an important feature of ACM and is demonstrated in Fig. 29 for a prototype ACM, observing the solar spectrum through a sodium line filter. The resultant spectrum obtained by FFT of the interferogram is shown in comparison with the KPNO solar atlas spectrum degraded to the same spectral resolution. This validates the heterodyne method. The attained S/N agrees with the simple formula given above to within a few percent. Fig. 30 contains the offset, central portion of an interferogram of a continuum source viewed through a 4.67 micron filter (80 cm^{-1} passband) with the lab prototype. The central peak is marked with a dot. The spatially displayed interferogram, on the two-dimensional 4.7 micron MWIR Rockwell array, is shown on the bottom of the figure. These data show that every aspect of the proposed ACM interferometer works as proposed and is ready for implementation.

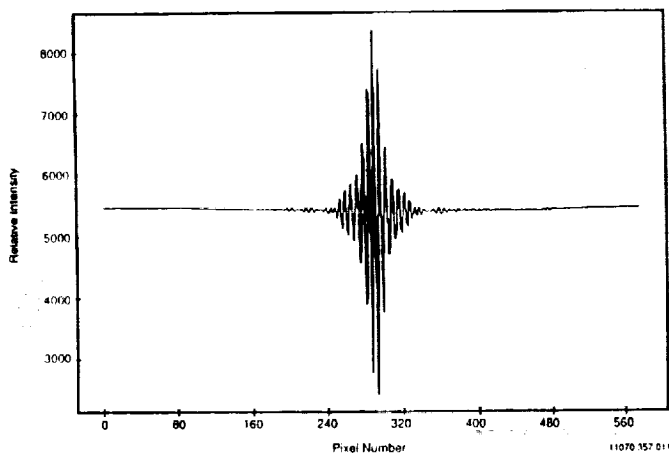


Figure 23: ACM's digital array scanner produces the spatially displayed interferogram by the superposition of the flux from all wavelengths simultaneously. Here, a traceogram, representing a single vertical scan of a broadband light source, is shown.

Figure 24: The Fourier transformation of the interferogram from Fig. 23 for a white light source, a tungsten lamp operated at low current, has a spectral long wavelength limit due to the silicon CCD response cutoff and a short wavelength limit due to the rapidly declining flux from the tungsten lamp. The characteristic quantum efficiency variations of a virtual phase CCD are superimposed on the black body spectrum of the tungsten lamp. The dynamic range of the virtual phase CCD is similar to that of the NICMOS arrays to be used in ACM, so that broadband measurements are clearly feasible with ir arrays. A corollary is that the much smaller wavelength band to be sampled with ACM will use a smaller fraction of the dynamic range of the array for ACM's spectroscopic measurements.

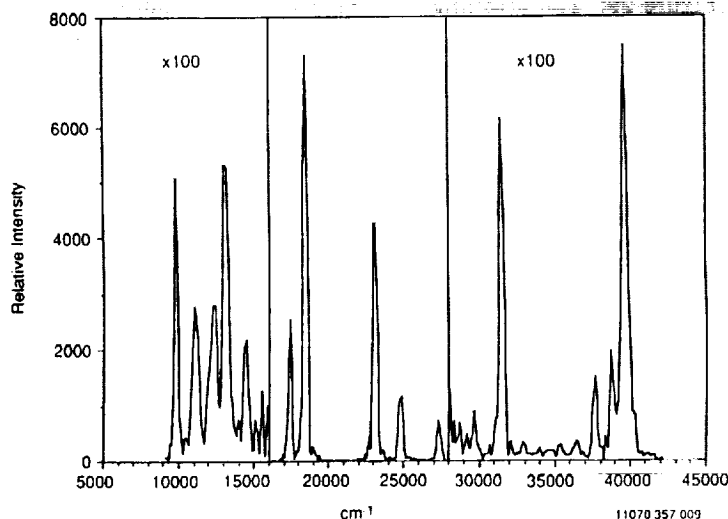
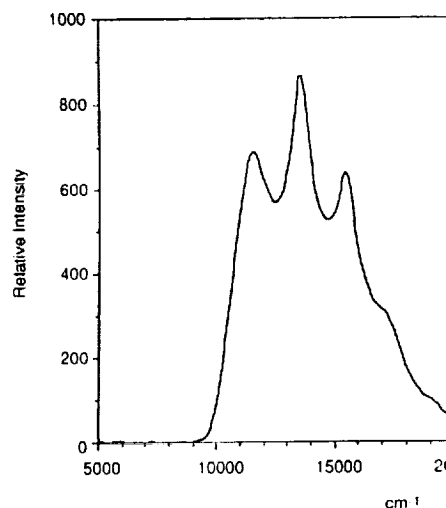


Figure 25: The mercury spectrum plot was obtained from the FFT of a single element of the Hg interferogram showing the spectrum illustrates the ability of digital interferometers to provide high quality spectra over broad wavelength intervals. In this case, the bandwidth is limited only by the wavelength range of the array detector and by the transmission components.

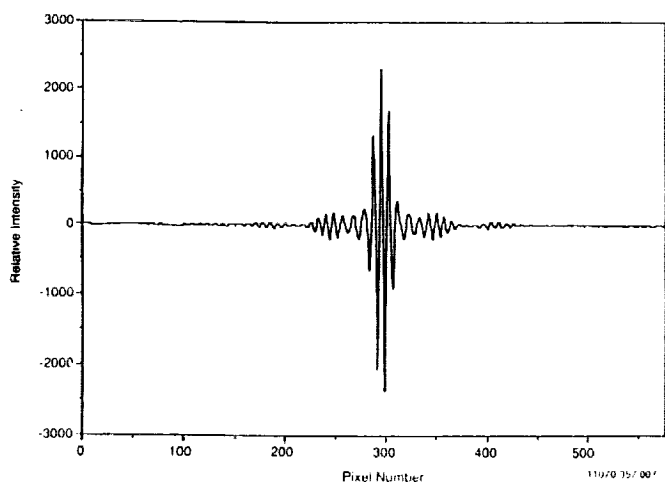


Figure 26: An example interferogram for a narrow band continuum source, an LED, taken from a single spatial pixel of Fig. 28, is characteristic of a narrow bandwidth but continuous spectral source. Since narrow bandwidth continua place lower demands on the dynamic range of the detector array, a correspondingly improved spectrum is obtained in the transform. This is a result of reducing the number of spectral elements being simultaneously superimposed to form the interferogram as described in the text.

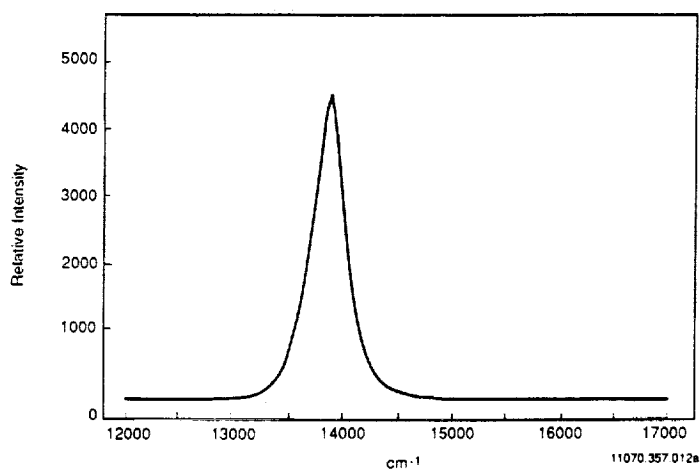


Figure 27: The LED spectral profile transformed from the interferogram shown in the preceding figure is a narrow band continuum source, analogous to the 5 micron and 3 micron narrowband continua ACM utilizes in attaining high spectral resolution.

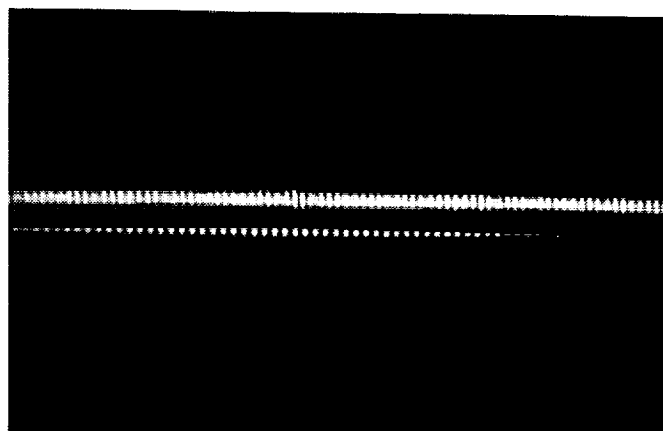


Figure 28: ACM achieves high spatial resolution along the entrance aperture as demonstrated here. This interferogram was obtained with a Hg placed above an LED lamp in the aperture. The spatial resolution is limited only by optical considerations and the detector dimensions (ie. pixel size). The interferograms may be treated independently or may be summed to increase the signal to noise.

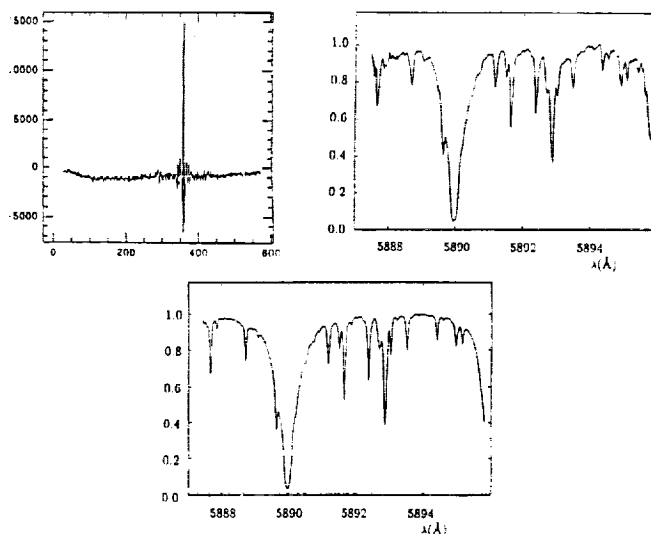
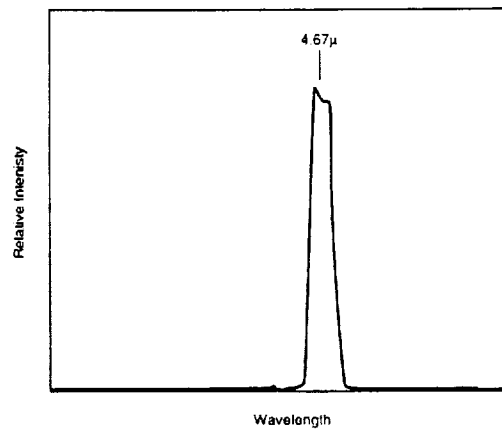
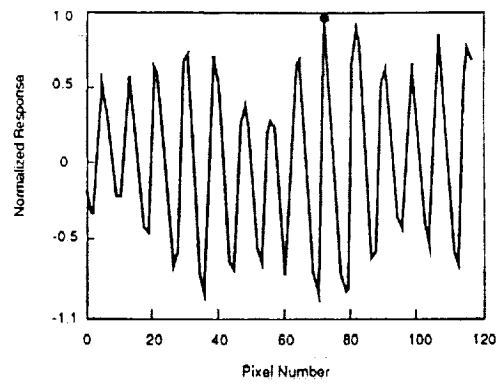
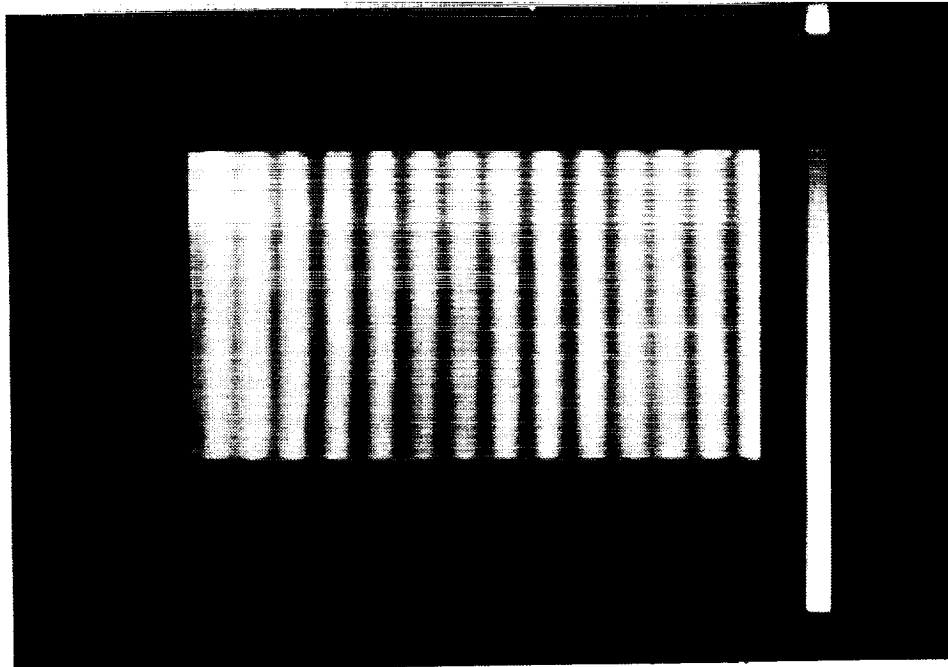


Figure 29: The attainment of high spectral resolution is shown here for an interferometer like ACM, but for visible wavelengths. The interferogram in the left portion of the figure is formed from the band limited input. The spectral resolving power is over 120,000 in the spectrum shown in the top right hand panel and includes the solar Fraunhofer Na I D2 line at 5890 Å. A comparison solar spectrum obtained from the KPNO solar atlas, also obtained with an FTS and convolved with a rectangular filter to degrade the spectral resolution to that of the measured profile is plotted. The spectra are equal to within the S/N, demonstrating the validity of the method. A spectral resolution of 120,000 at 0.5 microns is more difficult to obtain than a spectral resolution of 10,000 at 5 microns since the interferometer stability requirements are greatly reduced by the 10-fold increase in wavelength.



11070/357.047



11070/357.053

Figure 30: The infrared ACM uses a Rockwell HgCdTe MWIR array similar to that we have been. This figure shows the central portion of an interferogram obtained for a 4% 4.67μ filter with a 128 HgCdTe array similar to that proposed for ACM. The central peak is off set from the center (small ball). This interferogram was obtained to provide a spectral profile for the blocking filter limits the input radiation to ACM. That profile is shown in the middle part of the figure. The lowest dimensional array image of the interferogram prior to extraction as a row interferogram as shown at

1. The first part of the document is a list of the names of the members of the committee.

2. The second part of the document is a list of the names of the members of the committee.

3. The third part of the document is a list of the names of the members of the committee.

4. The fourth part of the document is a list of the names of the members of the committee.

5. The fifth part of the document is a list of the names of the members of the committee.

6. The sixth part of the document is a list of the names of the members of the committee.

7. The seventh part of the document is a list of the names of the members of the committee.

8. The eighth part of the document is a list of the names of the members of the committee.

9. The ninth part of the document is a list of the names of the members of the committee.

10. The tenth part of the document is a list of the names of the members of the committee.

11. The eleventh part of the document is a list of the names of the members of the committee.

12. The twelfth part of the document is a list of the names of the members of the committee.

13. The thirteenth part of the document is a list of the names of the members of the committee.

14. The fourteenth part of the document is a list of the names of the members of the committee.

15. The fifteenth part of the document is a list of the names of the members of the committee.

B SELECTED BIBLIOGRAPHIES OF INVESTIGATOR

The short bibliographical listing here specifies only those most prominent publications to the proposed ACM investigation.

B.1 Dr. William Hayden Smith

Smith, Wm. Hayden, T. McCord, and W. Macy (1981). Inhomogeneous Models of the Atmosphere from Spatially Resolved Line Profiles for CH₄ at 6196.8Å. *Icarus* **46**, 21-32.

Smith, Wm. Hayden, and W. V. Schempp (1990). Digital Array Scanned Interferometry. *App. Opt.*, in press.

B.2 Dr. Kevin H. Baines

Baines, K. H., W. H. Smith, and C. Alexander (1989). Spatial and temporal variations in abundance and cloud structure in the Jovian troposphere derived from CCD/Coudé spectroscopy. In *Time-Variable Phenomena of the Jovian System* (Belton, West, and Rahe, eds.) NASA Publication 494, 363-370.

B.3 Dr. Gordon L. Bjoraker

G. L. Bjoraker, H. P. Larson, U. Fink, and H. A. Smith (1981). A study of ethane in the 3 micron region. *Astrophys. J.*, **248**, 856-862.

G. L. Bjoraker, H. P. Larson, and V. G. Kunde (1986). The abundance and distribution of water vapor in Jupiter's atmosphere. *Astrophys. J.*, **311**, 1058-1072.

B.4 Dr. Pierre Drossart

P. Drossart, T. Encrenaz, and A. Tokunaga (1984). Variability of phosphine on Jupiter. *Icarus* **60**, 613-620.

B. Bezard, P. Drossart, E. Lellouch, G. Tarrago, J. P. Maillard (1989). Detection of phosphine on Saturn. *Astrophys. J. Lett.* In Press.

B.5 Dr. M. Bruce Fegley

J. S. Lewis and M. B. Fegley, Jr. (1984). Vertical distribution of disequilibrium species in the Jovian troposphere. *Space Sci. Revs.* **39**, 163-192.

M. B. Fegley, Jr. and R. G. Prinn (1985). Equilibrium and non-equilibrium chemistry in Saturn's atmosphere: Implications for the observability of PH₃, N₂, CO, and GeH₄. *Icarus* **299**, 1067-1078.

M. B. Fegley, Jr. and R. G. Prinn (1988). Chemical constraints on the water and carbon abundances in the deep atmosphere of Jupiter. *Astrophys. J.* **324**, 621-625.

M. B. Fegley, Jr. and R. G. Prinn (1988). The predicted abundances of deuterium-bearing gases in the atmospheres of Jupiter and Saturn. *Astrophys. J.*, **326**, 490-508.

B.6 Dr. Keith S. Noll

K. S. Noll, R. F. Knacke, A. T. Tokunaga, J. H. Lacy, S. Beck, and E. Seravyn (1988). Abundances of ethane and acetylene in the atmospheres of Jupiter and Saturn. *Icarus* **77**, 1-12.

K. S. Noll, R. F. Knacke, T. R. Geballe, and A. T. Tokunaga (1988). Detection of carbon monoxide in Saturn. *Astrophys. J. (Letters)* **309**, L91.

K. S. Noll, R. F. Knacke, T. R. Geballe, and A. T. Tokunaga (1988). Evidence for GeH_4 in Saturn. *Icarus* **75**, 409.

K. S. Noll, T. R. Geballe, and R. F. Knacke (1989). Arsine in Saturn and Jupiter. *Astrophys. J. (Letters)* **338**, L71.

B.7 Dr. Glenn S. Orton

G. S. Orton and A. P. Orton (1981). Saturn atmospheric temperature structure and heat budget. *J. Geophys. Res.* **85**, 5871-5881.

West, R. A., G. S. Orton, B. T. Draine, and E. A. Hubbell (1989). Infrared absorption features for tetrahedral ammonia ice crystals. *Icarus* **80**, 220-223.

B.8 Dr. Harold J. Reitsema

Reitsema, H. J., R. F. Beebe, and B. A. Smith (1976). Azimuthal brightness variations in Saturn's rings. *Astron. J.* **81**, 209.

Reitsema, H. J. (1978). Photometric confirmation of the Encke division in Saturn's Ring A. *Nature* **272**, 601.

Reitsema, H. J., B. A. Smith, and S. M. Larson (1980). A new Saturnian satellite near Dione's L_4 point. *Icarus* **43**, 116.

Hubbard, W. B., D. M. Hunten, H. J. Reitsema, N. Brosch, Y. Nevo, E. Carreira, F. Rossi, and L. H. Wasserman (1990). Results from the occultation of 28 Sgr by Titan's atmosphere. *Nature*, in press.

INSTRUMENT FACT SHEETS

Atmospheric Chemistry Mapper

1 Proposer Identification

Name of Instrument: Atmospheric Chemistry Mapper

Name of Proposer: Washington University

Address: Dept. of Earth and Planetary Sciences

Telephone Number: (314) 889-5638

FAX Number: (314) 726-7361

Date: February 5, 1990

2 Description

2.1 General Description

1. Science Objective, Targets, and Measurements

The Atmospheric Chemistry Mapper (ACM) provides high resolution spectral measurements in the 3-5 μm region. ACM makes brightside measurements of gaseous absorptions under solar illumination, and darkside measurements against the planet's blackbody emission. ACM thus provides clues to Saturnian atmospheric processes, its planetary evolution, Titanian atmospheric processes, its origin and evolution, and the rings' origin and evolution.

2. Key Instrument Interfaces

The Atmospheric Chemistry Mapper (ACM) is a simple, compact, and reliable Fourier Transform Infrared (FTIR) spectrometer. It has no moving parts. It is designed to be mounted on the High Precision Scan Platform (HPSP), co-aligned with the other optical instruments. It uses a completely passive radiative cooling system.

Table 1 shows key ACM specifications.

2.2 Instrument Development Approach Description

1. Design Approach

(a) Heritage

ACM is a Fourier Transform Spectrometer (FTS) equivalent in principle to other instruments which have been so successfully utilized in planetary exploration, including IRIS (Voyager) (Hanel, 1983), and ATMOS (Farmer and Rupert, 1986).

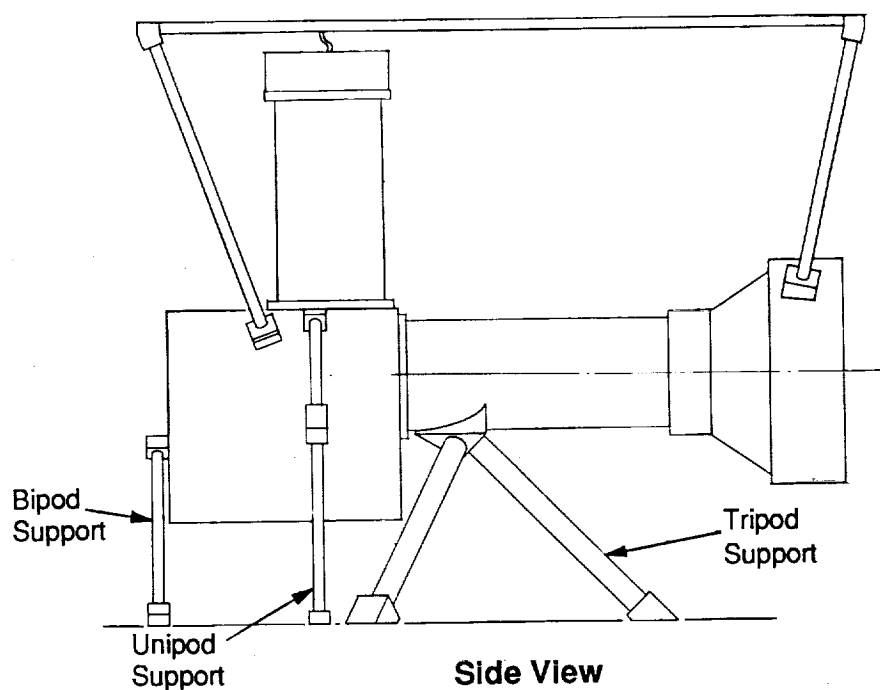
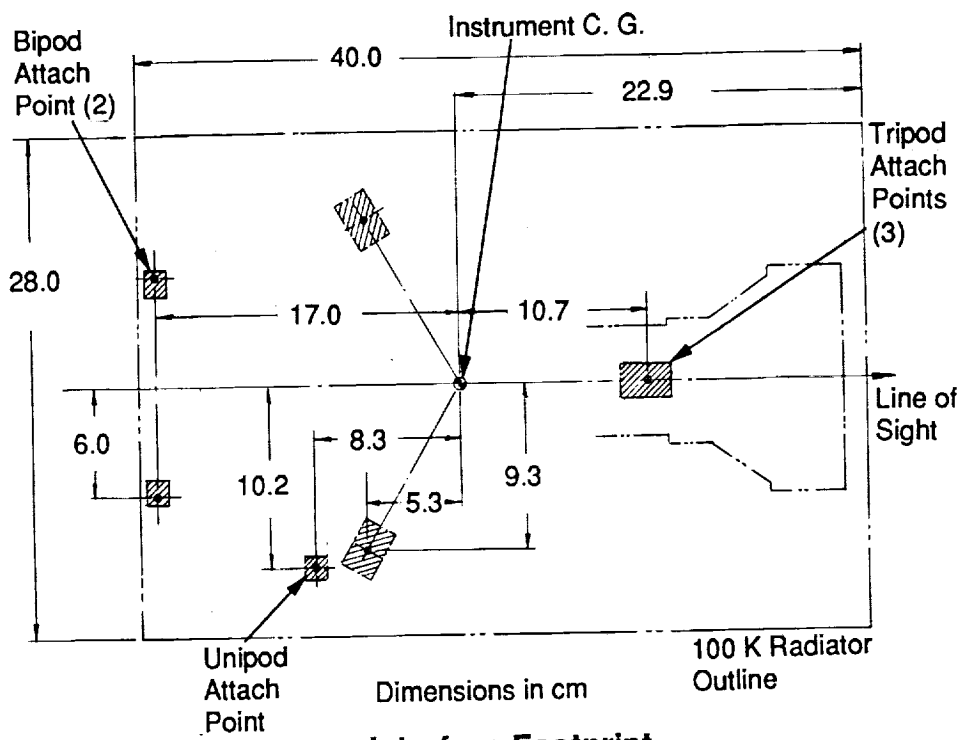
(b) Heritage Extent/Development

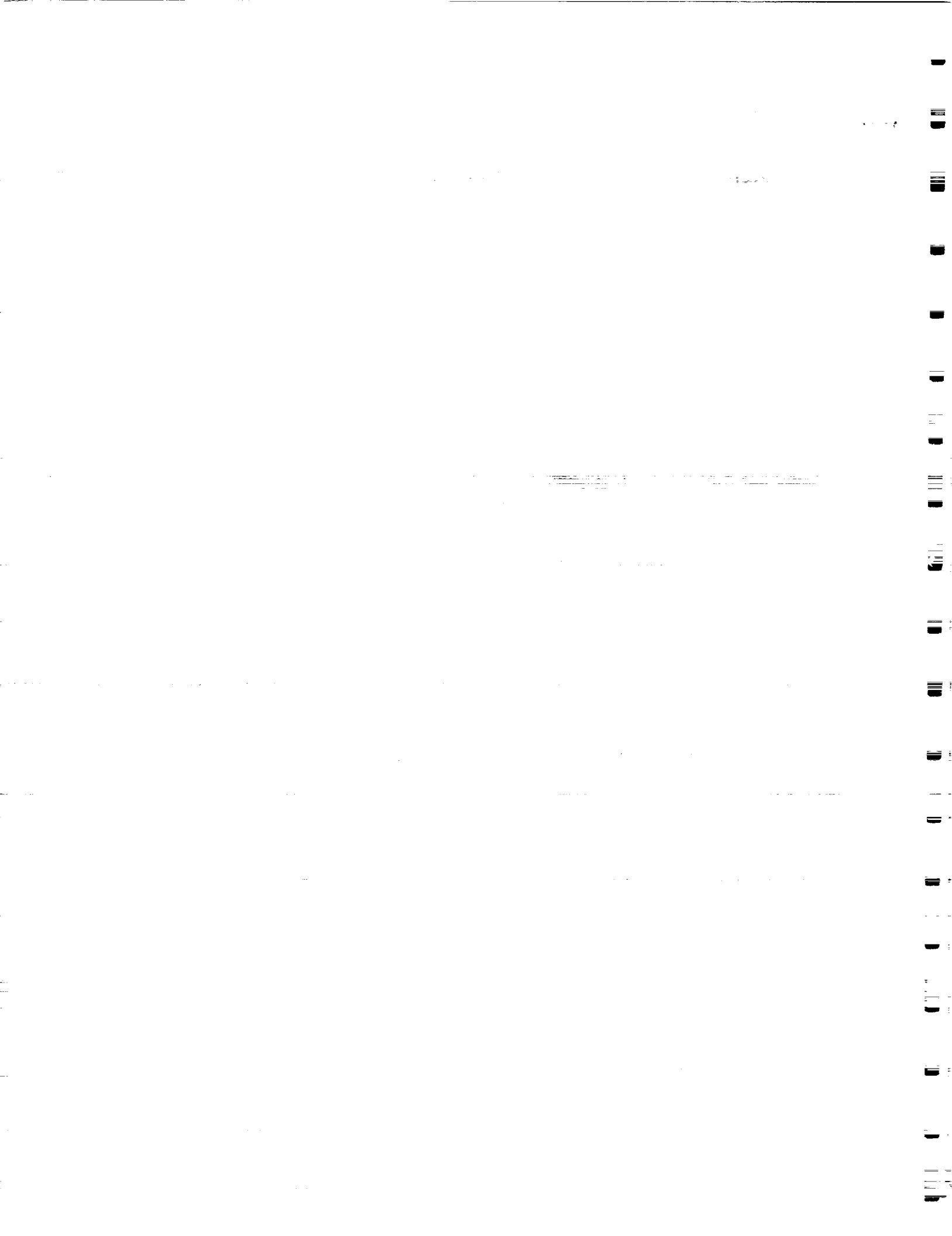
Digital array scanned interferometric principles were described more than 100 years ago by Fizeau (1862). Subsequently, modern development was initiated by Fellgett (1962), Funkhouser (1966). Caulfield reviewed digital array scanned interferometric applications in detail, while Kamia et al. (1971), Dohi and Suzuki (1972).

Table 1: ACM's key specifications

location:	HPSP
moving parts:	none
covers:	none required, dust insensitive
main aperture:	100 mm diameter, f/2, achromat
auxiliary aperture:	1.5 mm window slit
contamination:	main and aux element heaters sealed optics insensitive radiators
FOV, total:	1.2×102 mrad
FOV, ea. channel:	1.2×34 mrad
IFOV:	1.2×0.4 mrad
number of spectral channels:	3
spectral resolution:	0.2 cm^{-1} , all channels, nominal
channel 1, H ₂ O	$\sigma = 1885 - 1940 \text{ cm}^{-1}$, nominal
channel 2, CO	$\sigma = 2123 - 2168 \text{ cm}^{-1}$, nominal
channel 3, "3 μm "	$\sigma = 3255 - 3300 \text{ cm}^{-1}$, nominal
Exposure time for:	
SNR = 25	50 secs. (5 exp. of 10 secs)
SNR = 100	800 secs. (80 exp. of 10 secs)
interferometer:	Michelson with grating
detector:	256 \times 256 staring 3.0-5.3 μm HgCdTe array
detector temperature:	60K
detector cooling:	passive radiator, 400cm ²
instrument cooling:	passive radiator, 400cm ²
radiator surfaces:	$\epsilon \geq 0.85$, $\alpha \approx 0.9$ (black)
instrument/telescope temperature:	110K
mass:	<5.5Kg, including electronics
dimensions:	40cm \times 28cm \times 12cm, excluding electronics 15cm \times 15cm \times 9cm, electronics
power requirements:	<5 watts average, instrument +8 watts, heaters, when energized
processor:	SA3300
commanded data:	detector control parameters
housekeeping data:	temperatures, time of observation
output data:	raw detector image data
data rates:	<200 Kbps peak, <20 Kbps mean, typ.
EMI sources:	DC/DC converter
EMI receptors:	A/D converter

FOLDOUT FRAME





2. FOLDOUT FRAME

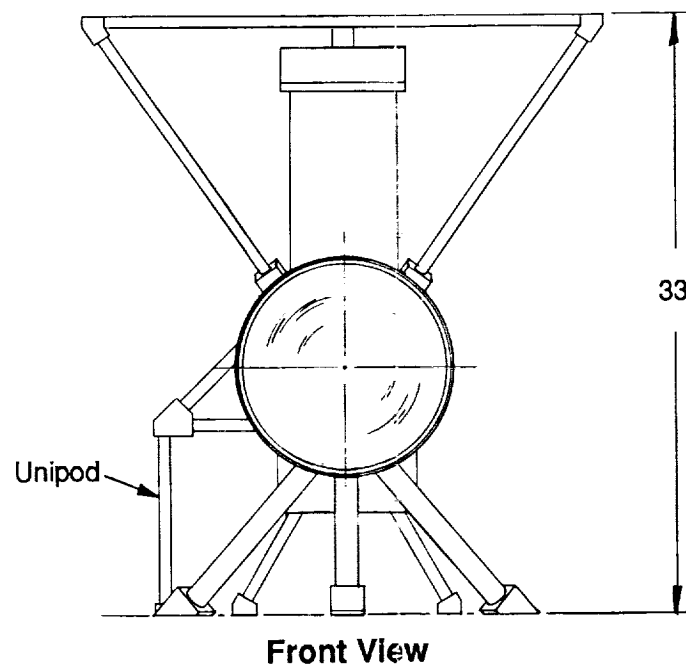
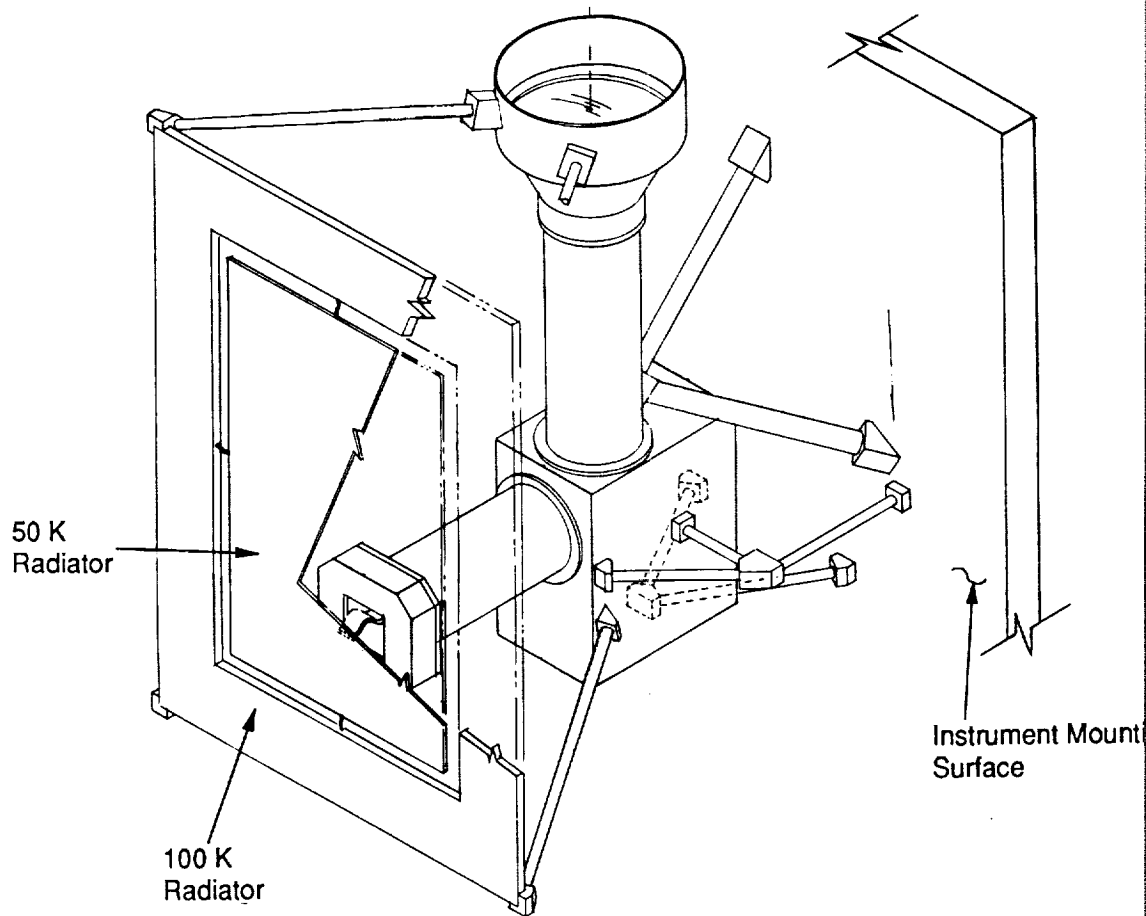


Figure 1: ACM mechanical configuration. The 50K radiator for the detector is placed inside a 100K radiator for the instrument case. The mounting structure minimizes heat leakage from wall to the instrument and detector. The electronics enclosure is not shown. The auxiliary occultation observations is shown.

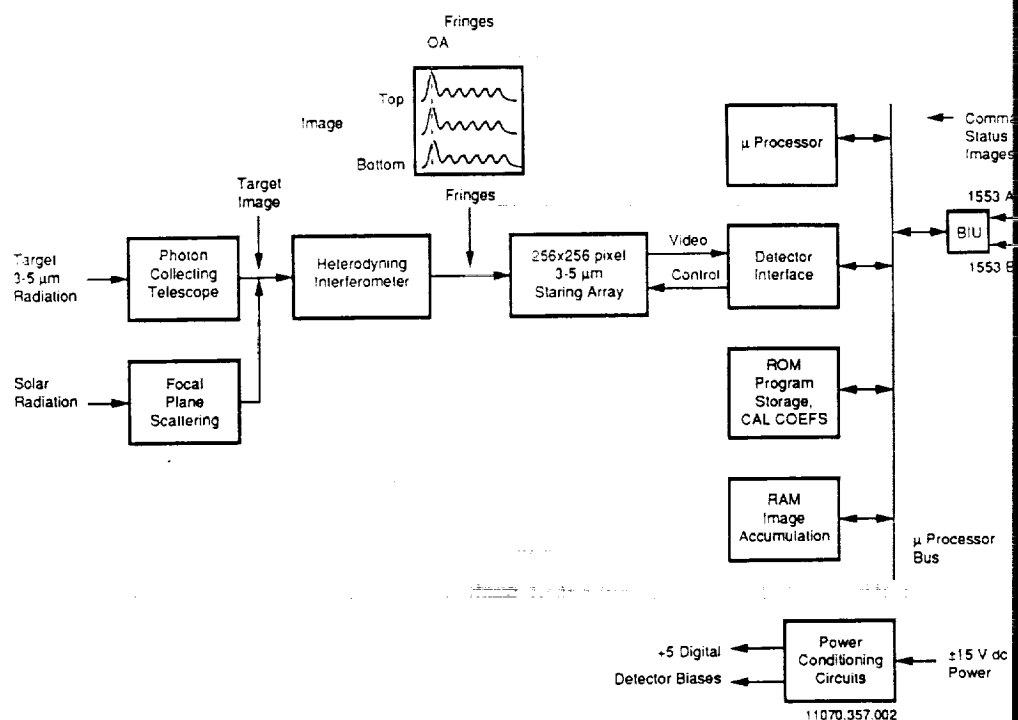


Figure 2: ACM block diagram. The instrument can be thought of as an infrared camera of 256×256 pixels coupled to a spectrometer that forms fringes on one axis and images on the other. There are no moving parts. Occultation flux enters through the auxiliary optical port.

et al. (1984), Barnes (1985), Barnes et al. (1986), and Smith and Schmitt (1986) have demonstrated specific advantages of various forms of self-scanned interferometers. Barnes (1985) has described a source doubling interferometer that uses heterodyning to correct detector pixel-to-pixel response variations for absorption against continuum sources, an important key development. Dohi and Suzuki (1986) et al. have utilized heterodyning methods with digital array scanned interferometers to attain high spectral resolution. Spectral resolving powers of 120,000 have been achieved in a facility instrument for the 3.6 m European Southern Observatory telescope (Schmitt et al., 1990). Jet Propulsion Laboratories has developed and patented a self-scanned interferometer (Breckinridge and Callaghan, U.S. Patent No. 4,523,846). V. Smith has an approved patent awaiting issuance. Further, we have now developed specific versions of digital array scanned interferometers with PIDDP support for high spectral resolution and high spatial resolution in the mid-infrared (3 to 5 μm) for the Cassini mission.

Details of our laboratory research with these instruments are discussed in Dohi and Schempp (1990).

(c) Hardware/Software Description

ACM is a specialized digital array scanned interferometer. Figure 2 shows the block diagram. Figure 3 shows ACM's optical path.

In the ordinary observation mode, incident light collected by the telescope is directed to a Michelson interferometer with a grating in one arm. Light at the grating wavelength forms a zero spatial frequency fringe at the interferometer output, which is imaged on a 3 - 5 μm staring 256×256 detector array.

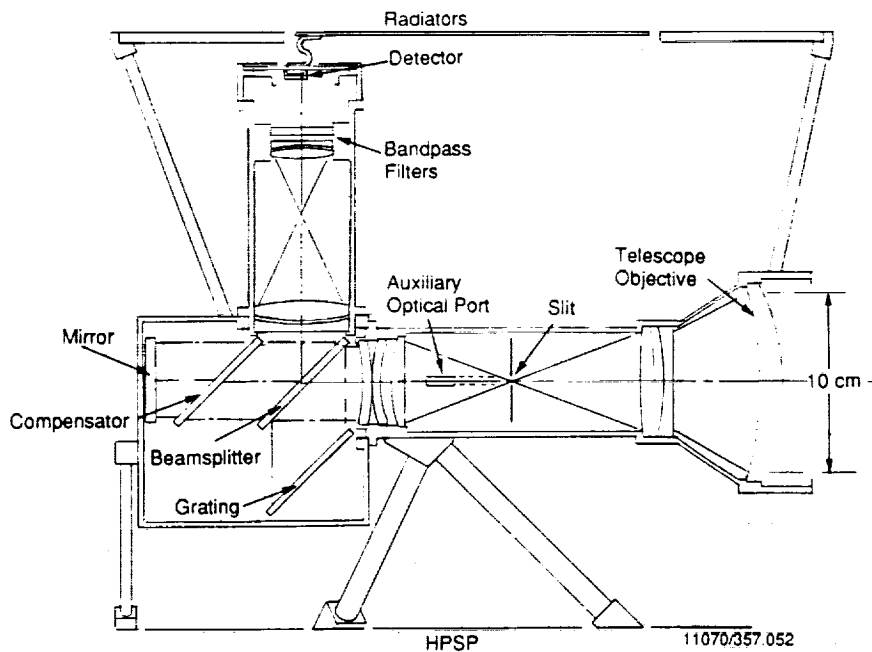


Figure 3: ACM's optical path. 3 - 5 μm light is collected with a 10 cm f/2 telescope, passes through a slit and on to an interferometer with a grating in one arm. Light at the Littrow wavelength forms zero spatial frequency fringes on the detector.

ACM attains a spectral resolution of over 10^4 by heterodyning, and bandpass limiting with two percent bandpass interference filters placed near the detector. ACM attains a spectral resolution equal to essentially the full resolving power of the grating, but retaining the throughput advantages of an interferometer, i.e. an aperture limits the field of view to the desired spatial elements.

In the solar occultation observation mode, sunlight enters through the auxiliary window, and is reflected into the spectrometer with small spherical reflectors placed next to the slit.

An associated electronics module, shown in Figure 4, is based on a SA3300 processor. It has several functions:

- Control and readout of the detector. Control is basically three clock lines in the horizontal and three in the vertical direction, to select a particular row and column address. Correlated double or triple sampling is accomplished in software. Bias voltages are programmable for flexibility in operation.
- Command, status, and buffered data to the BIU and S/C telemetry. Redundant BIU channels are implemented. Detector control parameters are commandable.
- Control of the telescope objective and auxiliary window heaters via telemetry and solid state switches.

2. Testing Approach

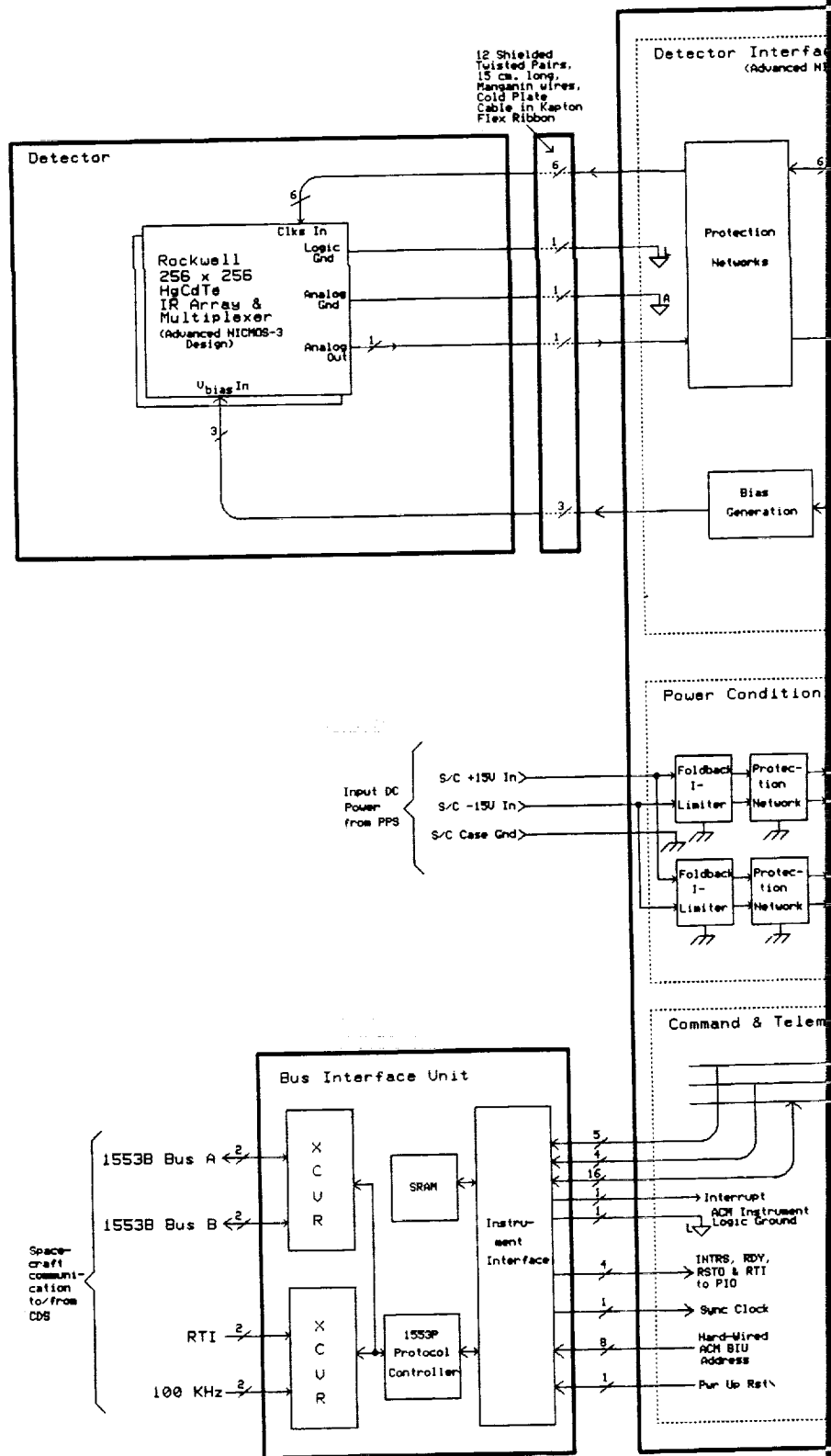
(a) Support Equipment: Common vs. shared

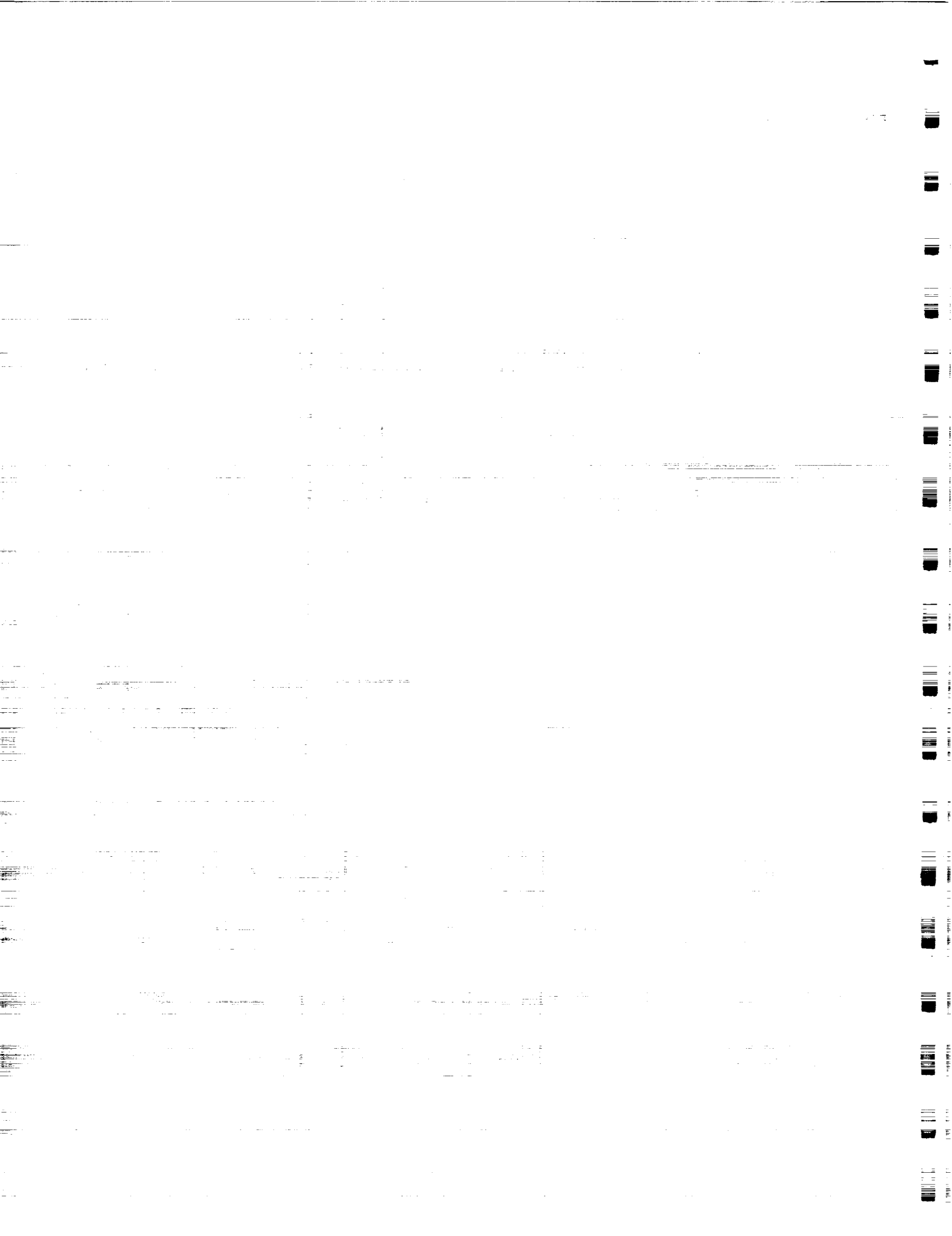
Final tests for ACM require simulating a 4K space environment, as well as a source of monochromatic collimated light, ideally at three wavelengths between 3 and 5 μm , one for each spectrometer channel.

ACM requires common cryogenic test equipment, such as LN2 dewars and vacuum pumps. It further requires common IR test equipment, such as blackbody sources, gas cells, collimating/focussing lenses, and apertures.

(b) Test Methodology

FOLDOUT FRAME





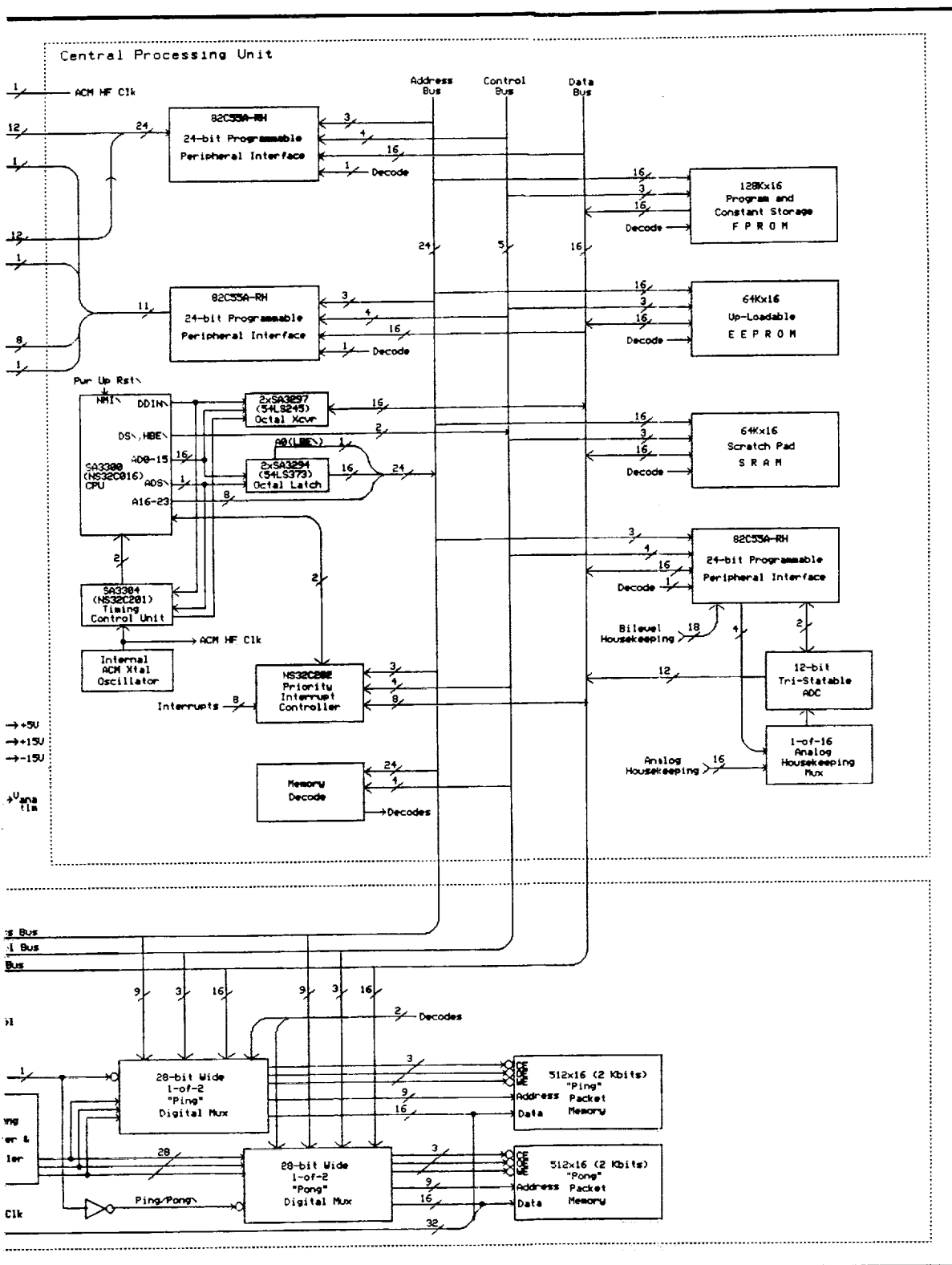


Figure 4: ACM employs microprocessor controlled electronics. Uplinked commands may be stored. Redundant DC/DC converters are employed for reliability. A standard interface with the simple interface with the detector is anticipated.

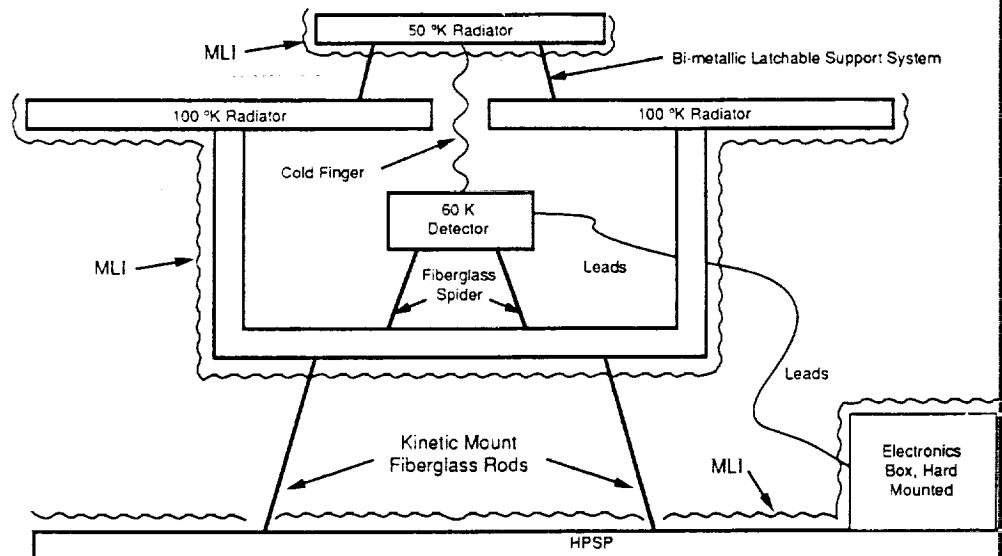


Figure 5: ACM's thermal structure. High thermal isolation between the warm HPSP mounting and the instrument is essential, and similarly between the instrument and detector.

Component level tests rely heavily on manufacturers. E.g. Rockwell characterizes detector parameters such as dark current, quantum efficiency, fixed pattern noise, well, gain, and yield. Optics houses characterize spectral transmissivity and aberrations and surface quality. PWB manufacturers provide continuous screening. Manufacturers also provide quality, reliability, and screening services including temperature testing and cycling. Ball routinely performs form, fit, and receiving inspection on all components.

Ball performs extensive module level testing. Mechanical parts made at Ball are tested for structural faults. The electronics module is tested using a simulated detector. The detector is tested using a simulated electronics module, easily implemented in the computerized IR Detector Evaluation Laboratory. The S/C interface is tested from hardware and software viewpoints using a S/C 1553 bus simulator. The interferometer, and re-imaging optics are tested individually and collectively with breadboard/brassboard sources, lenses, and apertures. Optics are tested with breadboard/brassboard detectors similar to flight models.

3. Instrument Design Description

(a) Context

ACM mounts on the HPSP, co-aligned with the other instruments. Figure 1 shows the physical outline of ACM. Not shown is an electronics module which is hard-mounted to the HPSP under its MLI blanket. Figure 2 shows ACM's major functional components, which consists of a photon collecting telescope, an auxiliary window for solar occultation, an interferometer, detector, and electronics. As shown in Figure 5, one radiator is for the optics (i.e. the instrument case), and one for the detector. ACM has a mechanical, thermal, and electronic interface with the HPSP.

i. Instrument Boundaries

Figure 1 shows the mechanical interface between ACM and HPSP. ACM is mounted along any of HPSP's three walls. It has been designed to be mounted in any of the three walls; it may be easily mounted between two other instruments.

The optical axis of ACM must be co-aligned with other instruments, within 100 mrad rms uncertainty in pointing angle. The slit should be co-aligned with the

as well. The look direction for the solar occultation mode is at least 45° from the optical axis, to prevent the other instruments from viewing the sun.

The electronics module is hard mounted to the HPSP wall, underneath the instrument case, and covered by the HPSP's MLI blanket. The instrument case is covered with a MLI blanket as well. Since ACM's optics and detector must run at 110 and 60K resp., and conducted and radiated heat from the HPSP is a major source of heat flux, HPSP temperatures above -40°C could require an increase in radiator size, or degrade ACM performance.

As shown in Figure 4, ACM has a signal and power electrical interface with the HPSP. Redundant 1553 interfaces via the BIU are provided, which relay telemetry commands, status, and housekeeping and image data from/to ACM to/from the S/C. DC power is used to power the electronics and, on infrequent occasion, a heater to defrost the telescope primary.

ii. Major Instrument Functions

• Primary

ACM is an infrared spectrometer. The instrument produces images which, after suitable data processing on the ground, represent spectra, in the $3 - 5\ \mu\text{m}$ region, of light present at an aperture of size $102 \times 1.2\ \text{mrad}$. Typically HPSP is pointed so that the $1.2\ \text{mrad}$ direction is normal to Saturn's axis, and HPSP slowly scans back and forth along the axis as the planet rotates, so that the entire surface is mapped sequentially.

This $102 \times 1.2\ \text{mrad}$ aperture is divided into three channels, each of size $34 \times 1.2\ \text{mrad}$. Thus channel 1 sees flux from a target area "above" channel 2, and channel 2 above 3. Channel 1 produces spectra in the $5.3\ \mu\text{m}$ region, channel 2 in the $4.7\ \mu\text{m}$ region, and channel 3 in the $3\ \mu\text{m}$ region.

Each channel is a collection of 85 spectra from 85 IFOV's of size $0.4 \times 1.2\ \text{mrad}$, each above the other.

Exposures in this mode require typically several hundred seconds. At the end of the exposure the interferogram image is reported to the S/C.

• Secondary

ACM has a solar occultation mode, as well as the main observing mode discussed above. Sunlight enters ACM through an auxiliary window, and impinges on three small spherical reflectors, one for each channel. Reflected light from the reflectors enters the interferometer just as light from the slit does in the usual observation mode.

Exposures in the occultation mode are typically one second long, and are accurately time tagged.

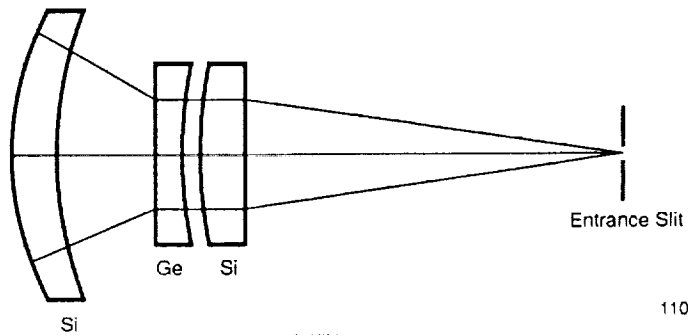
(b) Major Instrument Elements Description

i. Primary optical path

The primary optical path begins with a silicon-germanium-silicon, 200 mm EFL, $f/2$ Objective lens. It forms an image on an aperture whose width is $1.2\ \text{mrad}$. This lens system is athermalized, so that it maintains performance about the 100K environment provided by passive temperature control. It is optimized for the 3 to $5\ \mu\text{m}$ spectral region, and is shielded from all visible light by the choice of materials. An enlarged view of the lens system is shown in Figure 6.

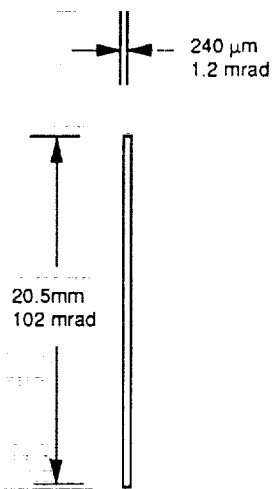
The slit is shown in Figure 7. It is $240\ \mu\text{m}$, or $1.2\ \text{mrad}$, wide, and $256 \times 80\ \mu\text{m} = 20.5\ \text{mm}$, or $102\ \text{mrad}$, long.

Following the slit, the light is recollimated and passes to a beamsplitter. Half the light is transmitted to a compensator plate and flat mirror. The other half impinges



11070/357.018

Figure 6: F/2 Telescopic Lens



11070/357.038

Figure 7: Spectrometer Entrance Aperture

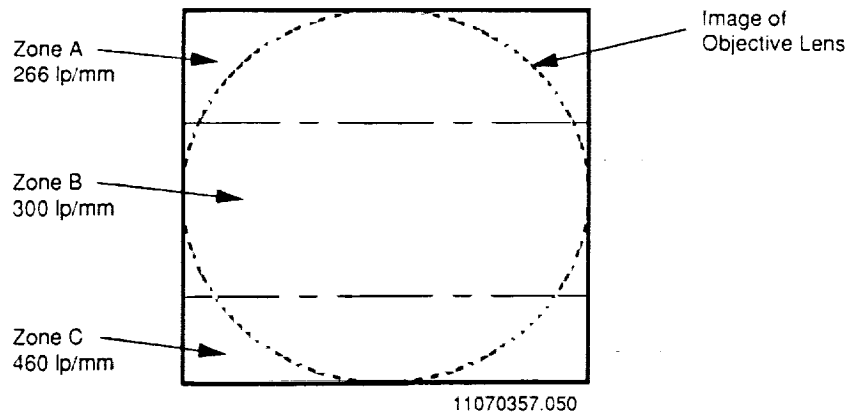


Figure 8: Spectrometer Grating

on a grating. The recollimation lens also projects a pupil onto the grating. This constrains all of the light passing through the slit to the active grating surface. The grating is composed of three sections, as illustrated in Figure 8. Each is designed for Littrow operation at the central wavelength of one of the three science spectral bands. The width of each sub grating is inversely proportional to the expected flux from Saturn. The wavelengths, grating periods and sub-grating widths are listed in Table 2.

Table 2: Grating Specifications

Band	1	2	3	
Central Wavelength	1885	2123	3255	cm ⁻¹
Grating period	266	300	460	lp/mm
Sub-grating width	3	33	3	mm

The recombined beams proceed from the beamsplitter towards the detector, passing through an anamorphic relay telescope and imager. This sub-system acts as a terrestrial telescope in the plane perpendicular to the slit, and as a reimager in the perpendicular plane. The telescope forms an exit pupil in the plane of the detector, while the imager forms an image of the slit. This creates a one dimensional image of the slit on the detector, with the light spread out in the perpendicular direction. This direction, then, is the interferogram that contains the spectral information. In the imaging direction, each 40 μm pixel row corresponds to 0.4 mrad.

The pupil is sized to encompass the detector when the optical axis of the system is placed in the middle of the 25th column of detector pixels, about 10% of detector width. Because the interference pattern is symmetrical across the center of the pupil, it is not necessary to record both sides. Accordingly, the detector is placed to gather a maximum of data from one of the two redundant halves of the pattern. This is illustrated in Figure 9.

The last elements of the optical system are the filters located near the detector surface. Each is a strip filter, covering several rows of pixels and limiting these rows to a specific spectral region. The dimensions and spectral coverage of the three filters

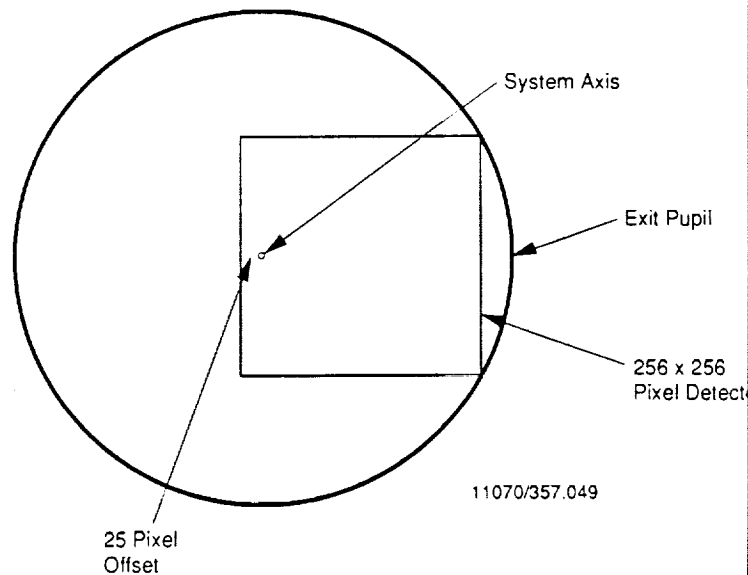


Figure 9: Focal Plane Image

are listed in Table 3.

Table 3: Detector Plane Filters

Spectral Band	1	2	3	
Central Wavelength	1885	2123	3255	cm^{-1}
Band width	55	45	45	cm^{-1}
Filter Width	3.48	3.28	3.48	mm
Lowest Pixel Row	1	89	169	
Highest Pixel Row	88	168	256	

ii. Auxiliary optical path

ACM observes solar occultations by the atmospheres of Saturn, Titan and the rings. In order to accommodate significantly higher flux levels without saturating the instrument in normal operations, a simple bypass of the large object is included.

A window is placed in the side of the housing behind the the slit plane as shown in Figure 10. This allows solar flux from a particular direction to enter the back of the slit plate at an angle well off normal. Mounted on the slit plate in the proximity to the slit itself, are a minimum of three segments of reflective material. The minimum configuration of three spheres is shown in Figure 11 for the auxiliary path. These "Pinhead Illuminators" are fabricated from small spheres, approximately 1 mm in diameter. Segments about 1 mm on a side are cut from them in such a way that, upon reflection, the solar flux will fill the $f/2$ acceptance cone of the camera lens. The virtual source of the reflected solar light lies close to the plane of the slit. An illuminated area of about 1 square millimeter provides flux reduced to the telescope, of $\approx 5,000$.

Since the detector images the slit, in one dimension, onto the detector array, a minimum of three separate "pinhead illuminators" are necessary for the auxiliary path for which observations are to be made. An alternative approach under consideration is to replace a collection of spherical reflectors with three cylindrical lenses, each of which is parallel to the slit.

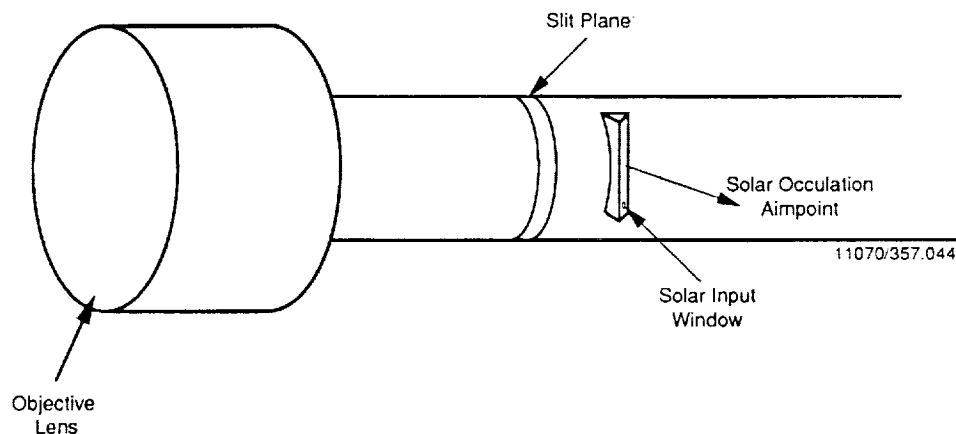


Figure 10: Auxiliary optical port geometry. In the solar occultation mode, sunlight enters the auxiliary slit and impinges on small spherical reflectors near the focal plane slit.

Because the light is dispersed into an $f/2$ cone, the pupil imaging will cause the light to be included within circles at the detector slightly displaced from the system pupil. By selecting the appropriate side of the slit for the chosen offset of the detector, the pupil will cover the entire detector in the non-imaging direction.

The window in the side of the ACM housing will be reduced to three very small apertures by masking. Light losses from the window, which may include filtering, will contribute to the adjusting of the power levels to that appropriate to the solar occultation mode.

It is important to suppress stray solar flux from entering the system in any manner other than from the "pinhead illuminators". To this end, the back of the slit plate, including the illuminators, will be coated with gold. The specular reflection of solar light from the flat regions of the slit plate will be trapped at the wall on the opposite side of the housing.

iii. Detector

ACM uses a staring array similar to the array currently under development for the NICMOS program. Table 4 shows its characteristics. It differs from NICMOS only in that MWIR HgCdTe is used (rather than SWIR). Figure 12 shows construction of the hybrid array. A pixel size of 40 microns permits the use of monolithic substrates without concern of breakage of the indium bump bonds.

Figure 13 shows design of the Si multiplexer. All 256^2 pixels are read out through one amplifier. Photocharge is integrated directly on the photodiode, initially reversed biased at 500mV. A FET places a corresponding voltage on the output bus when the pixel is selected with its row and column address. A pixel so selected is reset by asserting the RST signal. The device is straightforward to operate, requiring only a few clocks and biases.

Dark current is of critical importance. Figure 14 shows theoretical dark current per pixel for a Rockwell 4.7 micron device with 60 μm pixels extensively tested at Ball. In this region dark current is dominated by gain-recombination current. Shown also are laboratory measurements which agree well with theory. The proposed 40 μm device should have comparable dark current, since the pixels are smaller but the material lower bandgap.

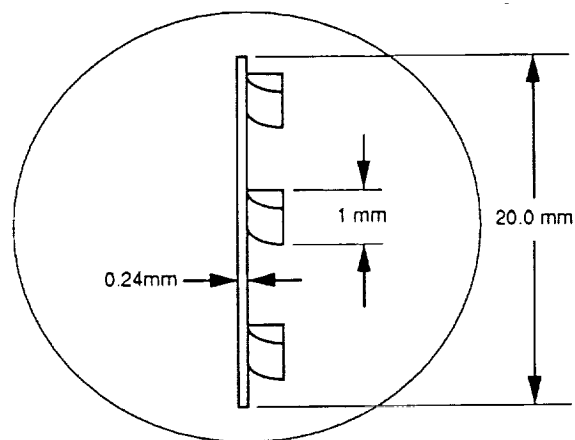


Figure 11: Auxiliary reflector placement. Shown is the minimum of three reflectors, one for each of separated channels. Using more reflectors will fill the detector completely.

Table 4: Focal Plane Array Requirements

type:	256 × 256 Rockwell Science Center array
spatial sampling:	0.4 × 1.2 mrad FOV/pixel 102 × 1.2 mrad FOV/array
quantum efficiency:	70% min at 5.3 microns
dark current:	<1 femtoamps at 60K
read noise:	<100 electrons/pixel
well depth:	>1 × 10 ⁵ electrons for 500 mV bias
pixel size:	40 microns at 85% fill factor
temperature:	60K, passive cooler

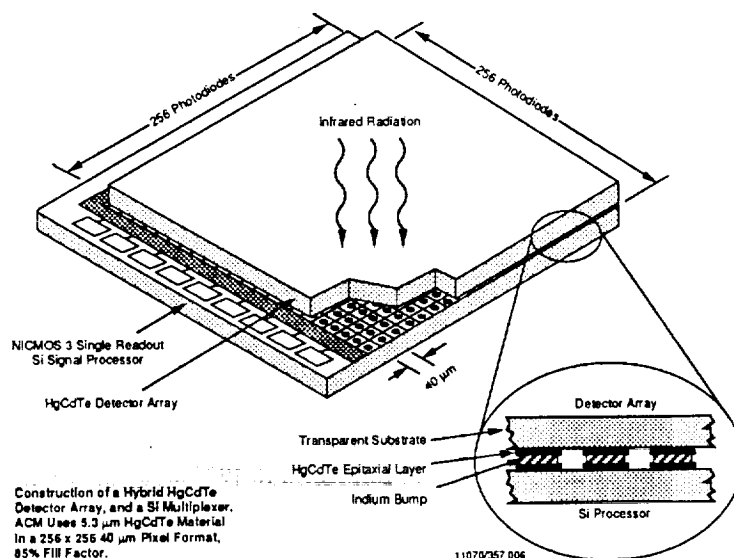


Figure 12: Construction of the hybrid HgCdTe array.

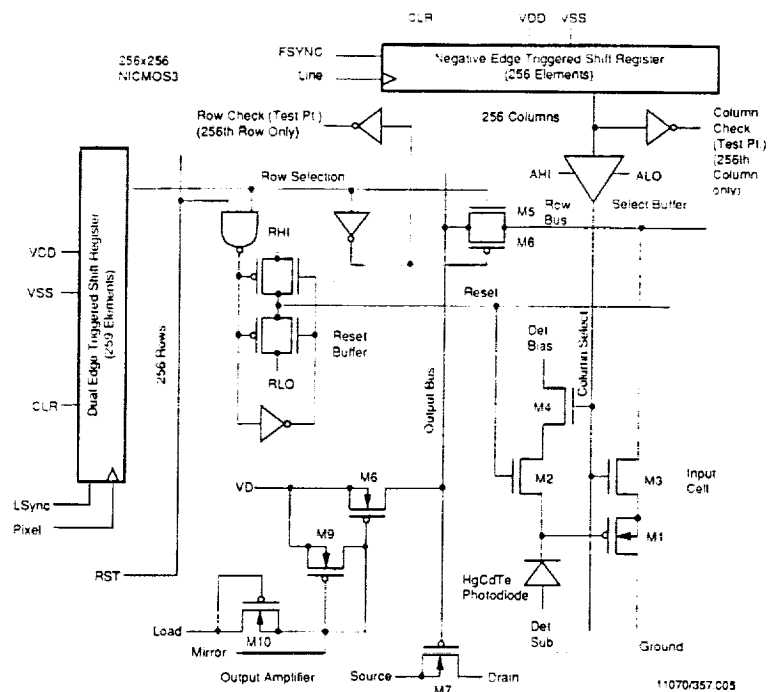


Figure 13: Si multiplexer organization. Each pixel is selected for readout or reset by its row and column addresses.

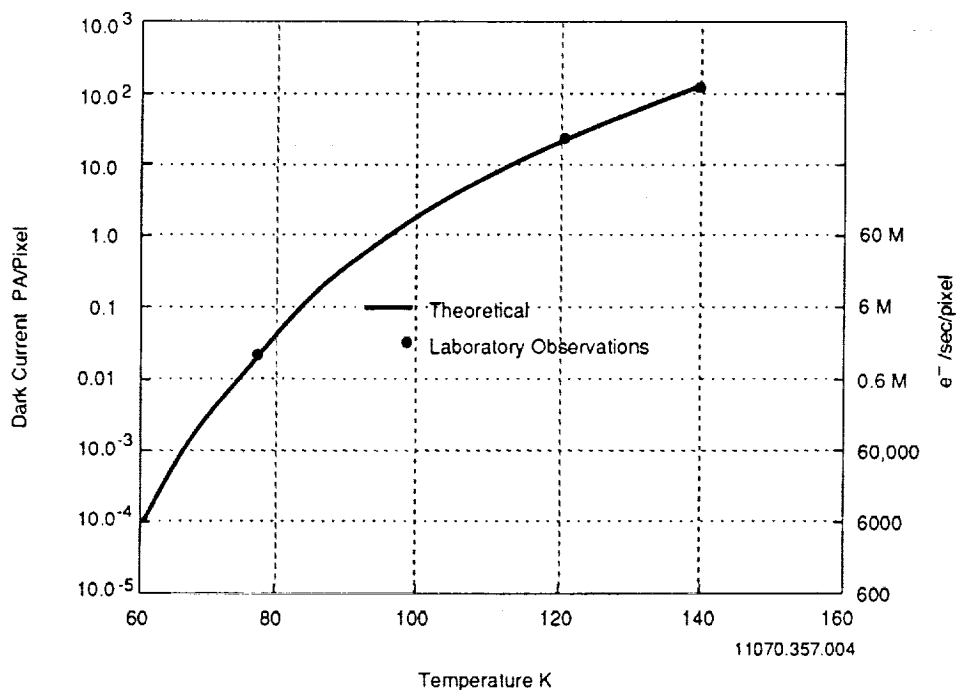


Figure 14: Mean dark current for Rockwell 4.7 micron 60 μm HgCdTe 128² array under nominal operating conditions. 40 μm currents can be expected to be proportionally smaller.

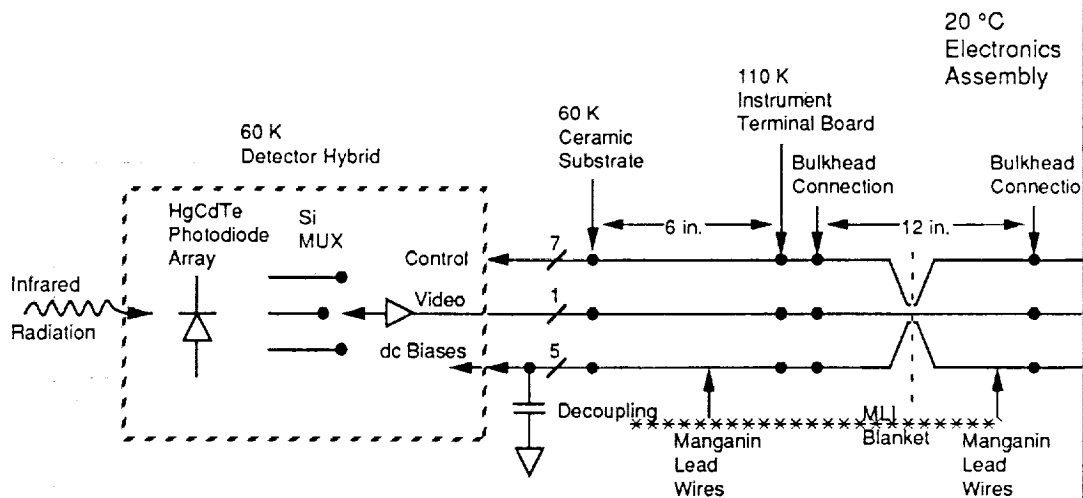


Figure 15: Detector system block diagram. The detector uses a 256^2 $40\text{ }\mu\text{m}$ Rockwell 5.3 micron HgCdTe photodiode array and a single readout Si multiplexer of NICMOS design.

Figure 15 shows the detector system. The detector at 60K is thermally isolated by a cold finger and short flexible metal strap to a 50K radiator. Short leads are brought from the detector case to a ceramic PWB also at 60K. Manganin wires provide thermal insulation to the instrument case at 110K, and relative to the case. The per wires provide thermal insulation between the case and the electronics assembly nominally at 20°C.

iv. Electronics

The electronics module, shown in Figure 4, has several functions:

- Control and readout of the detector. Control is simple, basically two horizontal lines in the horizontal and three in the vertical direction, to select row and column address. Correlated double or triple sampling is implemented in software. Bias voltages are programmable for flexibility in operation. Integration times are typically a few seconds or longer, readout speed is not a concern.
- Command, status, and data to the BIU and S/C telemetry. Microprocessor design with buffering RAM provides any desired protocol, data rate, and telemetry data. Commands may be loaded and executed later at time of need. Redundant BIU channels are implemented.
- Control of the primary lens heater via telemetry and solid state switch.

Reliability has been given serious consideration. Power supplies and water cooling are fully redundant. Radiation and single-event resistant parts and design techniques are used. The recommended SA3300 processor is proposed.

The electronics are packaged on three multi-layer PCBs in a 6"x6"x3.5" enclosure, so that the BIU and electronics form a 6"x6"x3.5" package thermally coupled to the HPSP and insulated so that operating temperatures are consistent with HPSP temperatures.

Table 1 shows size, mass, and power specifications. Figure 16 gives a detailed breakdown for the electronics.

v. Mechanical Structure

CIRCUITRY	I _{+5V}	P _{+5V}	I _{±15V}	P _{±15V}	TOTAL
Detector Array	10 mA	0.05 W	0	0	0.05 W
Det. I/F Elect.	50 mA	0.25 W	30 mA	0.9 W	1.15 W
CPU -- Osc.	20 mA	0.1 W	0	0	0.1 W
CPU -- Processor	100 mA	0.5 W	0	0	0.5 W
CPU -- Memory	50 mA	0.25 W	0	0	0.25 W
CPU -- Periphs.	100 mA	0.5 W	0	0	0.5 W
CPU -- Hskpg.	50 mA	0.25 W	25 mA	0.75 W	1.00 W
Cmd & Tlm. I/F	80 mA	0.4 W	0	0	0.40 W
Totals	460 mA	2.30 W	55 mA	1.65 W	3.95 W
Plus power supply losses (Efficiency = 0.8)					1.00 W
Overall total including power supply*					4.95 W

* Not including BIU power

11070/357.046

Figure 16: Detailed power budget for the electronic circuits.

ACM's mechanical outline is shown in Figure 1. The radiators are co-planar with other instrument radiators to avoid FOV conflicts. ACM is designed to be narrow, that it may easily be fit between two other instruments. No cover is required, since ACM is insensitive to dust contamination. The electronics module, not shown in the figure, fits under the instrument case against the HPSP mounting surface.

The instrument is composed of three subassemblies: a telescope (with an auxiliary optical port), interferometer, and detector optics. The telescope is designed to passively compensate for thermally induced optics defocus by using material combinations of composites and metals.

Structural support and thermal isolation between the instrument and HPSP is achieved by a quasi-kinematic mount system using thin wall, fiberglass struts. The mounting system accommodates differential thermal growth between the instrument and HPSP by (quasi-kinematic) flexure of the fiberglass struts in their respective low load directions.

The 100K thermal radiator is supported rigidly to the instrument. During ground handling and launch environment, thermally actuated latches will rigidly couple the two radiators together to provide structural support for the 50K unit. The latches will automatically release during on-orbit cooldown.

Table 5 lists component masses.

vi. Thermal Design

From a thermal point of view, two elements - the instrument and the electronics module, form the ACM. The thermal design of the latter is straightforward. The electronics module is covered with MLI and hard mounted to the HPSP. Little heat is lost through the MLI. The bulk of the 3 watts average power dissipation is conducted into the HPSP. Should the ICD not allow this heat to be passed to the HPSP, a small amount of MLI may be removed to expose an appropriately sized radiator.

The thermal design of the instrument case, shown in Figure 5, uses radiators and a high degree of thermal isolation from the HPSP. The detector is run at 60K to minimize dark current, and the optics at 110K to minimize parasitic flux and conduction to the detector. The detector is cooled with a simple flat plate radiator at 50K, and the instrument with a similar radiator at 100K. Five to ten degrees is reserved to get

the heat to the radiators without resorting to heat pipes.

A radiator at 55K, measuring 20cm × 20cm and having an emissivity dump 17.6mw to deep space. The electrical dissipation of the detector and the radiative load from the instrument case to the detector is an additional 4mw comes from radiation through MLI to the back of the conduction down the 15 40-gauge manganin leads adds a further 1.3mw. is supported from the 110K radiator with a combination of threads and latch which acts as a launch lock; in the unlatched condition, the cold load is negligible. The detector module is supported on a fiberglass adds a further 4.3mw, bringing the total to 13.6mw, a margin of 23%. Of this 14mw load on the cold radiator, 11mw must be passed through link or cold finger from the detector module to the radiator. This will be a copper wire attached at each end by indium solder or an e thermal impedance method. In this fashion the entire temperature difference is reserved for the wire itself, which will have an area-to-length ratio equal to 22-gauge OFHC copper wire 10cm long. This sizing includes the temperature on thermal conductivity, which is nearly a factor of 2 higher at 60K temperature.

The instrument radiator at 100K can dump 195mw, with an area of an emissivity of 0.85. The area in this case is based on the radiator being 31cm, but with a 20cm × 20cm area being either cut out or blocked by the radiator. The radiator is hard-mounted to the optics box. The window is covered with MLI. For sizing purposes, we have taken a 26cm × 31cm looking at -40°C. In this case, the total load to the optics box is:

- 90mw through the MLI
- 3mw from the leads (10 40-gauge and 5 30-gauge Manganin wires run to the electronics box)
- 84mw from the support system (kinematic mounts of a total of six fingers)

This gives a total of 177mw, compared to 195mw allowed, for a margin of 9%. Preliminary analysis indicates about a 2K rise in detector temperature and a 10K rise in HPSP temperature. Operation at temperatures warmer than this would necessitate larger radiators or degraded operation.

For the purpose of sublimating water deposited on the telescope primary optical window due to contamination from engine exhausts, we will provide a heater primary to 200K. Preliminary analysis indicates only 5 w heater power at the telescope, and 2 w at the window, if the radiators, intentionally for this purpose, are pointed towards the sun.

vii. Telescope Primary and Auxiliary Window Heater

These heaters are typically Minco Kapton elements bonded onto the outside of the structure, under its MLI blanket. Thermistors are adequate for temperature feedback.

(c) Instrument Testing Interfaces

i. Assembly Level

• Calibration

Rockwell determines detector parameters that cannot be calibrated in flight, such as spectral quantum efficiency, non-linear flux to signal conversions, and spatial maps of pixel gain and saturation levels. Ball has calibration facilities as well, and expects to verify many of these measurements.

Optical vendors are expected to provide spectral transmissivity and reflectivity curves, and aberration data, for optical components. Ball has extensive optical calibration facilities as well, and expects to verify many of these measurements.

- Testing

Rockwell performs wire bond tests, and temperature cycling tests on the detector. Rockwell characterizes (and Ball verifies) detector parameters such as dark current, fixed pattern noise, and yield.

Optics houses characterize surface quality. PWB manufacturers provide continuity and short screening. Electronic parts manufacturers also provide quality, reliability, and screening services, including temperature testing and cycling. Mechanical parts made at Ball are tested for structural faults. Ball routinely performs form, fit, and tolerance receiving inspection on all components.

- ii. Subsystem Level

- Calibration

- The electronics data acquisition system is calibrated for gain, bias, and temperature sensitivity.

- Testing

- Ball performs extensive module level testing.

- The electronics module is tested using a simulated detector. The detector is tested using a simulated electronics module, easily implemented in Ball's computerized IR Detector Evaluation Laboratory. The S/C interface is tested from hardware and software viewpoints using a S/C 1553 bus simulator.

- The telescope, interferometer, and re-imaging optics are tested individually and collectively on optical tables with breadboard/brassboard sources, lenses, and apertures. Optical tests often use breadboard/brassboard detectors similar to flight models.

- iii. System Level

Final tests for ACM require simulating a 4K space environment. Ball has thermal vacuum chambers with LN₂ refrigerated walls. One of these chambers will be used with He panels placed in front of the radiators.

- Calibration

- Radiometric and spectral calibration tests are required at the system level. For radiometric calibration a collimated source of known irradiance is required. Data processing software must be well developed at this point, since it is part of the signal processing flow.

- Spectral calibration requires a collimated source, either monochromatic or broad-band with distinctive lines of known wavelength. The latter can be provided by gas cells illuminated by blackbody light. Ideally three wavelengths between 3 and 5 μm are provided, one for each spectrometer channel.

- Testing

- Verifying thermal performance is the goal here. Of primary interest are detector and instrument temperatures with the radiators staring into thermal space, particularly as a function of HPSP temperature. Of secondary interest is the temperature of the telescope primary when heated, and unheated with the radiators staring at the sun at one A.U.

- (d) Instrument Operations

- i. Operational Modes

- ACM has two operational modes. The normal observing mode reports spectra observed through the telescope at relatively long time periods, typically several hundred

seconds. The solar occultation mode reports spectra observed through optical port at relatively short periods, perhaps once a second.

It can be seen the two modes have very different demands on pointing and data rates. However, so far as ACM's interface with the S/C is concerned, the two modes are nearly identical. ACM can be thought of as a camera returning raw video of resolution about $12 \text{ bits} \times 256 \times 256$ pixels, together with ACM's only auxiliary function is to control the telescope objective window heaters. They are energized for perhaps an hour at a time to remove contaminants, principally water, that have condensed on its surface and engine burns.

Detector control parameters such as frame time, number of detector integrations per frame, and area of the detector read out, are commandable. ACM requires usual housekeeping data and health checks, such as temperatures of instrument, telescope primary, and electronics; power supply voltages; processor self-tests; and telemetry loopbacks.

ii. Coordination with other instruments

ACM presents no special coordination problems with other instruments.

3 Mass

Table 5 shows ACM's mass breakdown.

Table 5: ACM mass breakdown

ELEMENT	MASS	
	Kg	lb
optical elements, detector	1.26	(2.77)
optics mounts	0.18	(0.40)
housing structures	1.34	(2.95)
radiators	0.28	(0.62)
support trusses, fittings	0.12	(0.26)
wiring, connectors	0.28	(0.63)
electronics, excluding BIU	1.36	(3.00)
BIU	0.25	(0.55)
TOTAL	5.1	(11.2)

4 Power

ACM is fully compatible with Vol IV, *Spacecraft Description*.

Table 6 shows the instrument power vs. mode for ACM.

ACM is immune to corona discharge at any pressure.

1.0 hours are required for warm-up/stabilization from the lowest allowable non-operating temperature.

Table 2-1.3 Instrument Power vs. Mode
(Fill in all blanks for each mode)

ACM (Atmospheric Chemistry Mapper)

Instrument Name _____

Instrument Mode*	Average Total** Power (W) at 30Vdc +/-0.75Vdc at Instr. Input	Location of Power Dissipation Percent (%) of Total in Item	Peak Power ***	
			Watts (W)	Duration (s)
1. OFF	0W	_____ % in _____ (Item) _____ % in _____ (Item)	0W	
2. ON	5W	99.9 % in <u>electronics</u> (Item) 0.1 % in <u>instrument</u> (Item)	9W	1 sec
3. Heaters ON	13W	55 % in <u>electronics</u> (Item) 45 % in <u>heater</u> (Item)	17W	1 sec
4.		_____ % in _____ (Item) _____ % in _____ (Item)		
5.		_____ % in _____ (Item) _____ % in _____ (Item)		
6.		_____ % in _____ (Item) _____ % in _____ (Item)		
7.		_____ % in _____ (Item) _____ % in _____ (Item)		

* Include Calibrate and Keep alive modes, if applicable (Use extra sheets if more modes)

** Including instrument power supply inefficiency plus quiescent BIU at 0.75W.

*** Including 4 W instantaneous for BIU, when providing data to the GPS; and any applicable actuator power (mini-dual drive and wax pellet actuators will be powered external to the instrument).

Table 6: Table 2-1.3, power vs. mode

5 Mechanical Configuration

ACM is fully compatible with Vol IV.

Table 7 shows sizes of ACM's mechanical components. ACM consists of two modules: the instrument itself; encompassing optics, detector and radiator; and a supporting electronics module.

Table 7: ACM module sizes

Deliverable Units Name(s)	Flight Size (cm)	State of Development
electronics module	15x15x9	conceptual
instrument	40x28x33	conceptual
radiator, detector	20x20	conceptual
radiator, instrument	26x31	conceptual

5.1 Location for instrument sensor, electronic package

Table 8 shows locations for mechanical components of ACM.

Table 8: ACM module locations

Location	Deliverable Units Name(s)
electronics module	HPSP wall, under instrument
instrument, with radiators	HPSP

5.2 Location constraints

The electronics module must not be located more than 0.5 m from the instrument.

5.3 Desired co-alignment and/or co-boresightment

ACM must be co-boresighted with the other optical instruments on HPSP. Section 4.2 discusses pointing and stability requirements.

5.4 Instrument sketch

Figure 1 shows ACM's mechanical outline and interface footprint.

- The FOV is 102×1.2 mrad. The long dimension of the FOV should be parallel to the slit-type instruments on HPSP, e.g. VIMS.
- The IFOV is 0.4×1.2 mrad.
- Since the radiators are co-planar with each other and with radiators on other instruments, their FOV is 2π sr.

6 Need for cover and/or pyrotechnic device

ACM requires no cover.

No pyrotechnic devices are used in ACM, or required for development.

7 Instrument safety/operational constraints

There is a possibility ACM can be damaged if its telescope is pointed at the sun for periods of time exceeding a few minutes at one A.U. Detector damage is the primary concern, with lens thermal runaway a secondary concern. At 9 A.U. there is no danger of such damage.

ACM can operate within 30° of the sun at 9 A.U.

8 Instrument sensitivity to stray light

ACM is insensitive to stray light from S/C structure or dust particles.

9 Electrical Interface Listing

ACM is fully compatible with Vol IV.

9.1 List of electrical interfaces between the instrument and the S/C

Table 9 shows electrical interface signals between ACM and the S/C.

Table 9: ACM to S/C electrical interface

Function	Number of Circuits
BIU low rate SCI bus	4
+15V	1 (2 preferred for redundancy)
-15V	1 (2 preferred for redundancy)
case ground	1 (2 preferred for redundancy)

10 Environmental

ACM is fully compatible with Vol IV.

10.1 EMI source - list and quantify

Table 10 lists ACM's EMI sources.

10.2 EMI receptors - list and quantify

Table 11 lists ACM's EMI receptors.

Table 2-1.1 EMI Sources Identification
Instrument Name ACM (Atmospheric Chemistry Mapper)

1. Motors (e.g., stepper, DC, DC Brushless)?
 Type None
 Current/Power (Assume 30 V dc bus voltage) _____
 In-Rush Current _____
 Speed/pulse rate _____
 Is there DC isolation? _____
 Is there isolation from local chassis? _____
- NOTE: For flight equipment, the isolated end-circuit shall present not less than 1.0 Megohms resistance, and signal circuits, not more than 400 pF of capacitance measured from each end-circuit terminal to circuit ground.
2. Relays (e.g., solid-state, reed, coaxial)?
 Type None
 Drive Current _____
 for contacts _____ for coils _____
3. High Power Electromagnetic Devices (e.g., TWTs, Magnatrons)
 Type None
 Frequency _____
 Power Level _____
 Emission data (if available) _____
 In-Rush Current _____
4. High Power Devices (e.g., Lasers)? None
 Type/modulation _____
 Power Level _____
 In-Rush Current _____
5. Power Converters
 Is there isolation? Yes
 Free-run Frequency 100K to 200KHZ
 Type (switching, linear) Switching-synchronous
 Ripple (frequency and amplitude) MIL-STD-461B

Table 10: Table 2-1.1, EMI sources

Table 2-1.2 EMI Receptors Identification
Instrument Name ACM (Atmospheric Chemistry Mapper)

1. Digital Circuits:

Technology Desired: _____

2. Analog Circuits:

High Precision/Low Level Circuits:	Yes	<input checked="" type="radio"/> No
Analog/Digital Converters (AD-DA Circuits):	<input checked="" type="radio"/> Yes	No
Multipliers/Dividers:	Yes	<input checked="" type="radio"/> No
Sensitive Telemetry Circuits:	Yes	<input checked="" type="radio"/> No

3. Radio Frequency Equipment:

--NONE--

If Yes, Describe:

Mixers:	Yes	No	_____
IF Stages:	Yes	No	_____
Local Oscillators:	Yes	No	_____
Phase-Locked Loops:	Yes	No	_____
Modulators:	Yes	No	_____

Instrument Receiver --NONE--

Type/MFR _____	Noise Figure _____
Frequency _____	Antenna(s): Type _____
Threshold Power _____	dB Gain _____
Bandwidth _____	Eff. Area _____
	Eff. Height _____

Table 11: Table 2-1.1, EMI receptors

10.3 Frequency bands - structural resonances

The radiators may have resonances between 0 and 100 Hz in the direction normal to

10.4 Low-level sensitivity

No low-level vibration sensitivities are expected.

10.5 Environmental tests instrument has been qualified to

ACM has not been qualified to any environmental tests.

10.6 Instrument operation during or after exposure to radiation enviro

ACM's optics, detector, and electronics are expected to operate satisfactorily in environment anticipated for the mission.

The SWIR version of the detector, currently under development by Rockwell for program, has been shown under test to exhibit no radiation effects up to 10Mrad (

Radiation hard electronic parts, including the SA3300 and supporting circuits, a ACM.

11 Thermal Control

ACM is fully compatible with Vol IV.

11.1 Heating/Cooling System

ACM is a cryogenic instrument. Its detector is designed to operate at 60K and the 110K. ACM uses continuously active radiators to achieve these temperatures. About dumped by the radiators to space, most of it by the instrument radiator. About half from HPSP through instrument supports, and the remainder radiation from HPS MLI blanket. No fluids are involved.

11.2 Type of thermal coupling

The instrument portion of ACM (the optics and detector) is thermally decoupled using low thermal conductivity mounting legs. ACM's electronic module should coupled to HPSP. Platform temperatures near the lowest specified operating point

11.3 Parasitic losses to the mounting point

ACM radiates to space about 200 mW.

11.4 Temperature control with the mass and power budget for each affe erable unit

For the electronics module, temperature control via MLI is acceptable.

ACM contains a heater for contamination control of the telescope primary lens window. During the heating phase, the element temperature are driven to at least : inary analysis indicates 5W at the telescope and 2W at the window are sufficient to temperatures.

11.5 Radiator size and field of view

ACM employs two radiators: one for the detector, one for the instrument case. ACM performance will degrade if the sun is in their FOV more than a few minutes at 9 A.U. ACM will have nominal performance if the radiators look at Saturn at distances greater than 30 Saturn radii.

The detector radiator is 20 cm × 20 cm, and has a 2π sr FOV. The instrument radiator is 26 cm × 31 cm (with a 20x20 cutout), and also has a 2π sr FOV, since the two radiators are co-planar.

11.6 Operating and non-operating temperature ranges

Table 12 shows temperature ranges for ACM.

Table 12: ACM temperature ranges

Deliverable Unit(s)	Operating Temperature	Non-operating Temperature	External surface Emissivity
detect. radiator	50K	-	> 0.9
instrm. radiator	100K	-	> 0.9
detector	60K	20 - 300K	N/A
instrument	110K	50 - 340K	> 0.9

11.7 “Special desires” for the proposed instrument

Good thermal isolation from HPSP is crucial for optimum ACM performance.

A clear “look” direction for the solar occultation port is necessary.

11.8 Number of one Watt RHUs for remotely located item(s)

RHU’s are not required for ACM.

11.9 Effect(s) of sun shades near instrument

A clear “look” direction for the solar occultation port is necessary.

11.10 Instrument thermal design – facilitate ground testing?

ACM’s design facilitates Solar Thermal Vacuum testing and verification.

12 Telecommunications

ACM is fully compatible with Vol IV.

ACM has no telecommunications sub-system.

13 Telemetry Measurement

ACM is fully compatible with Vol IV.

13.1 Identification of number of telemetry modes and formats

Although ACM may image through the telescope with long periods between frames the solar occultation port with short periods between frames, it has only one telemetry mode described in *Instrument Operations*. Detector parameters are always uplinked, and timing marks downlinked, in the same fashion.

ACM always reports raw detector images, as about $12 \text{ bits} \times 256 \times 256$ pixels. 112 bit image words into 16 bit packet words to avoid wasting bit space. Since telemetry is constrained to 8192 words, about 96 packets are required per frame. To further reduce data, an initial frame with 12 bit reporting may be transmitted, and succeeding frames with 12 bit differentials, since spectra typically change little from frame to frame. Engineering data, and timing marks are appended to each frame.

13.2 Commands stored within and timed from the instrument

ACM has the ability to store commands and execute them at timed intervals. This is useful in the solar occultation mode, where the frame rate approaches one per second.

14 Data System Intercommunication

ACM is fully compatible with Vol IV.

In lieu of Table 2-1.4, which seems awkward for describing ACM's data rates, a detailed discussion is submitted.

ACM requires an uplinked command to turn it off or on. It must be on for the main and auxiliary window heaters to be commanded off or on. If ACM is on, no data is transmitted until a command(s) specifying a sequence of timed frames is loaded and executed. Once the sequence begins, frame data is reported to the S/C on a frame by frame basis.

To sublimate contamination, ACM enables the heaters after engine burns, and after the heaters are to be taken. Approximately one hour is anticipated to clear the optics.

ACM takes data under four circumstances:

- Calibration. ACM requires deep space views to measure dark current. It also requires a known spectrum to identify changes in pixel response; the S/C calibration target spectrum, and the solar illuminated ring spectra are candidates. Calibration is performed before a sequence of observations. Each calibration target requires several frames, each frame from one to several hundred seconds in duration, depending on the target.
- Normal observations of Saturn, Titan, and Saturn's rings. Each frame requires several seconds, each mapping three 34×1.2 mrad slits of target, one of three spectra associated with each slit.
- Solar occultations by Saturn and Titan. Each frame is typically one second in duration. The entire array need not be reported, since not all pixels may be illuminated, and data processing (eg. summation) may be performed.
- Miscellaneous observations, eg. icy satellites.

14.1 Additional data to Volume IV-defined S/C-supplied standard services

No additional data services, in addition to the standard services, are required by ACM.

15 Command Structure/Formats

Command structure and format is discussed above in *Data System Intercommunication*.

16 Spacecraft Maneuver and Control

ACM is fully compatible with Vol IV.

16.1 Description of spacecraft/platform attitude

In general, ACM presents no special attitude control or rate demands. During data collection, ACM's radiators must not be pointed at the sun, and preferably not at Saturn.

ACM's most common data collection mode is mapping Saturn's surface. The long axis of ACM's slit should be parallel to the projection of Saturn's axis onto ACM's telescope primary lens. Most observations can be made at $20 R_S$ or greater.

When ACM is observing solar occultations, the other instruments on ACM will not be viewing the sun.

16.2 Description of in-flight calibration

Calibration of ACM requires no difficult attitude or rate demands.

ACM requires deep space targets to measure dark current. It also requires a known spectrum to identify changes in pixel response; the S/C calibration target, the solar spectrum, and the solar illuminated ring spectra are candidates. Calibration is normally performed before a sequence of observations. Each calibration target requires one or more frames, each frame from one to several hundred seconds in duration, depending on the target.

17 Accuracies

ACM is fully compatible with Vol IV.

17.1 Mechanical Alignment

Table 13 shows mechanical alignments of ACM.

17.2 Pointing and Stability

Table 14 shows pointing and stability requirements for ACM.

ACM's normal target reference is Saturn's geometric center.

ACM desires a 3σ pointing stability of $10\mu\text{rad}$ in 0.5 sec, and $100\mu\text{rad}$ in 100 sec. ACM is located on the HPSP.

ACM requires no scan slews.

In the solar occultation mode, ACM's line of sight differs from its usual LOS, and from the LOS of the other instruments on HPSP.

17.3 Induced Disturbances

ACM has no internal mechanical movements.

Table 13: ACM mechanical alignments

desired boresight control accuracy relative to instrument mounting interface	1 mrad (3σ)/axis
desired boresight alignment accuracy relative to instrument mounting interface	0.5 mrad (3σ)/axis
desired alignment control accuracy relative to other co-aligned/ co-boresighted instruments	1.4 mrad (3σ)/axis
desired alignment knowledge accuracy relative to other co-aligned/ co-boresighted instruments	0.7 mrad (3σ)/axis

Table 14: ACM pointing and stability

desired pointing control accuracy relative to inertial space (spacecraft control)	3.6 mrad (3σ)/axis
desired pointing knowledge accuracy relative to inertial space (spacecraft post reconstruction knowledge)	1.8 mrad (3σ)/axis
desired target-relative pointing control accuracy	1.8 mrad (3σ)/axis
desired target-relative pointing knowledge accuracy (post reconstruction)	0.9 mrad (3σ)/axis

18 Ground Operations

ACM is fully compatible with Vol IV.

18.1 Special ground operation listing

None.

18.2 Special instrument constraints listing

None.

18.3 Measures required to protect the instrument from contamination

None, other than the usual optical transportation covers and seals.

19 Ground support equipment

ACM is fully compatible with Vol IV.

The Cassini project office provides data processing equipment such as PC's and workstations. These may be required in the spacecraft assembly area or in the operations area during flight operations.

20 Reliability and Quality Control

ACM is fully compatible with Vol IV.

Every effort will be made to use standard parts in accordance with GSFC's Preferred Parts List PPL17 and NASA's Standard Parts List MIL-STD-979F grade 1. Non-standard parts are selected, procured, and screened to the same levels as standard parts. Levels are equivalent to M38510 Class S, JAN S for semiconductors, S or R for passive as available, and GSFC S-311-74 grade 1 for hybrid microcircuits. Qualification status is determined by existing test and application data, obtained from GIDEP, military, NASA, part manufacturers, or from BASD development programs. BASD developed qualification procedures may be submitted for approval prior to use. Technology, construction, quality control, application, and product maturity are all considered in choosing parts consistent with the 12 year mission.

21 Fault Protection

ACM has no assembly that requires power in the event of a fault protection action by the S/C.

22 Safety

ACM involves no hazardous materials.